Dynamics of Vortices in 2-dimensional Charged Fluids

by

George N. Stratopoulos

A thesis presented for the degree
of Doctor of Philosophy
at the University of Crete

Department of Physics, University of Crete
71003 Heraklion, Greece

January 1996

Δυναμική των Δινών σε Διδιάστατα Φορτισμένα Ρευστά

Γεώργιος Ν. Στρατόπουλος

Διδακτορική Διατριβή
που Υποβλήθηκε στο Φυσικό Τμήμα
του Πανεπιστημίου Κρήτης

Φυσικό Τμήμα, Πανεπιστήμιο Κρήτης
71003 Ηράκλειο

Ιανουάριος 1996

PREFACE

This thesis is based on work done by the author between September 1992 and December 1995 at the University of Crete, supported by the Greek General Secretariat of Research and Technology grant No 91ΠΕΝΕΔ358, by a Research Fellowship from the Greek Ministry of Education and a Research Fellowship from the Research Center of Crete. No part of it has been previously submitted for any degree, either in this or any other university.

With the exception of the review in chapter I and part of chapter IV it is believed that the material in this thesis is original work. Chapter III is based on a paper [28] published in Physica D. The work in chapter V is based on a paper [29] to appear in Physical Review B and a Crete preprint [30].

I would like to warmly thank my supervisor Prof. T.N. Tomaras and Prof. W.J. Zakrzewski for their guidance and encouragement. I would also like to thank D. Apostolakis, M. Panagiotakis, G.A. Papadogonas and N. Primikirios for creating a stimulating environment during my graduate years at Crete.

I thank my parents for their love and support. Among many other reasons, I am grateful to E. Papadimitraki for her love and for the enthousiasm she inspired me.

Dynamics of Vortices in 2-d Charged Fluids

by

George N. Stratopoulos

Ph.D. Thesis, 1996

Abstract

The work in this thesis is concerned with the study of some aspects of the physics of flux vortices within the framework of a dynamical Ginzburg-Landau model, relevant to the description of a superconductor or of an idealized bosonic plasma.

It is shown that a non-relativistic scalar field coupled minimally to electromagnetism supports in the presence of a homogeneous background electric charge density the existence of smooth, finite-energy topologically stable flux vortices. The static properties of such vortices and vortex-pairs are studied in detail. By using a constrained variational calculation, the interaction potential of two minimal vortices is obtained.

It is proven analytically that a free vortex is spontaneously pinned, while under the action of an external force it moves with a calculable speed perpendicular to it. Finally, the motion of vortices under the influence of several external probes is studied numerically. It is shown that up to a fine "cyclotron" internal motion, also studied in detail, two vortices brought together, rotate around each other, while a vortex and an antivortex move in formation parallel to each other. The drift of the vortex under the influence of a homogeneous external current, in a direction opposite to the current is also demonstrated. The velocities of the vortices in the above cases are measured to be in remarkable agreement with recent theoretical predictions.

Δυναμική των Δινών σε Διδιάστατα Φορτισμένα Ρευστά

Γεώργιος Ν. Στρατόπουλος

Διδακτορική Διατριβή, 1996

Περίληψη

Το αντικείμενο αυτής της διατριβής είναι η μελέτη της φυσικής των δινών μαγνητικής ροής στα πλαίσια μιας δυναμικής επέκτασης της θεωρίας Ginzburg-Landau, κατάλληλης για την περιγραφή ενός υπεραγωγού ή ακόμη ενός ιδεατού μποζονικού πλάσματος.

Ενα μη-σχετικιστικό βαθμωτό πεδίο συζευγμένο με το ηλεκτρομαγνητικό δυναμικό επιδέχεται, παρουσία ενός ομογενούς ηλεκτρικού φορτίου υποβάθρου, τοπολογικά ευσταθείς λύσεις πεπερασμένης ενέργειας, που αντιστοιχούν σε δίνες μαγνητικής ροής. Οι στατικές ιδιότητες απομονωμένων δινών καθώς και ζευγών αλληλεπιδρώντων δινών μελετώνται λεπτομερειακά. Χρησιμοποιώντας έναν μεταβολικό υπολογισμό με δεσμούς κατασκευάζεται το δυναμικό αλληλεπίδρασης μεταξύ δύο δινών.

Αποδεικνύεται αναλυτικά ότι οι δίνες παρουσιάζουν "συμπεριφορά Hall", δηλαδή ότι μία δίνη κάτω από την επίδραση μιάς εξωτερικής δύναμης κινείται κάθετα στην εφαρμοζόμενη δύναμη. Η κίνηση των δινών κάτω από την δράση διαφόρων εξωτερικών αιτίων διερευνάται με την βοήθεια αριθμητικών προσομοιώσεων. Δείχνεται πως ένα ζεύγος δινών περιστρέφεται γύρω από το κέντρο μάζας του, ενώ μία δίνη και μία αντι-δίνη κινούνται σε ευθείες παράλληλες τροχιές. Υπό την επίδραση ενός ομογενούς εξωτερικού ρεύματος η δίνη κινείται σε κατεύθυνση αντίθετη στο ρεύμα. Οι ταχύτητες των δινών στις παραπάνω περιπτώσεις βρίσκονται σε εξαιρετική συμφωνία με τις θεωρητικές προβλέψεις.

Contents

CHAPTER I
Introduction

Solitons

Linear equations combine a number of good properties which make their study feasible and tractable. Due to their simplicity, an extensive study of linear systems has been carried out and numerous mathematical tools and techniques have been developed to cope with them. Yet linear equations are far too simple to describe realistic systems and only nonlinear equations can account for the complicated behaviour we observe in nature. In fact nonlinearity emerges in all the fields of scientific study.

A particularly interesting class of nonlinear equations is those which possess so called 'soliton' solutions. Roughly speaking solitons are solutions of non-linear equations which have finite energy with a localized, non-dispersive energy density. The term soliton is used with a variety of connotations in the natural sciences. To the mathematician the term is usually reserved for particle-like kink, pulse or envelope excitations appearing in totally integrable Hamiltonian systems. These are extremely rare and are associated with equally special properties. Real physics is never concerned with such strict soliton systems. Many of the physically important soliton characteristics like for example the existence of stable particle-like excitations do not impose any constraints to their dynamical behaviour, while in the rigorous mathematical definition of solitons, the elastic collision between a pair of them is a fundamental property. Physicists in particle and

condensed matter physics, use 'soliton' to describe a wide variety of stable, finite-energy particle-like field patterns in various dimensions which retain some central physical nonlinear properties but few of the precise mathematical ones.

Theoretical studies show that phenomena such as water waves, light pulses in optical fibres, magnetic-flux quanta in superconducting devices and coherent excitations of biomolecules can be solitons. Computer simulations show that solitons can form in the presence of such realistic features as frictional loss mechanisms, external driving forces and thermal fluctuations. The solitons will exist under these circumstances for sufficiently long to be important features of the corresponding physical systems. A typical example in condensed matter physics where soliton notion applies, is the formation of magnetic flux lines in high T_c superconductors, where flux lines contribute significantly to thermodynamic and transport properties of these systems.

Superconductivity

In sufficiently low temperatures there are many metals and alloys which conduct electricity without any resistance. This phenomenon first discovered by Onnes in 1911 [1] is called superconductivity and the materials which exhibit such behaviour are called superconductors. It was soon understood that the classical treatment of the phenomenon of superconductivity was insufficient. Apart from the currents formed in superconducting materials (supercurrents), the only other currents which flow without dissipation are the orbiting electrons in atomic and molecular systems. By analogy supercurrents must be quantum currents and superconductivity a macroscopic quantum effect.

The theoretical explanation, of the phenomenon of superconductivity puzzled physicists for many decades. Since Onnes discovery, several phenomenological models have been proposed [2] to account for the thermodynamical and the electrodynamical properties of superconductors. However a thorough comprehension of superconductivity was only achieved with the formulation of the microscopic theory, developed by Bardeen, Cooper and Schrieffer [3] generally referred as BCS theory. The essential qualitative fea-

ture of the BCS theory is that superconductivity results from an attractive interaction between electrons mediated by phonons. The effect of the interaction on two isolated electrons is to bind them to an entity called a Cooper pair [4], in which the centre of mass momentum is zero and the electrons have opposite spin. Electrons which form Cooper pairs are responsible for the supercurrents and are known to be in the "superconducting state" to distinguish them from those which remain in the "normal state" i.e. those which are free fermionic states and contribute to dissipative currents.

A large class of superconducting phenomena is well described by a set of phenomenological equations proposed by Ginzburg and Landau [5]. The theory, usually referred as GL theory, was actually preceded the microscopic theory and in fact soon after the formulation of BCS theory it was shown that in certain domains of temperature and magnetic field the GL equations are a rigorous consequence of the microscopic theory [6]. The theory was based on the pioneering work of Landau [7] on second order phase transitions. He made the important observation that such a transition is associated with an abrupt change in the symmetry of the system, and that the system of lower energy can be characterized by a parameter which is the measure of its departure from the configuration in the more symmetric phase. To extend Landau theory of phase transitions to superconductivity, G-L introduced a quantity to characterize the degree of superconductivity at various points in the material, a quantity called the order "parameter" and denoted $\Psi(\mathbf{r})$. The order parameter was defined so as to be zero for a normal region and unity for a full superconducting region. Rather to allow for supercurrent flow, $\Psi(\mathbf{r})$ was taken as a complex function and interpreted as analogous to a "wave function" for the superconductivity. Due to their simple form, GL equations are widely in use in systems where they are known to be valid, and form the theoretical basis for a large variety of phenomena.

Encouraged by the wide region of validity of the GL equations, several attempts to derive a generalized GL theory for time dependent phenomena (TDGL), have been made during the past three decades, TDGL equations were formulated either departing from the microscopic theory [8], [9], [10] or by introducing phenomenological extensions of the GL theory [11], [12]. Of

particular interest to the work presented hear is the formulation of Feynman [11]. Noting that the energy density in G-L theory looks like that of a non-linear Schroedinger theory, Feynman naturally assumed that he could extended this analogy to the time dependent theory. Despite the numerous time-dependent models, none of them has succeeded to be established as the standard dynamical extension of the G-L theory.

Magnetic Flux Lines

The fundamental macroscopic property of a superconductor is the displacement away from it of a magnetic field (the Meissner effect [13]). If a normal metal is cooled below its superconducting transition temperature the magnetic flux is abruptly expelled. Thus the transition when it occurs in a magnetic field, is accompanied by the appearance of whatever surface currents are required to cancel the magnetic field in the interior of the specimen. This effect distinguishes a superconductor from a perfect conductor.

The exclusion of magnetic field is correct provided that the magnetic field is not too strong. As a magnetic field is turned on, a certain amount of energy is expended to establish the magnetic field of the screening currents that cancels the field in the interior of the superconductor. If the applied field is large enough it becomes energetically favourable for the specimen to revert back to the normal state, allowing the field to penetrate. The manner in which penetration occurs with increasing field strength classifies the superconducting materials in two different types.

Type I Below a critical field $H_c(T)$, there is no penetration of flux; when the applied field exceeds $H_c(T)$ the entire specimen reverts to the normal state and the field penetrates perfectly.

Type II Below a critical field $H_{c1}(T)$ the magnetic flux is totally excluded. When the applied field exceeds an upper critical value $H_{c2}(T) > H_{c1}(T)$, normal state is restored completely. For intermediate values of the applied field there is a partial penetration of flux, and the sample develops a rather complicated microscopic structure of both normal and superconducting regions known as the mixed state.

It is nowadays well established by a wealth of experimental evidence

[14] that in the mixed state of type II superconductors, the magnetic field partially penetrates the sample in the form of thin filaments (often called vortices) of flux. Within each filament the field is high, and the material is not superconducting. Outside of the core of the filaments, the material remains superconducting and the field decays exponentially. Furthermore the magnetic flux of the vortices is quantized. Each vortex carries a quantum of flux[15] [16] equal to $\frac{\hbar}{2e} = 2.07 \times 10^{-7}$ gauss cm^2.

The study of the dynamics of flux-vortices in ordinary or high$-T_C$ superconducting films under the influence of a variety of external probes and in various conditions of temperature, has been an area of vigorous experimental as well as theoretical research during the past few decades. The interest stems from the fact that thermodynamic and transport properties of these systems are affected by the soliton contributions. The models used in the literature range from phenomenological ones based on an hydrodynamic description [17], [18], [19], to time dependent extensions of GL equations either relativistic [12] or non-relativistic [9], [20]. One issue that has not been settled yet is the question of the origin of the so-called Magnus force which acts on a flux- vortex. A lot of effort based on the microscopic theory has been devoted to this issue [9], [10], [21], [22], but no consensus has achieved yet.

The interest on vortex dynamics was recently renewed, after it was experimentally observed [23]-[26] that the Hall voltage changes sign in the superconducting mixed state. This inverse of the sign is attributed to the motion of vortices in a direction opposite to the applied current. Such a behaviour is not expected within the standard models of vortex motion in superconductors and considerable effort has been done to theoretically understand this phenomenon [9], [19], [20].

In this work we will we be concerned with the study of the physics of vortices within the framework of a field theoretical model which was introduced in reference [27] and studied extensively in subsequent works [28], [29]. The motivation for carrying this study is twofold:

1) Mathematically is an interesting system possessing topological solitons which exhibit unusual dynamical behaviour.
2) The model is relevant to the theoretical treatment of several physical systems like plasma and superconductivity.
In particular the model offers a natural explanation for the origin of the Magnus force, and succeeds to predict the anomalous sign Hall effect. It is thus believed that the model might prove reasonable starting point for the understanding of the dynamics of an isolated Abrikosov vortex in thin superconducting films.

This thesis is laid out as follows. In chapter II we introduce the model, we analyze its topological properties and we show that it supports the existence of stable flux-vortices. Small oscillation analysis around the trivial vacuum is performed, to obtain an energy gap in the excitation spectrum of the system. In the following chapter we study in full detail the static properties of the isolated flux vortices. Also the vortex-pair system is studied and the interaction potential of two single vortices is obtained numerically. Chapter IV, deals with the canonical structure of the model. A direct link between the dynamical behaviour of the vortices and the topological features of the model is established. We also demonstrate the analogy of vortexs dynamics to the Hall motion and we obtain analytical predictions concerning the motion of the vortices. Finally in chapter V we describe in detail numerical simulations of the motion of a vortex pair as well as of a vortex-antivortex system. Furthermore we present numerical results which show that an isolated vortex under the influence of an external current moves in a direction opposite to the external current.

CHAPTER II
The Model

2.1 Introduction

When the electrons in a superconductor form a Cooper pair, the total spin of the pair is integer and thus Cooper pairs obey Bose statistics. According to Bose statistics, in sufficient low temperatures the single particle quantum state with lowest energy is occupied by a macroscopically large number of particles. This is the phenomenon known as the Bose-Einstein condensation, and the particles in the lowest level comprising what is called the *condensate.* When the electrons in a superconductor form a Cooper pair, the total spin of the pair is integer and thus Cooper pairs obey Bose statistics. It is generally believed that below the transition temperature T_c the Cooper pairs undergo an analogous condensation. The dynamics of the Cooper condensate might be handled in a similar manner to that of a superfluid one. The only difference is that the condensate is charged , i.e. it describes a charged quantum fluid.

We introduce a phenomenological effective model to study the physics of charged quantum fluids, emphasizing the issue of vortex dynamics within this model. The model combines features of the successful G-L theory for the static properties of superconductors and of the dynamical Gross-Pitaevskii [7] model for neutral quantum fluids, into a non-linear Schroedinger type

equation. The model is the most general one can write down in terms of the condensate wave function ψ, minimally coupled to electromagnetism. The equation of motion for ψ is taken to be of first order in time derivatives, and since the physical system does not have any kind of relativistic invariance the pure electromagnetic part is taken as an arbitrary positive definite combination of $\mathbf{E}^2$ and $\mathbf{B}^2$. To make contact with the G-L theory a quartic Mexican hat type potential is introduced. Also the condensate realizes a uniform positively charged background due to the ions which are taken to be rest. The role of the ions is to form the condensate but after that their role can be ignored, so that the effective theory does not contain these degrees of freedom. The only symmetries of the model are the electromagnetic U(1) gauge invariance together with the rotational and translational symmetry in time and in the two spatial dimensions. The ion lattice breaks spontaneously the Galilean invariance of the original fundamental model by the definition of a preferred reference frame.

The model - with the arbitrary coupling constants of the electromagnetic part equal to one - was first proposed in reference [27], but in a sense it had been already introduced by Feynman [11] without the phenomenological potential term for Ψ. Several other authors have considered similar systems [31], [33] while an attempt to derive the model from first principles was reported [10] recently.

In section II we introduce the model. Since the bulk of our results refer to configurations independent of the third spatial coordinate we formulate it directly in two space dimensions. In the following section III we derive the main analytical results about the properties of the vacuum sector of the model. In section IV we briefly report some results from homotopy theory, which we subsequently apply in our model (section V) to show that it supports topologically stable vortex solutions.

2.2 General Features

We will be dealing with a non-relativistic complex scalar field Ψ (the condensate) minimally coupled with coupling q to the electromagnetic potential

(A_0, A_i). To make the model physically sensible and mathematically consistent it is necessary to introduce a background (positive-ion) charge density to neutralize the system. For simplicity we take it to be constant and homogeneous throughout. Since the system at hand is not Lorentz or Galilean invariant, the pure Maxwell part of the model is modified accordingly to allow for two arbitrary parameters in front of the terms E^2 and B^2. We concentrate on the physics of infinitely long straight vortices i.e. on field configurations uniform along the third spatial direction and define the model directly in two space dimensions by the lagrangian

$$\mathcal{L} = \frac{i\gamma}{2}[\Psi^* \mathcal{D}_t \Psi - c.c.] + \gamma q \Psi_0^2 A_0 - \frac{\gamma^2}{2m}|\mathcal{D}_i \Psi|^2 + \frac{1}{8\pi}(\epsilon \mathbf{E}^2 - \mu B^2) - V(|\Psi|) \tag{2.2.1}$$

with $\mathcal{D}_t\Psi = (\partial_t + iqA_0)\Psi$, $\mathcal{D}_i\Psi = (\partial_i - i\frac{q}{c}A_i)\Psi$, $B = \epsilon_{ij}\partial_i A_j$, and $E_i = -\frac{1}{c}\partial_t A_i - \partial_i A_0$. γ, m, q, ϵ and μ are parameters, c is the speed of light and the spatial indices i, j range from 1 to 2. As it will become clear, although the specific form of the potential V changes the details of the profile of the vortex solutions, it does not affect their dynamical behaviour. For the discussion of vortex dynamics V could even be absent but in order to make contact with a variety of models of physical interest we will allow for a mexican hat phenomenological potential

$$V(|\Psi|) = \frac{1}{8}\, g\, (\Psi\Psi^* - \Psi_0^2)^2 \tag{2.2.2}$$

with quartic self-coupling g . Rescale fields and coordinates according to

$$x_i \to \frac{\sqrt{\mu m}\, c}{\sqrt{4\pi}\Psi_0 q\gamma}\, x_i \qquad t \to \frac{\mu m^2 c^2}{4\pi \Psi_0^2 q^2 \gamma^3}\, t$$

$$\Psi \to \Psi_0 \Psi \qquad A_0 \to \frac{4\pi \Psi_0^2 q \gamma^3}{\mu m^2 c^2}\, A_0 \qquad A_i \to \frac{\sqrt{4\pi}\Psi_0 \gamma}{\sqrt{\mu m}}\, A_i \tag{2.2.3}$$

to obtain, in terms of the dimensionless quantities t, x_i, Ψ, A_0 and A_i used from now-on, the lagrangian

$$\mathcal{L} = \frac{1}{2}(\Psi^*(i\partial_t - A_0)\Psi + c.c.) + A_0 - \frac{1}{2}|D_i\Psi|^2$$
$$+ \frac{1}{2}(\frac{1}{\beta}\mathbf{E}^2 - B^2) - \frac{1}{8}\kappa^2(\Psi\Psi^* - 1)^2 \qquad (2.2.4)$$

with $B = \epsilon_{ij}\partial_i A_j$, $E_i = -\partial_t A_i - \partial_i A_0$ and $D_i = \partial_i - iA_i$. We keep the same symbols to simplify our notation.

Classically the model depends on the two free dimensionless parameters κ and β defined by

$$\kappa^2 = \frac{g\mu\, m^2c^2}{4\pi q^2\gamma^4} \qquad \beta = \frac{\mu^2 m^3 c^4}{4\pi\,\epsilon\, q^2\gamma^4\ \Psi_0^2} \qquad (2.2.5)$$

An overall factor ${g\Psi_0}^4/\kappa^2$ was dropped from $\mathcal{L}$ since it does not enter the equations of motion. It plays though the role of $1/\hbar$ in the quantum theory and determines the necessary condition for the validity of our semiclassical approximation

$$\frac{\kappa^2}{g{\Psi_0}^4} \to 0 \qquad (2.2.6)$$

In this limit we expect the quantum solitons to resemble closely their classical ascendants studied below.

The equations of motion on the other hand read

$$i\dot{\Psi} = -\frac{1}{2}\mathbf{D}^2\Psi + A_0\Psi + \frac{1}{4}\kappa^2(\Psi^*\Psi - 1)\Psi$$
$$\frac{1}{\beta}\dot{E}_i = \epsilon_{ij}\partial_j B - J_i \qquad (2.2.7)$$

The Gauss constraint and the remaining Maxwell identity

$$\frac{1}{\beta}\,\partial_i E_i = \rho \qquad \dot{B} = -\epsilon_{ij}\partial_i E_j \qquad (2.2.8)$$

complete the set of field equations of the model. The charge and current densities ρ and J_i respectively, are given by

$$\rho = \Psi^*\Psi - 1 \qquad J_i = \frac{1}{2i}[\Psi^* D_i\Psi - (D_i\Psi)^*\Psi] \qquad (2.2.9)$$

The Lagrangian 2.2.4 is invariant under the local (gauge) transformations,

$$\begin{aligned} \Psi' &= exp(\imath\Lambda(\mathbf{x},t))\Psi \\ A_i{}' &= A_i + \partial_i\Lambda \\ A_0{}' &= A_0 - \partial_t\Lambda \end{aligned} \tag{2.2.10}$$

where $\Lambda(\mathbf{x},t)$ is an arbitrary function of space and time, It is easy to check that under the set of transformations 2.2.10, a total differential is added in the Lagrangian 2.2.4 which has no effect in the equations of motion.

2.3 The Energy Spectrum

Equations 2.2.8 and 2.2.7 admit the one parameter family of trivial vacuum solutions

$$\Psi = exp(i\alpha) \qquad A_i = 0 \qquad A_0 = 0 \tag{2.3.1}$$

for arbitrary constant value of α.

We perform small oscillations analysis around a trivial vacuum to derive the energy spectrum of the model. To proceed analytically one has first to eliminate the degeneracy of the vacuua. Since α in 2.3.1 is arbitrary and constant, we define the vacuum by setting its value equal to zero or equivalently setting $\Psi = 1$. It is then convenient to use the following parameterization for Ψ:

$$\Psi = (1+\Phi)e^{i\Theta} \tag{2.3.2}$$

The gauge freedom is eliminated by imposing the gauge fixing condition $\nabla\mathbf{A} = 0$. The Lagrangian 2.2.4 is rewritten keeping only up to quadratic terms in the fields.

$$\mathcal{L} = -\partial_t\Theta(1+2\Phi) - 2\Phi A_0 - \frac{1}{2}(\partial_i\Theta^2 + \partial_i\Phi^2 + A_i^2) \tag{2.3.3}$$

$$+\tfrac{1}{2\beta}(\partial_i A_0^2+\partial_t A_i^2)-\tfrac{1}{2}B^2-\tfrac{1}{2}\kappa^2\Phi^2$$

The equations of motion read

$$\partial_t\Phi+\partial_i^2\Theta \;=\; 0 \tag{2.3.4}$$

$$\partial_t\Theta \;=\; \frac{1}{2}\partial_i^2\Phi-A_0-\frac{1}{2}\kappa^2\Phi \tag{2.3.5}$$

$$\frac{1}{\beta}\partial_i^2 A_0+2\Phi \;=\; 0 \tag{2.3.6}$$

$$\frac{1}{\beta}\partial_t^2 A_i \;=\; \partial_k^2 A_i-A_i \tag{2.3.7}$$

We take the Laplacian at eqs. 2.3.5 and the time derivative of 2.3.4 and we combine them with 2.3.6 to eliminate Θ and A_0. Finally we obtain the equation

$$\partial_t^2\Phi \;=\; \frac{1}{4}\kappa^2\partial_i^2\Phi-\beta\Phi-\frac{1}{4}\partial_i^4\Phi \tag{2.3.8}$$

By substituting $A_i = A_i^0\; e^{i(\omega t-\mathbf{kx})}$ and $\Phi = \Phi^0\; e^{i(\omega t-\mathbf{kx})}$ at 2.3.7, 2.3.8 we obtain the following dispersion relations

$$\omega^2 \;=\; \beta+\frac{1}{4}\kappa^2|\mathbf{k}|^2+\frac{1}{4}|\mathbf{k}|^4 \tag{2.3.9}$$

$$\omega^2 \;=\; \beta(|\mathbf{k}|^2+1) \tag{2.3.10}$$

As it follows from 2.3.10 the system has a mass gap, since ω does not disappear at $|\mathbf{k}| = 0$. In particular for $|\mathbf{k}| = 0$, $\omega^2 = \beta$ and the energy gap of the model is given by the relation $G = \beta^{\frac{1}{2}}$.

2.4 Topology and Homotopy Theory

The analytical treatment of the equations of motion 2.2.7 derived in the previous section, turns out to be a very difficult task. This is a generic feature of non-linear classical field theories in more than one spatial dimension. For a typical system of this sort no systematic method of obtaining even a single non-trivial classical solution in analytic form is available as yet. To study such systems, one has to implement indirect methods.

A powerful tool which enables us to handle analytically a class of non-linear field theoretical systems is the mathematical branch of topology. The main consequence of topology when dealing with such topologically non-trivial systems, is that enables us to classify the solutions of the corresponding equations according to a certain mapping that divides the space of solutions into many distinct subspaces. This classification in turn, enables us in some cases, to construct exact non-trivial solutions. Of particular interest is a class of solutions called "topological solitons". Topological solitons are stable localized finite energy solutions of non linear field theories in 1, 2, and 3 spatial dimensions, which owe their stability to general topological properties of the corresponding theory. They have been a subject of intense study in field theory over the last twenty five years, mainly because they apply in a variety of physical problems. Among the best known examples [34] are domain walls and magnetic bubbles in a ferromagnetic continuum, vortices in HeII or in superconductor, topological defects in liquid crystals, as well as skyrmions and monopoles which are particle-like solutions in generic models of high energy physics.

The common feature of topologically non-trivial field theories is that the space of non singular finite energy solutions can be divided to subspaces - usually called topological sectors - which are disconnected in the normal topological sense: it is not possible to continuously deform a solution in one component into a solution in another one. Since the time evolution is continuous this implies that if a solution is in one component at any one time, then it is in the same component at all times. In other words the transition from one sector to another is forbidden [35].

An integer number can be associated with each sector, called topological

index or topological charge. Topological charge is then a conserved quantity. Conservation of topological charge has a different origin than the well known Noether conservation charges. In the latter case the conserved quantities are a result of the existence of a continuous symmetry of the Lagrangian, while in the former case they are a consequence of the fact that the space of non singular solutions is not-connected.

In most of the cases it is easy to carry out the relevant analysis, and determine the topological properties of the corresponding systems. For instance, consider a Lagrangian for a scalar field Φ in n-dimensions (spatial), and a degenerate potential $V(\Phi)$. Denote by M the space which corresponds to the minima of the potential. Then denote by X the space which corresponds to spatial infinity. The condition that a solution to the equation of motion is of finite energy implies that the asymptotic values of $\Phi(\vec{r})$ must be zeros of $V(\Phi)$ i.e.

$$lim\ \Phi(\vec{r}) \rightarrow \Phi_0, \qquad as \quad |\vec{r}| \rightarrow \infty \tag{2.4.1}$$

This condition can be considered as a mapping from X into M. From topology theory we know that mappings from one space to another can be classified into homotopy sectors. Mappings within one sector can be continuously deformed into each other, whereas mappings from two different sectors cannot be continuously so deformed. Thus if we have a particular solution then it is its behaviour at infinity, that classifies it to a certain homotopy sector, and the solution has to remain in this sector independently of its time evolution. As a result, the stability of a soliton-like solution, against decaying to a state in a different sector, is assured.

Furthermore, some general results are available in mathematical literature which enable us to determine whether a field theory is topologically non-trivial. These can be stated in the following form[34]:

$$\pi_n(S_n) = Z, \tag{2.4.2}$$

$$\pi_n(S_m) = 0 \qquad \text{for} \qquad n < m, \tag{2.4.3}$$

$$\pi_n(S_1) = 0 \qquad \text{for} \qquad n > 1, \tag{2.4.4}$$

where $\pi_n(S_m)$ refers to the homotopy group of mappings of S_n into S_m and Z refers to the group of integers. The zero on the right hand side of 2.4.3, 2.4.4 implies that the group is trivial i.e. that in these cases all mappings can be deformed into one another.

Although in the previous example the classification was a consequence of the behaviour of the fields in the spatial infinity, this is not always the case. For instance in the non-linear O(3) model the homotopy classification arises from the behaviour of the fields throughout the space.

To summarize, implementation of topology and homotopy theory enables us to establish the existence of localized, finite energy solutions even in cases where an analytical treatment is extremely difficult. We end the section with a final remark: Non trivial topology is a sufficient condition but not a necessary one. As it is stated in [36], [37], it is possible to have soliton like solutions even in a topologically trivial field theory.

2.5 Flux Quantization

We now focus to the homotopy classification of finite-energy configurations in our model. The energy of our system is the sum of four positive terms $W = W_d + W_b + W_e + W_v$ with

$$W_d = \frac{1}{2}\int d^2x |D_i\Psi|^2 \qquad W_b = \frac{1}{2}\int d^2x\, B^2$$

$$W_e = \frac{1}{2\beta}\int d^2x\, \mathbf{E}^2 \qquad W_v = \frac{1}{8}\kappa^2 \int d^2x\, (\Psi\Psi^* - 1)^2 \tag{2.5.1}$$

For W_v to be finite $|\Psi(\mathbf{x})|$ must tend to the minimum of the potential i.e. to 1, as $|\mathbf{x}|$ tends to infinity. Note that in contrast to relativistic models [12],[38], where the potential term is introduced in order to impose that particular boundary condition for $|\Psi|$ at infinity, here it could be absent since finiteness of W_e already implies that behaviour. More specifically any configuration with W_e finite, has to be neutral. A localized configuration

with non-zero net electric charge leads to an electric field behaving like $1/r$ at large distances and this makes W_e diverge. This neutrality requirement translates into a boundary condition for $|\Psi|$ at infinity. In fact $|\Psi|$ must tend to one, since otherwise it will lead to infinite charge at large distances. It is possible of course to interpolate to a neutral singular configuration but only at an infinite energy cost. One could in principle contemplate a logarithmically divergent energy due to a non-zero finite charge but it is impossible to allow for an asymptotic value of $|\Psi|$ different from one. Furthermore as it is demonstrated in the next chapter even without V the field equations do support the existence of non-trivial soliton solutions. We thus have to impose the conditions

$$Q = \int d^2x \; \rho = 0 \tag{2.5.2}$$

and

$$|\Psi(\mathbf{x})| \to 1 \quad and \quad |D_i\Psi| \to 0 \quad as \quad |\mathbf{x}| \to \infty \tag{2.5.3}$$

The phase of the complex field is not fixed by these boundary conditions at infinity. The field Ψ approaches the value $e^{i\alpha}$ where the phase angles α form points in a circle S_1. Since in $2+1$ dimensions, the spatial boundary is also S_1 the finite-energy field configurations are classified according to the first homotopy group of S_1 into disjoint topological sectors characterized by an integer topological index (or "charge") N. Actually N describes the number of times the phase α is wound around the circle at spatial infinity and is also called winding number. Furthermore winding number has to be integer in order for Ψ to be continuous.

Let (r, ϕ) parameterize the space; then at $r = \infty$

$$N = \frac{1}{2\pi} \int_0^{2\pi} \frac{d\alpha}{d\phi} \, d\phi \tag{2.5.4}$$

But the condition 2.5.3 tells us that as $|\mathbf{x}| = r' \to \infty$

$$A_i \to -i \frac{\delta_i \Psi}{\Psi} \tag{2.5.5}$$

Hence A_ϕ, the tangential component at $r \to \infty$ becomes

$$A_\phi = \frac{1}{r}\frac{d\alpha}{d\phi} \tag{2.5.6}$$

Hence

$$N = \frac{1}{2\pi}\int_0^{2\pi} A_\phi\, r\, d\phi = \frac{1}{2\pi}\oint \mathbf{A}\, d\mathbf{l} = \frac{1}{2\pi}\int_S d^2x\, B \tag{2.5.7}$$

Thus we see that the magnetic flux is quantized within our model, in accord with Ginzburg-Landau theory as well as the experimentally observed flux quantization in superconductivity. It may seems surprising that magnetic flux quantization is obtained purely from classical considerations. But as Coleman [35] has pointed out equation 2.5.7 is not exactly the flux-quantization condition in superconductivity. In equation 2.5.7 the quantum flux is a constant depending on the parameters which initially appeared in the classical Lagrangian 2.2.1 and which are arbitrary. It is only in the quantum level, where these parameters will so be related to physical constants, as to yield the full flux quantization condition.

From equation 2.5.7 follows that N can be expressed as the volume integral of a topological density defined as $\tau_1 = \frac{B}{2\pi}$

$$N = \frac{1}{2\pi}\int d^2x\; B$$

Equivalently one can use an expression for topological density depending on Ψ

$$N = \frac{1}{2\pi i}\int d^2x\; \epsilon_{kl}\partial_k\Psi^*\partial_l\Psi \tag{2.5.8}$$

or the manifestly gauge invariant formula

$$N = \frac{1}{2\pi i}\int d^2x\,\tau, \qquad \tau = \frac{1}{2\pi i}[\epsilon_{kl}(D_k\Psi)^*(D_l\Psi) - iB(\Psi^*\Psi - 1)] \tag{2.5.9}$$

which as it is shown later can be directly associated with other physical properties of the system.

CHAPTER III
Static Properties of the Vortices

3.1 Isolated Vortices

3.1.1 The Ansatz

In the previous chapter, it is shown that due to general topological arguments, soliton solutions in our model are in principle possible. Aside from these general existence arguments, we would like to find explicit solutions in any given non-trivial topological sector. We will particularly concentrate on the search of static axially symmetric solutions of the field equations. The most general ansatz for such a configuration with topological charge N is in polar coordinates (r, ϕ) given by

$$\Psi(\mathbf{x}) = X(r)\, e^{iN\phi} \qquad A_0(\mathbf{x}) = f(r) \qquad \mathbf{A}(\mathbf{x}) = \frac{N}{r}(1-\alpha(r))\hat{\phi} \tag{3.1.1}$$

At infinity 2.5.3 implies the boundary conditions

$$X(r) \to 1 \qquad \alpha(r) \to 0 \tag{3.1.2}$$

The field configuration described by the above ansatz, is localized, of finite energy and carries magnetic flux. It is clear that by adding a third dimension on which the fields have no dependence, this configuration is equivalent to

a magnetic flux tube, which often called vortex line. Within the ansatz the electric and the magnetic fields are

$$\mathbf{E} = -f' \hat{r} \qquad B = -\frac{N\alpha'}{r} \tag{3.1.3}$$

while the electric charge and current densities take the form

$$\rho = X^2 - 1 \qquad \mathbf{J} = \frac{N}{r}\alpha X^2 \hat{\phi} \tag{3.1.4}$$

Finally the field equations reduce to the following set of ordinary nonlinear differential equations

$$X'' + \frac{1}{r}X' - \frac{N^2}{r^2}X\alpha^2 = \frac{1}{2}\kappa^2(X^2-1)X + 2fX \tag{3.1.5}$$

$$\frac{1}{\beta}\left(f'' + \frac{1}{r}f'\right) = -\rho \qquad \alpha'' - \frac{1}{r}\alpha' = \alpha X^2 \tag{3.1.6}$$

The behaviour of the solutions around the origin $r = 0$ is dictated by the requirement of smoothness and by the equations themselves to be

$$X(r) \to c_1\, r^{|N|} \qquad \alpha(r) \to 1 + c_2\, r^2 \qquad f(r) \to c_3 + \frac{1}{4}\beta\, r^2 \tag{3.1.7}$$

where c_1, c_2 and c_3 are undetermined constants.

Equations 3.1.5,3.1.6 though simpler than the parent equations, are not amenable to an analytic solution, but one can implement asymptotic analysis to show that the fields decay exponentially. To study the behaviour of the fields for large $r \gg 1$ we use the following ansatz :

$$\begin{aligned} f &\longrightarrow v_1\, r^v\, e^{-\omega} \\ X &\longrightarrow 1 + s_1\, r^s\, e^{-\sigma} \\ \alpha &\longrightarrow (t_1 + t_2\, r^{-1})\, r^t\, e^{-\tau} \end{aligned}$$

where $v, v_1, \omega, s, s_1, \sigma, t, t_1, t_2, \tau$, are undetermined constants of order one.

Substituting α, X in the right part of 3.1.6 and equating the coefficients of $r^t\, e^{-\tau}$ and $r^{t-1}\, e^{-\tau}$ we obtain : $\alpha \to t_1\, r^{1/2}\, e^{-r}$.

Substitution of the asymptotic form of f, X in the left part of 3.1.6 yields a relation between f and X. Specifically the following equations must hold : $\omega = \sigma$, $v = s$, and $v_1 = -\frac{2\beta s_1}{\sigma^2}$.

Determination of σ, and thus of the asymptotic behaviour of X is a more complicated problem. After the replacement of the asymptotic form of the fields, and keeping only the higher terms, equation 3.1.5 becomes :

$$(\sigma^2 - \kappa^2 + \frac{4\beta}{\sigma^2}) s_1 r^s e^{-\sigma} = N^2 t_1^2 r^{-1} e^{-2r} \qquad (3.1.8)$$

Note that we are not allowed to neglect the right part of the above equation unless σ is smaller than 2. Omission of a similar term in the Abelian-Higgs model has led to wrong formula for the asymptotic behaviour of the Higgs field [39]. To proceed further, we assume that $\sigma < 2$. Then the right part 3.1.8 is dropped and equation 3.1.8 yields

$$\sigma^4 - \sigma^2 \kappa^2 + 4\beta = 0 \implies \sigma^2 = \frac{\kappa^2 \pm \sqrt{\kappa^4 - 16\beta}}{2} \qquad (3.1.9)$$

An argument that prefers + sign than − in 3.1.9 comes from the relativistic Abelian-Higgs model [12]. In fact the equations for static vortices in that model are identical to equations 3.1.5, 3.1.6 when $\beta = 0$. In that case asymptotic behaviour for the Higgs field is given by 3.1.9 with $\beta = 0$ and retaining the + sign in front of the root. Thus we expect that + sign remains when β smoothly turns on. Apparently equation 3.1.9 has no real solution when $\kappa^4 < 16\beta$. Moreover it does not always yields a $\sigma < 2$. In either of those cases, our assumption on the value of σ has to be reconsidered. Assuming that $\sigma \geq 2$, equation 3.1.8 has to be resolved retaining all terms. Actually the fall-off of the matter field is determined by that particular term on the right hand side of 3.1.8, and turns out to be

$$X \longrightarrow 1 + s_1 r^{-1} e^{-2} \qquad (3.1.10)$$

where s_1 is related to t_1 by the equation $s_1 = (4 + \beta - \kappa^2)^{-1} t_1^2$

Asymptotic analysis leads us to the quite "paradoxical" result, that - at least in a certain region of the parameter space - the behaviour of the fields

at large r is independent of the parameters of the model. On the other hand one must bear in mind, that the asymptotic behaviour of the fields actually refers to very large r, where all the fields have already reached their vacuum values and thus it is of no physical consequence.

3.1.2 Variational Method

Being unable to solve analytically the equations at hand we proceeded numerically. After some experimentation we decided that among the various methods available the variational approach is the most convenient. The method is based on the fact that the field equations 2.2.7 and 2.2.8 for static solutions are identical to the conditions for the minimization of the energy functional 2.5.1 under the Gauss-law and charge neutrality constraints. This is true even after we insert into the energy functional the spherically symmetric ansatz 3.1.1 and leads in that case directly to equations 3.1.5, 3.1.6. We can thus use the variational method and minimize the energy in order to find approximate solutions of our equations.

We approximate the fields of the ansatz by a set of trial functions depending on some number of variational parameters. We then evaluate the energy as a function of these parameters and minimize the resulting expression. The position of the minimum in the parameter space determines the approximate solution, whose energy is the value of the energy functional at the minimum. The variational ansatz we used, compatible with the boundary conditions at large r is :

$$X(r) = 1 + e^{-kr} \sum_{l=0}^{m} z_l \frac{r^l}{l!} \qquad \alpha(r) = e^{-r} \sum_{l=0}^{m} \alpha_l \frac{r^l}{l!} \tag{3.1.11}$$

$$f'(r) = e^{-kr} \left[\frac{c_{-1}}{r} + \sum_{l=0}^{m} c_l \frac{r^l}{l!}\right] + e^{-2kr} \left[\frac{d_{-1}}{r} + \sum_{l=0}^{2m} d_l \frac{r^l}{l!}\right] \tag{3.1.12}$$

To determine the exponential fall-off of the gauge field we used information from asymptotic analysis. Strictly speaking the exponential decay of Ψ

should be determined in a similar way. Numerically though, it is more accurate to leave k as an independent variational parameter. The optimum value of k often deviates from what asymptotic analysis results. This is no contradiction. The variational ansatz is more effective when the exponential cutoff e^{-kr} is close to the rate of decay of the condensate, in the region where the value of Ψ is away from its vacuum value. And that rate is not in principle determined by the asymptotic form of the fields at large r. Yet one may insist on reproducing the exact asymptotic form of Ψ, but this frustrates the other variational parameters, which are forced to take unnaturally diverse values in order to lead to the right solution. This induces in general higher numerical errors.

Plugging the above expressions for X and f' into Gauss' constraint equation 3.1.6a we determine the coefficients c_{-1}, d_{-1}, c_i and d_i in terms of the z_i. The boundary conditions at the origin give $\alpha_0 = \alpha_1 = 1$, $z_0 = -1$ for the $N = 1$ vortex. For higher-N vortices one has more conditions due to the faster fall-off of X at $r = 0$. Thus, for the $N = 2$ vortex we obtain in addition to the above that $z_1 = -k$. Finally, the vanishing of the total electric charge eliminates one more of the unknown coefficients of the variational ansatz. In our computations as it will be explained below, we achieve satisfactory accuracy for $m = 10$, i.e. with 16 and 15 independent variational parameters for $N = 1$ and $N = 2$ respectively.

Having solved explicitly Gauss' constraint as well as the neutrality condition, we insert the variational ansatz into the energy functional, we compute analytically the spatial integrals to end-up with a polynomial of fourth order in the variational parameters. A quasi-Newton minimization procedure in then used to evaluate its minimum. The method converges fairly rapidly within four or five iterations despite of the large number of parameters. The physical nature of the problem and the proper choice of the variational ansatz which restricts the fields to the right subspace of the configuration space, are the two factors to which it is reasonable to attribute this rapid convergence.

Figure 3.1 shows the profiles of the $N = 1$ vortex solutions for two different sets of values of the parameters of the model. In figures 3.1a and 3.1b we plot the magnitude of the electric current J, the magnetic field B,

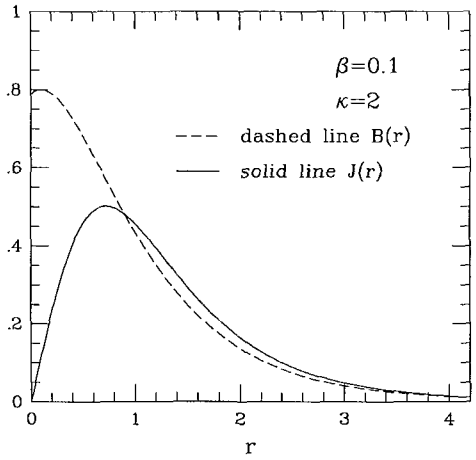

fig.1a

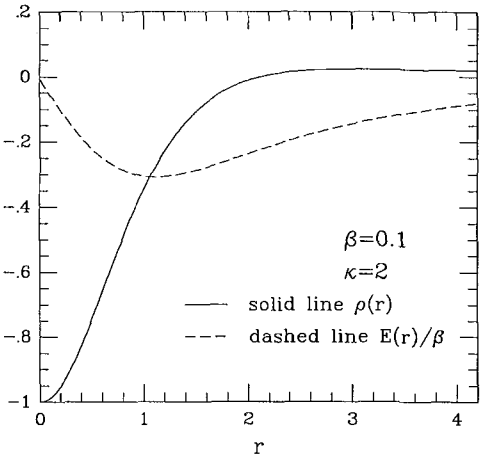

fig.1b

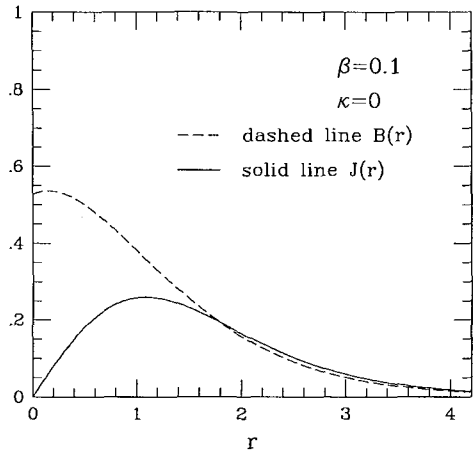

fig.1c

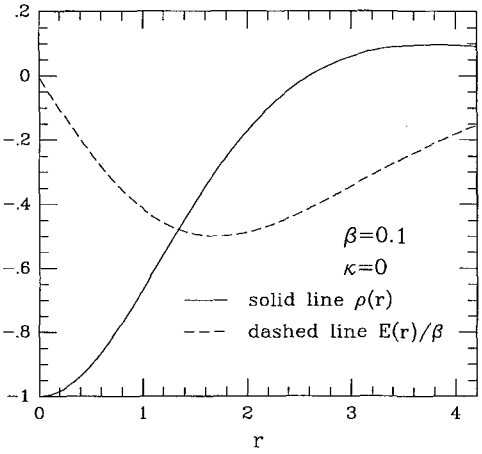

fig.1d

Figure 3.1 : $N = 1$ *vortex profiles. (1a) and (1b) correspond to* $\kappa = 2$ *and* $\beta = 0.1$, *while (1c) and (1d) to* $\kappa = 0$ *and* $\beta = 0.1$

the charge density ρ and the magnitude of the electric field E divided by β as functions of the radius r from the center of the vortex for $\beta = 0.1$ and $\kappa = 2$. Similarly, in figures 3.1c and 3.1d we have the same quantities but for $\beta = 0.1$ and $\kappa = 0$, the case with no quartic potential.

Before we proceed with further results a few comments about the accuracy of our numerical computations are in order. To obtain an estimate of the error induced by the truncation of the configuration space, we minimized the energy for various values of m in order to check the stability of our results against a broadening of the trial ansatz 3.1.11, 3.1.12. The energy at the minimum for $m = 10$ differed from the one for $m = 11$ in the sixth significant digit. Thus we conclude that our energy calculations are correct to within one part in 10^5 or so. To eliminate the danger that during a minimization process we were accidentally trapped in a local minimum, we repeated each run several times starting with different initial configurations. An additional test is provided by the accuracy with which we verify the virial relation

$$W_b = 2W_e + W_v \tag{3.1.13}$$

obtained by the well known scaling argument of Derrick [40]. We define

$$\Delta = \frac{2W_e + W_v - W_b}{W_b} \tag{3.1.14}$$

and check that in all our calculations Δ is smaller than 10^{-4}. Finally, the spherical symmetry of the ansatz provides another test of the accuracy of our results. Notice that the ansatz is spherically symmetric in the sense that a spatial rotation by some angle γ can be compensated by a global internal U(1) rotation by $N\gamma$. This means that the corresponding generator $Q - NL$ where L is the field angular momentum to be defined in the next chapter, must vanish for the solution. Q is zero by construction and we check, by explicit evaluation of the integral of the angular momentum density, that for all solutions L is also zero to within one part in 10^4.

Figure 3.2 shows the values of the ratio $R = E_{N=2}/2E_{N=1}$ of the energy of the double vortex to twice the energy of the single one, as well as the value of the energy of a single vortex itself divided by π for various sets of the parameters of the model. For $\beta = 0$ and for static configurations our model reduces to the Ginzburg-Landau equations for a superconductor

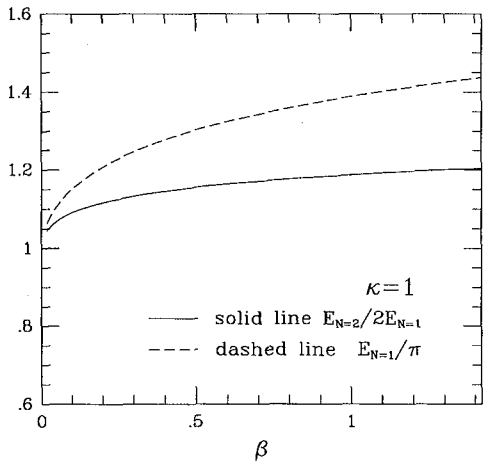

fig.2a

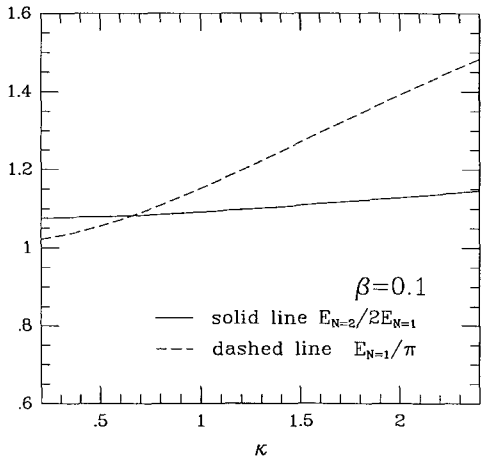

fig.2b

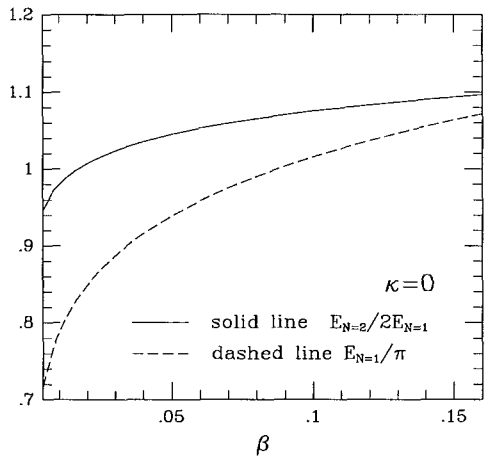

fig.2c

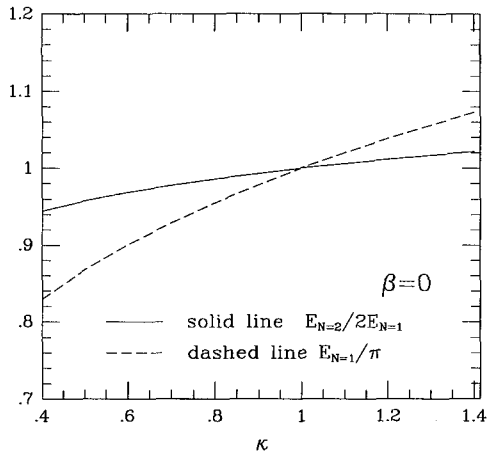

fig.2d

Figure 3.2 : *Plots of* $R = E_{N=2}/2E_{N=1}$ *and of* $E_{N=1}/\pi$ *as functions of* κ *or* β *for the values of the second parameter as shown. (2d) corresponds to the Ginzburg-Landau model, while (2c) to the no- potential case.*

and κ corresponds exactly to the ratio of the penetration depth to the coherence length defined there.

Figure 3.2d is in perfect agreement with the results obtained previously in the context of the Ginzburg-Landau theory [41] [12] [38]. We divided all energies by π to make easier contact with previous results concerning the Ginzburg-Landau theory, in which for $\kappa = 1$ the $N = n$ vortex solution has energy $E_n = n$. The fact that the energy of a vortex is an increasing function of the parameters κ and β is easily understood by the following argument: (we give the argument for κ). Start with the solution of the static equations for some value of the parameter κ and a given β which we keep fixed. By construction it satisfies Gauss' constraint and is neutral. It can thus be used as a trial initial configuration for the energy minimization for a different value $\kappa' < \kappa$. The energy $E(\kappa')$ of the solution for κ' is smaller than the value of the energy functional for the above configuration. The latter is equal to the energy of the solution for the value κ minus the positive quantity $(1/8)\,(\kappa^2 - \kappa'^2)\,\int d^2x\,(\Psi\Psi^* - 1)^2$, where Ψ is the solution for κ. Thus, $E(\kappa') < E(\kappa)$. Q.E.D. A similar argument with a little extra care due to Gauss' constraint applies to β.

The other extreme, the no-potential case $\kappa = 0$ is shown on figure 3.2c. The critical value of β for the $N = 2$ vortex to have the same energy with two well-separated single vortices is 0.0167.

The critical line separating the parameter space into regions-I and -II, according to the value of R being smaller or larger than one respectively, is shown on figure 3.3. Regions-I and -II correspond in the Ginzburg-Landau case to ordinary type-I and type-II superconductors.

single vortices far from each other. In contrast to the Ginzburg-Landau case there exists inside region-I another critical line separating the parameter space into two subregions according to whether $E(N = 3)$ is larger or smaller than 3 times $E(N = 1)$. Consistent with the well known facts about the Ginzburg-Landau model this line too passes through the point $(\kappa = 1, \beta = 0)$. The subregion with $E(N = 3) < 3E(N = 1)$ is further split into two subsubregions depending on the value of the ratio $E(N = 4)/4E(N = 1)$ being larger or smaller than one, and so on.

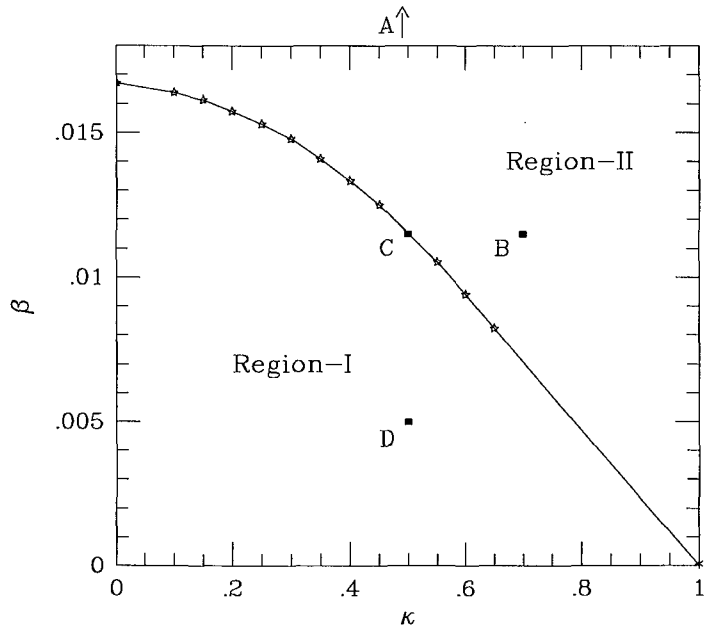

Figure 3.3 : *Regions-I and -II of the parameter space.*

It is interesting to compare the energy of a triple vortex to that of three single vortices far from each other. In contrast to the Ginzburg-Landau case there exists inside region-I another critical line separating the parameter space into two subregions according In the context of a relativistic model we would talk about stable and unstable higher-N vortices. For instance, a vortex with $N = 2$ and energy larger than twice the energy of a single one could not be absolutely stable against decay to two single vortices. In the model at hand though as we will see later a completely different picture arises [27].

3.2 Penetration depth and coherence length

In this section we study the dependence of the size of the $N = 1$ vortices on the variation of the two parameters of the model. In accordance to the case of the vortices in real superconductors, we introduce two characteristic

lengths ; the penetration length λ which is related to the decay rate of the magnetic field, and the coherence length ξ, which defines the characteristic distance for variations of Ψ.

It is easy to derive some general features as for example that ξ is a decreasing function of κ by simple inspection on the exact form of the energy functional 2.5.1. The potential term is proportional to κ^2, which as we mentioned earlier, forces Ψ to attain its vacuum expectation value (V.E.V.). Therefore when κ increases it becomes energetically more unfavourable to have $\Psi \neq 1$, and consequently Ψ attains its V.E.V. sooner. The same argument applies to β. Equation 2.5.1 implies that the electrostatic energy term W_e is proportional to the inverse value of β. At the same time because of Gauss law 2.2.8, the strength of the electric field is linear to β. The latter results a linear dependence of W_e on β. Given that the presence of the electrostatic term also forces Ψ to relax to its V.E.V. we conclude that the variation of β has a similar effect to that of κ. Regarding the region where $\Psi \neq 1$ as a measure of the coherence length, the previous considerations justify our initial assertion.

At that point we would like to dissociate the size of the fields from their asymptotic behaviour derived in the previous section. Physically the size of a field is related to the distance where the field varies from its vacuum value significantly. While in many cases that distance is similar to the rate of decay of the field at large r, this is not a general rule. Consider for example the asymptotic behaviour of the condensate as that arises from the analysis of the previous section. According to equation 3.1.10 for $\kappa \geq 2$ and $\beta = 0$ the asymptotic form of Ψ is independent of κ. If we now try to associate the coherence length with the asymptotic behaviour of Ψ, we end up with a result which contradicts our earlier statement that ξ is a decreasing function of κ.

Apart from those general remarks, in order to obtain solid results we have to resort to numerical methods. We use the same minimization technique which described earlier to construct the vortex solutions for various values of the parameters and we then evaluate their size. To determine the characteristic lengths of the fields we adopt the following definition for "length" : The length of each field is associated to the square root of the

normalized second moment of the energy density. More precisely it is used that part of the energy density which is related to each field. For example, the penetration length is evaluated by the formula :

$$\lambda = \frac{1}{W_b} \int d^2x \, \mathbf{x^2} \, w_b \tag{3.2.1}$$

A similar formula is used for the evaluation of the coherence length, where W_b and w_b are substituted by $(W_e + W_v)$ and $(w_e + w_v)$ respectively.

Since the potential term and the electrostatic term have a similar effect on the size of the vortex, we consider it more convenient to isolate each term and study their effect separately. We first examine the case where there is no potential, i.e. κ is fixed to zero while β varies. Our starting point is the evaluation λ and ξ for two widely different values of β ; $i) \beta = 1$ and $ii)$ $\beta = 10^6$. The corresponding numerical results are $\lambda = 0.96$, $\xi = 0.76$ and $\lambda = 0.62$, $\xi = 0.026$ respectively. Note that while ξ undergoes a significant change, λ is quite insensitive to the value of ξ. We could contemplate partly on that result in the sense that given the values of ξ, it is easy to predict the behaviour of λ. After Ψ has attained its vacuum value (i.e. $r \geq \xi$), the gauge field decays with a rate equal to one. In particle physics terminology we would say that the gauge field due to the spontaneous symmetry breaking acquires a mass equal to the square V.E.V. of the Higgs field, i.e. equal to one. Thus its size is roughly of order one plus a fraction of the coherence length ($c\xi$ with $c \leq 1$). The factor c was introduced to take into account the fact that the gauge field decreases, though with a lower pace, even for $r \leq \xi$. Taking into account the dependence of ξ on the variation of β, we conclude that λ is a decreasing function of β. Moreover when ξ is small (i.e. $\xi < 1$) the dominant term - the rate of decay outside the core - is independent of β and thus λ is a slowly decreasing function of β.

In the same line of reasoning, and assuming that our prediction about the dependence of λ on β is correct, we may conclude that the magnetostatic energy W_b is a slowly increasing function of β. In fact in the previous numerical calculations we found, that for $\beta = 1$, W_b was equal to $0.314\,\pi$ and for $\beta = 10^6$, W_b was equal to $0.496\,\pi$ One could not in principle contemplate that such a tremendous change in the parameter β would result a

W_b of the same order. Yet it possible to explain that result using qualitative arguments. To do so we recall that $\alpha(r)$ is a smooth monotonous function which attains its maximum value at $r = 0$ and which asymptotically goes to 1 at large r. Assuming that the region where α varies from its asymptotic value is comparable to λ, and recalling the relation between $\alpha(r)$ and $B(r)$ in 3.1.3, we realize that the strength of the magnetic field in the two cases is comparable and so we end up with the same relation for the spatial integral of B^2.

Similar considerations along with scaling analysis can provide us useful insight to the relation between β and ξ. Therefore we apply in detail the well known scaling argument of Derric [40] Suppose that a certain configuration of the fields $\Psi = \Psi(\mathbf{x})$ and $\mathbf{A} = \mathbf{A}(\mathbf{x})$ is a static solution of the equations of motion and thus a stationary point of the energy functional 2.5.1 with finite energy

$$W = W_d + W_b + W_e + W_v$$

The energy of the configuration $\Psi = \Psi(\frac{\mathbf{x}}{\nu})$ and $\mathbf{A} = \mathbf{A}(\frac{\mathbf{x}}{\nu})$ where ν is some constant is then given by

$$W(\nu) = W_d + \nu^2 W_b + \frac{1}{\nu^4} W_e + \frac{1}{\nu^2} W_v \qquad (3.2.2)$$

By our hypothesis $\nu = 1$ is a stationary point of $W(\nu)$. Hence applying the condition $W'(\nu = 1) = 0$ to equation 3.2.2 yields the virial relation $2W_e + W_v = W_b$ which in the absence of potential term reduces to $2W_e = W_b$. An immediate consequence of that relation combined with the behaviour of W_b, is that large alterations on the value of β result a small change on the value of W_e. On the other hand as stated earlier W_e is linear to β and thus the field configuration for Ψ must change drastically in order to retain the value of W_e at the same order. To illustrate that point we introduce $\mathcal{E}$ defined as follows:

$$\partial_i \mathcal{E}_i = \Psi^* \Psi - 1 \qquad (3.2.3)$$

Apparently from Gauss law 2.2.8 follows that $E_i = \beta \mathcal{E}_i$ and $W_e = \beta \tilde{W}_e$, where $\tilde{W}_e = \frac{1}{2} \int d^2x \, \mathcal{E}_i^2$. Thus when β increases, $\tilde{W}_e$ decreases so as to

retain W_e at the same order of magnitude. Note that $\tilde{W}_e$ is a quantity independent of β and it only depends on the spatial distribution of Ψ. Let us now study deformations of the profile of $\Psi(r)$ and their effect to $\tilde{W}_e$. We first consider smooth deformations of $\Psi(r)$ which modify the form of the profile without altering its scale. The exact formula for $\tilde{W}_e$ in terms of Ψ reads

$$\tilde{W}_e = \int_0^\infty dr\, r^{-1} \left(\int_0^r dr'\, r' \left(\Psi^*(r')\Psi(r') - 1 \right) \right)^2 \qquad (3.2.4)$$

and it is legitimate to assume that such deformations could only result to a multiplication of $\tilde{W}_e$ by a numerical factor of order one. If instead we act to $\Psi(r)$ with a scale transformation of the form $\Psi'(r) \rightarrow \Psi(\nu r)$, it will result to a change : $\tilde{W}_e \rightarrow \tilde{W}'_e = \nu^{-4}\tilde{W}_e$.

From the previous considerations we realize that it is mainly a change on the scale of Ψ which balances the variation of β. Furthermore this statement is quantified as follows : When β changes to β' the scale of the Ψ field changes according to the law $\frac{\beta'}{\beta} = \Lambda\, \nu^4$ where ν is the scaling factor and Λ is a number of order one, which depends on β and β'. A scale transformation on Ψ results to a change on the size of the field. Consequently one derives the following relation for the coherence length : $\xi \propto \beta^{\frac{1}{4}}$

Having determined qualitatively the behaviour of ξ we proceed with numerical calculations to check the validity of our conclusions. We performed a number of numerical calculation for several values of β and the results are illustrated in table *I*. In column one we insert the value of β. In columns two and three the values of λ and ξ are written, where the lengths are determined by computing the first moment of the energy density. In columns four and five we insert the values of λ and ξ, where the lengths are determined by equation 3.2.1 i.e by computing the second moment of the energy density.

The coincidence of the numerical results to our prediction is remarkable. Although our reasoning was quite rough and vulnerable it is justified by that accordance. At the same time numerical results reveal the limits of our analysis. The values of β are exposed as powers of 16 and thus according to our prediction the magnitude of ξ has to underdouble each time. While for large β this prediction is quite accurate, for small β the deviation increases.

Even then, this deviation is explicable. When we studied deformations of Ψ we did not take into account their effect on the gauge field. In the limit where $\xi \ll \lambda$ (or equivalently for large β) their effect is insignificant, but as λ and ξ become comparable their coupling is getting more important and our analysis less reliable.

Table *I*

β	λ_1	ξ_1	λ_2	ξ_2
16^{-1}	1.23	1.34	1.41	1.57
16^{0}	0.96	0.76	1.12	0.89
16^{1}	0.77	0.41	0.92	0.48
16^{2}	0.67	0.21	0.85	0.24
16^{3}	0.63	0.11	0.83	0.12
16^{4}	0.62	0.053	0.82	0.061
16^{5}	0.62	0.026	0.82	0.030
16^{6}	0.62	0.013	0.81	0.015
16^{7}	0.62	0.006	0.81	0.007

We can implement the same kind of reasoning to study the effect of κ, when the electrostatic term is absent. There are only two minor differences. The potential has quadratic dependence to scale transformations while W_e has quartic. Besides, the potential is quadratic to κ while W_e is linear to β. Thus the corresponding relation between ξ and κ is expected to be : $\xi \propto \kappa^{-1}$. Numerical study confirms that prediction. The numerical results for various values of κ and $\beta = 0$ are illustrated in table *II*. The columns are as those of table *I*, where in column one instead of values of β are inserted the values of κ.

As in the case of β, the results are in accordance to our predictions and the same comments concerning limitations of our analysis apply also to the case of small κ. Note that values of κ, are written in powers of 2 and thus, coherence length is expected to underdouble each time.

Table *II*

κ	λ_1	ξ_1	λ_2	ξ_2
2^0	1.23	1.21	1.43	1.40
2^1	1.00	0.71	1.18	0.82
2^2	0.82	0.40	1.00	0.46
2^3	0.72	0.21	0.90	0.25
2^4	0.66	0.11	0.85	0.13
2^5	0.63	0.055	0.82	0.064
2^6	0.62	0.027	0.81	0.032
2^7	0.62	0.014	0.81	0.016

Finally having determined the dependence of λ and ξ on each of the parameters β and κ separately, we would like to comment on the combined effect of the potential and the electrostatic term. So far, it appears that as far as the static properties of the vortices are concerned, both terms have similar effect. So when both are present, the behaviour of λ and ξ may change quantitavely but not qualitavely. In particular, when one of the two terms dominates, the behaviour will be much like as if the other term is absent. It is easy to estimate which is the dominant term simply by comparing β and κ. The two terms have equivalent effect when $\kappa = 2$ and $\beta = 1$ and that equivalence is preserved when κ is multiplied by a power of 2 and β is multiplied by the same power of 16. Thus by comparing the two numbers $n_1 = log_2(\frac{\kappa}{2})$ and $n_2 = log_{16}(\beta)$ we can immediately determine the dominant term.

3.3 The two-Vortex System

Our main goal in this section is to compute the energy of two single vortices as a function of their separation d. Again we proceed numerically and choose a variational ansatz with the following characteristics: 1) The complex field vanishes at the points $(\pm\frac{d}{2}, 0)$ on the x-axis. 2) For large d the configuration reduces to two well-separated axially symmetric single vortices at a distance d from each other, while 3) for $d \to 0$ it takes the form of an axially symmetric $N = 2$ vortex located at the origin.

To formulate an ansatz, we first fix the phase of the matter field. This is equivalent to a choice of gauge. Parameterising the condensate as $\Psi(\mathbf{x}) = X(\mathbf{x})\, e^{i\Theta(\mathbf{x})}$, we choose the phase factor Θ to be [38]

$$\Theta(x,y) \;=\; tan^{-1}\Big[\frac{2xy}{x^2 - y^2 - \frac{d^2}{4}}\Big] \tag{3.3.1}$$

At large distances from the origin, as the argument $\mathbf{x}$ varies by 2π, Θ undergoes a rotation by 4π. Furthermore Θ is undefined, at the points $(\pm\frac{d}{2},0)$ (where the magnitude of Ψ vanishes) instead at the point $(0,0)$. For the magnitude X of the complex field Ψ we write

$$X(\mathbf{x}) \;=\; \omega\, X^{(1)}(|\mathbf{x}_-|)\, X^{(1)}(|\mathbf{x}_+|) + \,(1-\omega)\,\frac{(|\mathbf{x}_-|)\,(|\mathbf{x}_+|)}{r^2}\, X^{(2)}(r) \;+\; \delta X \tag{3.3.2}$$

where $\mathbf{x}_\pm$, correspond to the points $\mathbf{x} \pm \frac{d}{2}$, $X^{(1)}$ and $X^{(2)}$ are the previously determined solutions for the $N = 1$ and $N = 2$ vortices respectively and ω is a weight factor. The first term, for $\omega = 1$, reproduces an asymptotic configuration of separated vortices which is quite accurate for $d \ll \lambda$, where by λ is denoted the size of the vortices. In the second term the factor $\frac{(|\mathbf{x}_-|)\,(|\mathbf{x}_+|)}{r^2}$ has the effect of replacing the double zero of $X^{(2)}$ with two zeros at $\mathbf{x} = \pm\frac{\mathbf{d}}{2}$. For $\mathbf{d} = 0$ and $\omega = 0$ this second term reproduces the field of a $N = 2$ vortex.

The function δX contains the variational parameters and is written in the form

$$\delta X \;=\; (|\mathbf{x}_-|)\,(|\mathbf{x}_+|)\, cosh^{-1}(kr) \sum_{m=0}^{l}\sum_{n=0}^{m} z_{mn}\, r^{2m}\, cos(2n\phi) \tag{3.3.3}$$

The first factor on the right hand side of equation 3.3.3 ensures that Ψ vanishes at $\mathbf{x} = \pm\frac{\mathbf{d}}{2}$, the second factor introduces an exponential cutoff and the third term is an expansion into powers of r and cosines of argument $2n\phi$ which takes in account the symmetry of the field configuration.

In a similar manner we formulate the variational ansatz for the gauge potential.

$$\mathbf{A}(\mathbf{x}) = \omega\,\mathbf{A}^{(1)}(|\mathbf{x}_-|) + \omega\,\mathbf{A}^{(1)}(|\mathbf{x}_+|) + (1-\omega)\,\mathbf{A}^{(2)}(r) + \delta\mathbf{A}(\mathbf{x}) \quad (3.3.4)$$

where $\delta\mathbf{A} = \delta A_r\,\hat{r} + \delta A_\phi\,\hat{\phi}$ with δA_r and δA_ϕ defined by

$$\delta A_r = r\,cosh^{-1}(r) \sum_{m=0}^{l}\sum_{n=0}^{m} \alpha^r_{mn}\, r^{2m}\, sin(2n\phi) \quad (3.3.5)$$

$$\delta A_\phi = r\,cosh^{-1}(r) \sum_{m=0}^{l}\sum_{n=0}^{m} \alpha^\phi_{mn}\, r^{2m}\, cos(2n\phi) \quad (3.3.6)$$

The angular dependence of the fields was restricted to the form given above by the requirement on the configuration to be invariant under spatial reflection with respect to either one of the coordinate axes.

Once the ansatz for Ψ and $\mathbf{A}$ are formulated we use the same numerical procedure as in the isolated vortex case to determine the optimum values of the variational parameters $\alpha^\phi_{ij}, \alpha^r_{ij}$, z_{ij} and k. ω is in a sense also a variational parameter, the relative weight of N^1 and N^2 vortex solutions in the configuration, but we have chosen for it the value that minimizes the energy obtained from the ansatz without variational corrections ($\delta X = \delta A_r = \delta A_\phi = 0$). The dominant source of error in our results is due to the truncation of the configuration space. Again an estimate is obtained from the change in the value of the quantity of interest as we vary the number of variational parameters. To achieve an error of the order of 0.1% in the total energy for all values of d, it was enough to set $l = 1$ for $d > 3$, while for $d < 3$ it was necessary to take $l = 2$ i.e. a richer variational ansatz with 18 parameters. The uncertainty in W_e was a little larger, something like $0.2 - 0.3\%$, but since W_e contributes always a small fraction to the total energy, this error is negligible. Contrary to the isolated vortex case we did not perform the spatial integrations analytically. Instead we carried out these integrations numerically. Appropriate choice of the grid and the boundaries reduced the corresponding error to the order of 0.01%.

In figure 3.4 we plot the energy divided by π of the two-vortex system as a function of their separation d for four sets of the parameters κ and β

corresponding to the points A, B, C and D shown in figure 3.3, from well inside region-II, to somewhere in region-I. We have included the point C on the critical line with ($\kappa = 0.5$, $\beta = 0.0115$). Figure 3.4a corresponds to parameter values far from the critical line in region-II. The force between the vortices is everywhere repulsive. In all other cases one immediately recognizes a region of attraction and a region

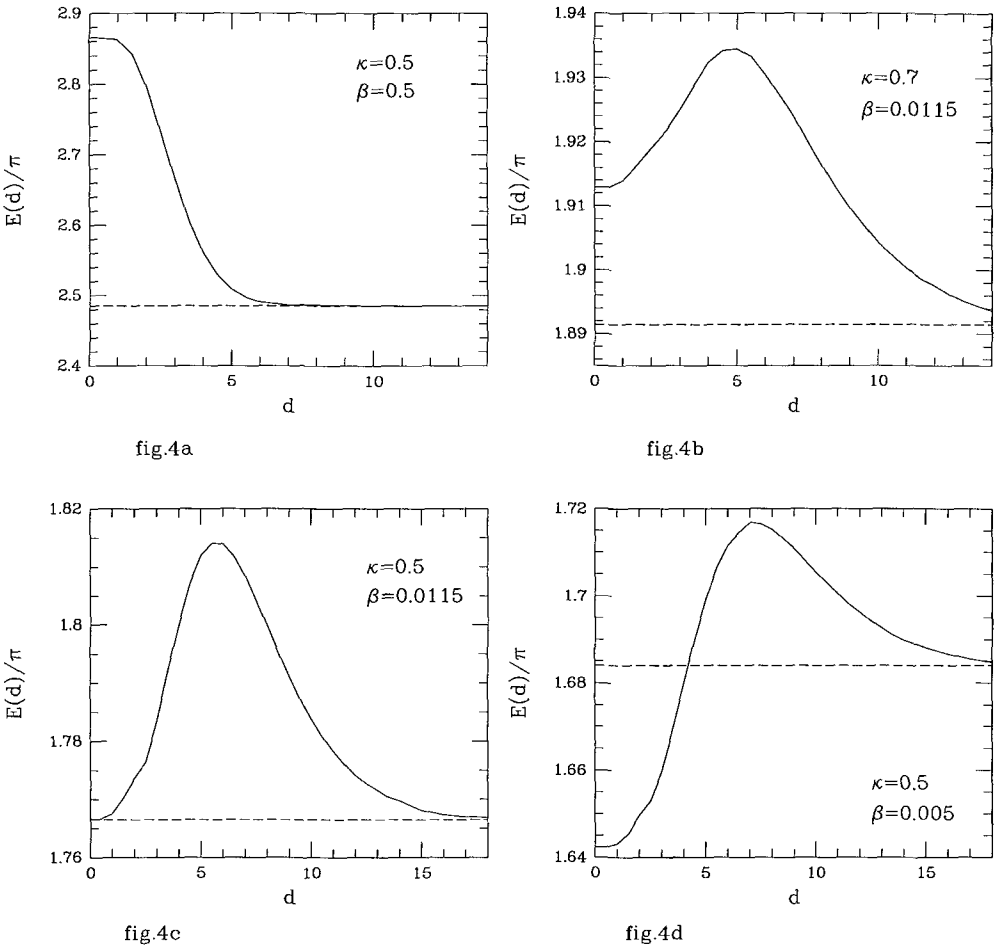

Figure 3.4 : *The energy of the two-vortex system as a function of their separation for the values of parameters corresponding to the points A, B, C and D of figure 3.3. The dashed line is drawn at twice the energy of a single vortex.*

of repulsion of the two solitons. The local extremum in the energy leads to the exciting possibility of the existence of dumb-bell shaped doubly-charged static solutions of the field equations for a rather wide range of parameters. We will have the opportunity to elaborate later when considering the dynamics of a pair of vortices.

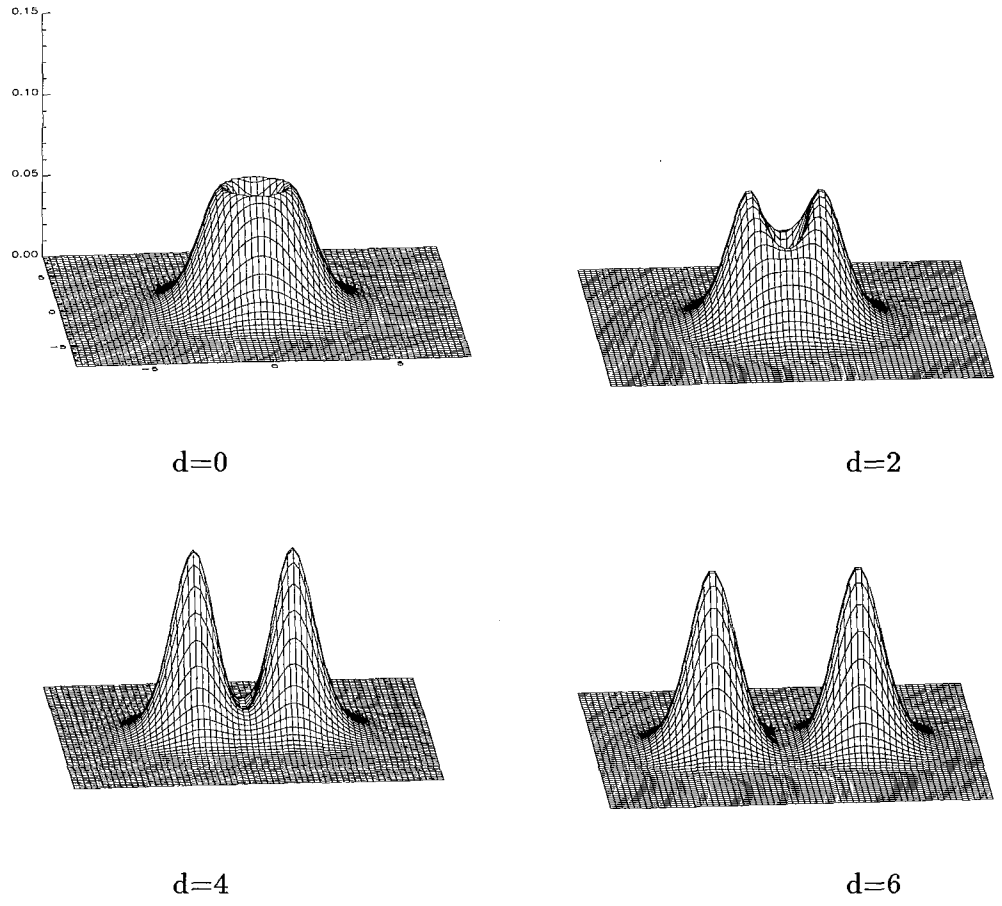

Figure 3.5 : *The total energy density of the two vortices* $d = 0$, 2, 4 *and* 6. $\kappa = 0.5$ *and* $\beta = 0.0115$.

Finally, figures 3.5, 3.6, 3.7 and 3.8 show the total energy density w_t, the gauge-invariant topological density τ, the magnetic field B and the electrostatic energy distribution w_e respectively, of the optimum two-vortex configuration corresponding to the parameter values ($\kappa = 0.5$, $\beta = 0.0115$)

on the critical line. The pictures in each one of them refer to distances $d =$ 0, 2, 4, 6.

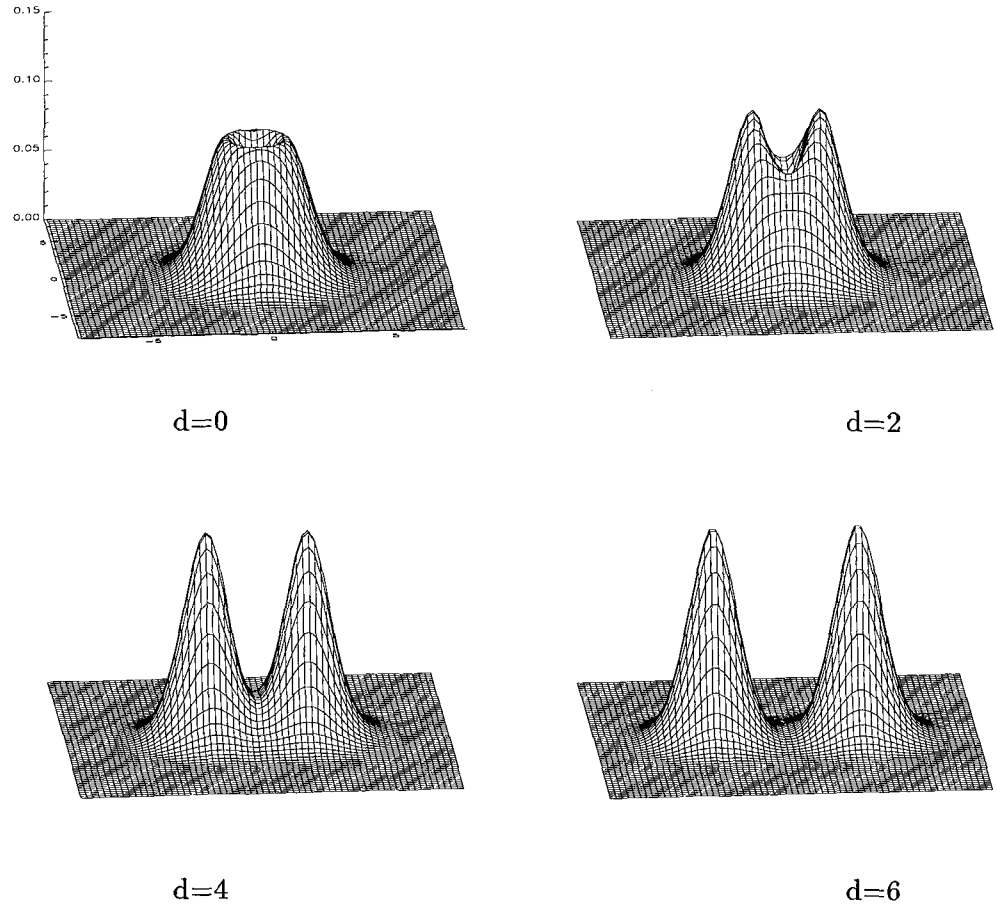

Figure 3.6 : *The topological charge density τ of the two vortices for $d = 0,\ 2,\ 4$ and 6. $\kappa = 0.5$ and $\beta = 0.0115$.*

Notice that of the two definitions $B/2\pi$ and τ of the topological density the former follows less closely the energy distribution and as such it offers a bad description of the two vortex positions. We have checked, although we do not show it here, that the topological density in terms of the complex field alone is even worse in that respect.

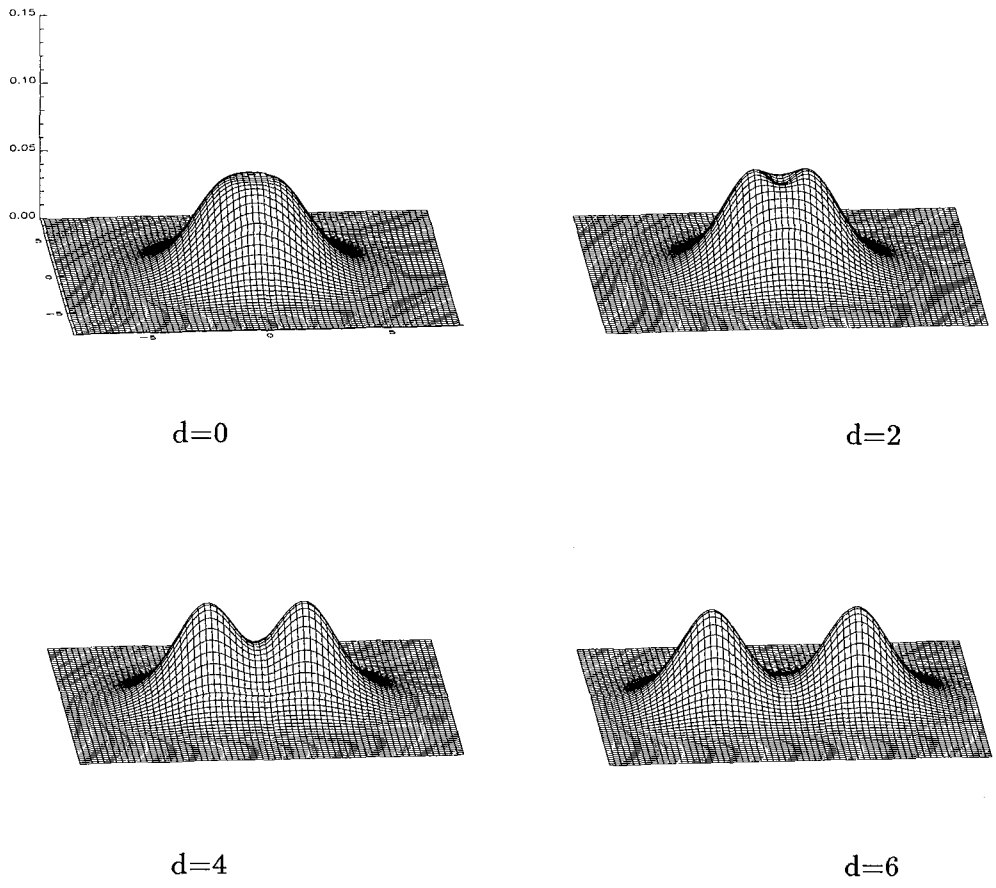

Figure 3.7 : *The magnetic field of the two vortices for* $d = 0$, 2, 4 *and* 6. $\kappa = 0.5$ *and* $\beta = 0.0115$.

Notice also that the distribution of w_e does not follow that of the total energy. It spreads over the whole region between the two vortices and is actually responsible for the bump in their interaction energy. Being so small in magnitude it does not alter the final picture that the two vortices can be safely considered far from each other already for $d = 4$.

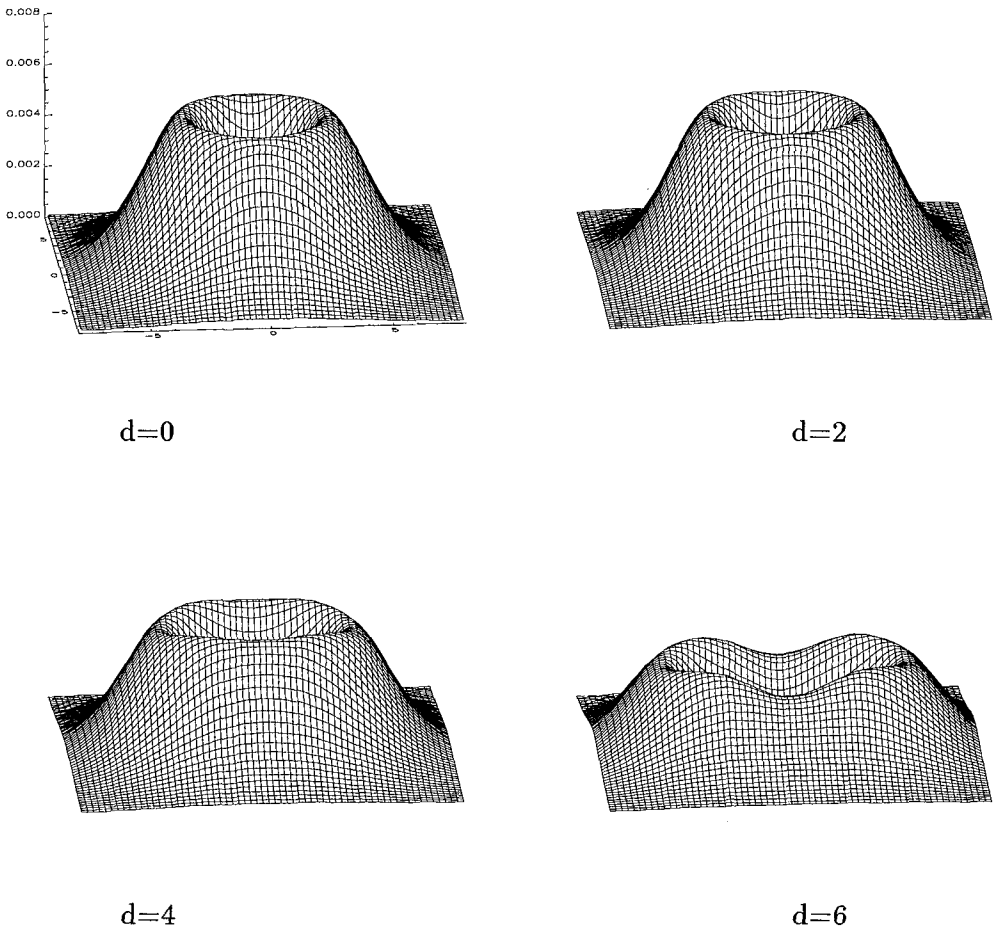

Figure 3.8 : *The electrostatic energy density of the two vortices* $d = 0$, 2, 4 *and* 6. $\kappa = 0.5$ *and* $\beta = 0.0115$.

These features of w_e as well as its negligible magnitude compared to w_t are also shown on figure 3.9 for the case of an axially symmetric $N = 1$ configuration with $\kappa = 0.5$ and $\beta = 0.0115$. The virial relation given in the previous section shows that W_e is never dominant. It can at most be $1/3$ of $W_t - W_d$ for any value of the parameters.

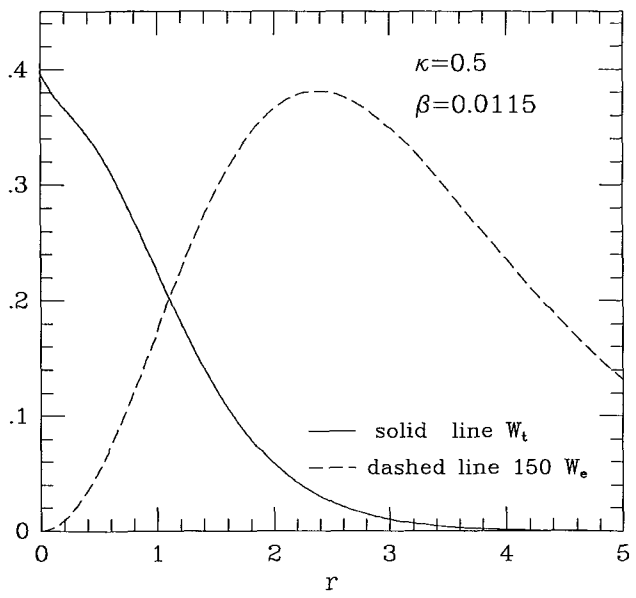

Figure 3.9 : *Plot of the densities* w_t *and* $150w_e$ *for an isolated* $N = 1$ *vortex.* $\kappa = 0.5$ *and* $\beta = 0.0115$.

We end this section with a remark about the numerical procedure used to compute W_e at each step of the iterative minimization process. We exploited the linearity of the Poisson equation to compute once and for all the electric field created by the charge density due to the configuration (3.10) to (3.12) in terms of the parameters of the ansatz. Thus the calculation of the electric field after each iteration is immediate. One does not have to solve the Poisson equation again but just plug into the general formula the new values of the parameters. W_e is finally given by a straightforward spatial integration. This way the computation is more accurate and much faster.

3.4 Fitting to a type-II Superconductor

In this section we roughly compare the underlying physics of the model to the physics of a typical type-II superconductor. To make contact with superconductivity the parameters q, m, and γ are fixed to the values : $q = \frac{2e}{\hbar}$, $m = 2m_e$, $\gamma = \hbar$. The electric charge of Ψ was set equal to $2e$ as well as its mass equal to $2m_e$ in order to account for the results of the microscopic theory of superconductivity, namely that the charge carriers are pairs of electrons [4] (the Cooper pairs). The background density Ψ_0 is determined by fitting it to the density of the superconducting electron pairs $\Psi_0^2 = n_s$. Because n_s is the density of the Cooper pairs in the physical three dimensional space, the dimensionality of Ψ is $[L]^{-3/2}$. To avoid any confusion with dimensions we note that here the model is considered as three dimensional $(3 + 1)$ and thus the dimensionality of the lagrangian density 2.2.1 is $[L]^{-3}$. Though in contrast to the convention we adopted in section 2.2 where the model was directly defined in two space dimensions, its three dimensional foundation is well defined and consistent.

To estimate n_s we write it as $n_s = \frac{1}{2}pn_f$ where n_s is the density of superconducting electron pairs, n_f is the density of the free electrons in the metal and p is the ratio of the superconducting over the free electrons in the metal. As typical value for n_f is considered $n_f = (2A^o)^{-3}$, and we indicatively set $p = 0.01$ in our calculations.

Yet there are three undefined parameters, namely κ, μ and ϵ. Since the physical origin of the potential term is arbitrary and given that the electrostatic term suffices to ensure the asymptotic convergence of Ψ to Ψ_0, the potential term is ommited i.e. we focus to the special case where $g = 0 \Rightarrow \kappa = 0$. To justify physically the introduction of ϵ in the model we may assert that the presence of ϵ in the Lagrangian 2.2.1 incorporates the screening effect on the electric field due to the presence of the normal electrons. In a similar manner μ accounts for the magnetic susceptibility of the normal phase as well as for the induced currents of the normal electrons. In the case we restrict our analysis to non magnetic materials, and assuming that the normal state currents are negligible - which is correct in thermal equilibrium - μ can be set equal to one. The only remained free parameter

is then ϵ. Its value is relevant to essential properties of the model like the energy spectrum and the coherence length. The claim of reproducing the physics of a superconductor will determine its value.

Having fixed the parameters of the model we are ready to proceed to the calculation of some of the fundamental properties of the superconducting state. Before embarking upon we add a comment about notation. In section 2.2 we used equation 2.2.3 to rescale fields and coordinates while we retained the same notation for the rescaled quantities. Since here we alternatively use both rescaled and original dimensionful fields and coordinates, we will use a tilde to denote the rescaled quantities and distinguish them from the dimensionful ones.

a) Quantization of magnetic flux

As it follows from section 2.5 quantization of magnetic flux is built-in the model. Specifically the claim for finite energy fixes the asymptotic behaviour of $\mathbf{A}$ which subsequently yields

$$\tilde{\Phi} = \int d\tilde{x}^2 \, \tilde{B} = \epsilon_{ij} \int d\tilde{x}^2 \, \tilde{\partial}_i \tilde{A}_j = 2\pi N \tag{3.4.1}$$

Using equation 2.2.3 to restore dimensions with $g = 0$, $\mu = 1$, magnetic flux reads

$$\Phi = \epsilon_{ij} \int dx^2 \, \partial_i A_j = \frac{\sqrt{m}c}{\sqrt{4\pi}\Psi_0 q\gamma} \frac{\sqrt{4\pi}\Psi_0\gamma}{\sqrt{m}} \epsilon_{ij} \int d\tilde{x}^2 \, \tilde{\partial}_i \tilde{A}_j$$

$$\Longrightarrow \Phi = 2\pi N \frac{c}{q} = N(137\pi e) \tag{3.4.2}$$

Thus the model succeeds to derive the right formula for the quantum of magnetic flux which in CGS units equals to 2×10^{-7} Gauss cm^2.

b) Penetration depth

Let us consider a superconducting specimen in the presence of an external magnetic field $\mathbf{H_0}$ in thermodynamical equilibrium [7]. It is assumed that the specimen occupies the half space namely the half of positive x coordinate, while the magnetic field is homogeneous and constant in the rest

half space and is parallel to the z-axis. Because of the symmetry of the system under consideration, the distribution of any physical quantity can only depend on coordinate x. In combination to Maxwell equation $\nabla \mathbf{B} = 0$ the latter reduces to $\partial_x B_x = 0$ which in turn implies $B_x = 0$. Symmetry considerations also allows us to impose $B_y = 0$, which renders B_z as the only non vanishing component of $\mathbf{B}$. The system possesses translational symmetry in the z-axis and thus it is essentially 2-dimensional. We thus ignore the third direction and invoke equations 2.2.9, 2.2.7 to describe the relevant physics in the limit of weak H. ($H \ll H_{c_1}$ where H_{c_1} is the lower critical field of a type-II superconductor). The weak H condition excludes any significant influence of the magnetic field on the density of the superconducting electrons, which is translated to the field $\tilde{\Psi}$ being in its ground state, i.e. $|\tilde{\Psi}(\tilde{\mathbf{x}})| = 1$.

To find the distribution of B_z (which we denote as $\tilde{B}$ from now on to be consistent to our notation) inside the specimen we combine the second part of eqs. 2.2.7 with the curl of $\mathbf{J}$ as that is given from 2.2.9 to obtain

$$\partial_x^2 \tilde{B} = (\tilde{\Psi}^* \tilde{\Psi}) \tilde{B} = \tilde{B} \tag{3.4.3}$$

which yields an exponential decay for the magnetic field into the superconductor. Note that in the derivation of 3.4.3, we imposed $\tilde{E}_i = 0$ which is a consequence of the fact that $\tilde{\Psi}$ is in its ground state, and thus the charge density is zero.

According to 3.4.3 the magnetic field penetrates into the specimen only to distances ~ 1. Denoting penetration length in rescaled units as $\tilde{\lambda}$ we write $\tilde{\lambda} = 1$ In dimensionful units we get $\lambda = \frac{\sqrt{m}c}{\sqrt{4\pi}\Psi_0 q \gamma} \tilde{\lambda} = \frac{109.3}{\sqrt{p}} A^o$ which becomes $\approx 10^3\, A^o$ if we substitute the value of p. This result is in accordance to the penetration depth of a typical type-II superconductor [42] which is about $10^{-5} - 10^{-6}$ cm.

c) Energy Gap

In the BCS theory of superconductivity the energy gap is given by the formula $\Delta = 1.76 k_B T_c$. [42]. Substitution of a typical value of $T_c = 10\, K^o$, results an energy gap $\Delta = 1.5 \times 10^{-3}\, eV$. According to our earlier derivation of section 2.3, the energy spectrum of the model has a gap which in the

absence of the potential term depends only on β, $\tilde{\omega} = \beta^{\frac{1}{2}}$. Note that we use $\tilde{\omega}$ which is dimensionless to distinguish from ω which has dimension $[T]^{-1}$. By restoring units and dimensions, the energy gap becomes

$$G = \hbar\omega = \hbar\tilde{\omega}\frac{m^2c^2}{4\pi\Psi_0^2 q\gamma^3}$$

which after the proper substitutions yields $G = \sqrt{\frac{\pi p}{8\epsilon}}A.U.$ In order to fit the value of G to that of Δ, ϵ and p must meet the following relation: $\frac{\epsilon}{p} \approx 10^8$ which for $p = 0.01$ results $\epsilon = 10^6$

d)Coherence Length

We use the same definition of the coherence length ξ to that adopted in section 2.2, i.e. ξ defines the characteristic distance for variations of Ψ in the vortex state. In that section, a relation between ξ and β was established, namely

$$\xi = c\beta^{-\frac{1}{4}}$$

where c is a numerical factor of order one. To evaluate β we substitute the value of ϵ derived earlier, in equation 2.2.5 to obtain $\beta = 3.5\,10^4$. The value of the coherence length for that particular value of β is $\approx \frac{10}{\sqrt{p}}A^o$. which fits well to the existing experimental data for type II superconductors.

The previous calculations were rough based on several assumptions such as the effective mass of the Cooper pair, the fraction of the superconducting electrons, the magnetic properties of the material etc. Nevertheless the output contains useful information and the viability of the model as a candidate effective theory of superconductivity is established. We complete this section by briefly discussing whether the model is adequate to describe vortex physics in plasma. In that case, in first approximation parameter ϵ is equal to one while γ, m,μ, and q take similar values to those of the superconductor case. Then for a typical value of plasma density, $|\Psi_0|^2 = 10^{-6}A^{o\,-3}$, ξ, λ take values of order $10\,A^o$ and $10^4\,A^o$ respectively. Yet the dependence of ξ, λ on the density is given by

$$\xi \propto \Psi_0^{-1/2} \qquad\qquad \lambda \propto \Psi_0^{-1}$$

Thus, higher densities from the one considered above result a value for the coherence length which is comparable to the radius of Bohr. But at Bohr's length scale our effective field theory is not applicable. On the other hand, for low densities the model yields a penetration depth several orders of magnitude larger than the corresponding coherence length.

CHAPTER IV
Hall Motion

4.1 Introduction

The study of the dynamical behaviour of topological solitons has attracted a rather intense interest over the past few decades. Among the most unexpected features of topological solitons is their unusual dynamical response to external probes. The magnetic bubbles undergo a skew deflection under the influence of a magnetic field gradient. The behaviour of vortices in pure superconducting films at very low temperature is a puzzle yet unsolved. Recent theoretical studies in relativistic field theories [44] [43] have demonstrated that skyrmions and monopoles exhibit scattering patterns that are highly unusual from the point of view of familiar scattering processes of ordinary particles. Meanwhile, 90^o scattering patterns have been reported in a large number of numerical studies of topological solitons in a variety of relativistic systems [46], [47], [48], [49], [50].

In a recent paper [51], the fundamental simplicity which underlies the skew deflection of magnetic bubbles, was established. In particular the gross features of bubble dynamics were shown to be similar to those of the familiar Hall effect. Later on it was proved [27] that the non-relativistic Abelian-Higgs model, exhibits an identical dynamical - Hall - behaviour. Furthermore it was demonstrated [28] that Hall behaviour is a common

feature of a whole class of non relativistic topological solitons. In contrast to the relativistic systems where the theoretical explanation of the unusual scattering patterns remains an interesting open question, the origin of Hall behaviour is well understood and is directly linked with the topological properties of the corresponding systems.

The purpose of this chapter, is to demonstrate the analogy between the dynamical behaviour of the vortices and of the Hall effect. In section II we study the dynamics of vortices in our model. The canonical structure of the model is derived and it is shown that the unambiguous linear momentum is essentially the first moment of the topological density. The momentum conservation law in the absence of any external fields is shown to imply the spontaneous pinning of isolated vortices, while the application of an external force results in the motion of the vortex at a constant calculable speed in a direction $(N/|N|)\ 90^0$ relative to it. For completeness in section III we study the plane motion of charged particles in the presence of an external perpendicular to the plane magnetic field, and discuss its relevance to our model. Finally in section IV we formulate necessary conditions for the manifestation of the above Hall-behaviour in the dynamics of topological solitons.

4.2 Vortex Dynamics

4.2.1 Canonical structure of the model

In order to investigate the dynamics of vortices we start with the canonical structure of the model. We follow the standard procedure [52] applied to gauge theories to determine its fundamental Poisson brackets. As mentioned in a previous section to eliminate the redundant degrees of freedom due to the gauge invariance of the model we impose the condition

$$\nabla \cdot \mathbf{A} = \mathbf{0}$$

Since the action does not depend on $\dot{A}_0$, A_0 is a dependent variable

satisfying the Gauss law constraint which we solve to obtain

$$A_0(\mathbf{x},t) = -\frac{\beta}{2\pi}\int d^2x'\ ln|\mathbf{x}-\mathbf{x}'|\,(\Psi^*\Psi(\mathbf{x}',t)-1) \tag{4.2.1}$$

(use was made of $\nabla^2\ ln|\mathbf{x}-\mathbf{x}'| = 2\pi\delta(\mathbf{x}-\mathbf{x}')$). With the above gauge-fixing condition the purely electromagnetic part of the action takes the form

$$S_A = \frac{1}{2}\int d^2x\ [\ \frac{1}{\beta}(\mathbf{E}_T{}^2+\mathbf{E}_L{}^2) - B^2\ ] \tag{4.2.2}$$

where the transverse and the longitudinal parts of the electric field are $\mathbf{E}_T = -\dot{\mathbf{A}}$ and $\mathbf{E}_L = -\nabla A_0$ respectively.

The canonical momentum π_k conjugate to A_k is then $\pi_k = \partial\mathcal{L}/\partial\dot{A}_k = -E_k^T/\beta$, while Ψ and $\pi \equiv \partial\mathcal{L}/\partial\dot{\Psi} = i\Psi^*$ are conjugate of each other. Thus, the fundamental Poisson brackets are

$$\begin{aligned}\{\Psi(\mathbf{x},t),\Psi^*(\mathbf{x}',t)\} &= -i\delta(\mathbf{x}-\mathbf{x}')\\ \{A_i(\mathbf{x},t),\dot{A}_j(\mathbf{x}',t)\} &= \beta\delta^T{}_{ij}(\mathbf{x}-\mathbf{x}')\\ \{\Psi(\mathbf{x},t),A_i(\mathbf{x}',t)\} &= 0 = \{\Psi(\mathbf{x},t),\dot{A}_i(\mathbf{x}',t)\}\end{aligned} \tag{4.2.3}$$

where the transverse δ function is defined as $\delta^T{}_{ij}(\mathbf{x}-\mathbf{x}') \equiv \equiv (\delta_{\mathbf{ij}} - \nabla^{-\mathbf{2}}\partial_{\mathbf{i}}\partial_{\mathbf{j}})\delta(\mathbf{x}-\mathbf{x}')$. Finally, the Hamiltonian (total energy) of the system is

$$H = \int d^2x\ [\ \frac{1}{2\beta}(\mathbf{E}_T{}^2+\mathbf{E}_L{}^2) + \frac{1}{2}B^2 + \frac{1}{2}|\mathbf{D}\Psi|^2 + \frac{1}{8}\kappa^2(\Psi^*\Psi-1)^2\ ] \tag{4.2.4}$$

All other Poisson brackets are obtained from the ones given above. It is straightforward to check that

$$\begin{aligned}\{A_0(\mathbf{x},t),\Psi(\mathbf{x}',t)\} &= -\frac{i\beta}{2\pi}ln|\mathbf{x}-\mathbf{x}'|\ \Psi(\mathbf{x}',t)\\ \{A_0(\mathbf{x},t),A_i(\mathbf{x}',t)\} &= 0 = \{A_0(\mathbf{x},t),\dot{A}_i(\mathbf{x}',t)\}\end{aligned} \tag{4.2.5}$$

as well as that the equations of motion 2.2.7 and 2.2.8 coincide with Hamilton's equations

$$\begin{aligned}\dot{\Psi}(\mathbf{x},t) &= \{\Psi(\mathbf{x},t),H\}\\ \dot{A}_k(\mathbf{x},t) &= \{A_k(\mathbf{x},t),H\}\end{aligned} \tag{4.2.6}$$

$$\dot{\pi}_k(\mathbf{x},t) = \{\pi_k(\mathbf{x},t), H\}$$

We are now ready to proceed with the construction of the field momentum and angular momentum for the model at hand, valid in all topological sectors. We will show [27] [51] that the corresponding conservation laws describe the basic feature of vortex motion in the absence of external forces, namely spontaneous pinning.

4.2.2 Momentum and angular momentum in all sectors

The Noether expression for the linear momentum in our model is

$$P_k^N = \int d^2x \, (-\pi\partial_k\Psi - \pi_j\partial_k A_j) \tag{4.2.7}$$

It is derived under the assumption that all fields approach their vacuum values fast enough as $r \to \infty$ so that all integrals are meaningful and surface terms appearing in intermediate steps are zero. It is straightforward to check that the above expression is ill-defined for any vortex configuration with non-zero topological charge. Under the same assumptions though which led to 4.2.7 the latter can be brought to the form

$$P_k = -\epsilon_{ki}\int d^2x \; x_i \; \epsilon_{lm}(\partial_l\pi \; \partial_m\Psi + \partial_l\pi_j \; \partial_m A_j) \tag{4.2.8}$$

which is well-defined for any smooth finite-energy field configuration with arbitrary topological charge. The two expressions 4.2.7 and 4.2.8 differ by exactly those surface terms which were omitted from the former and make the latter finite and unambiguous in all topological sectors.

All the defining properties of the momentum are verified for P_k. This is no surprise. They are formally valid for P_k^N and this differs from P_k only by surface terms. In any case, one can directly and unambiguously show using the equations of motion 2.2.7, 2.2.8 and the Poisson brackets derived above first, that P_k is conserved

$$\frac{d}{dt}P_k = 0 \tag{4.2.9}$$

second, that it is the generator of spatial displacements

$$\{P_k, \mathcal{F}\} = \partial_k \mathcal{F} \tag{4.2.10}$$

and finally, that it is gauge-invariant. The only condition on the configuration $\mathcal{F} = (\Psi, A_0, A_i)$ necessary for the derivation is that A_0 vanishes faster than r^{-1} as $r \to \infty$. All our vortices have A_0 approaching zero at infinity exponentially fast and consequently they safely belong to this set of configurations. Furthermore, using Gauss' constraint we can rewrite the momentum in the manifestly gauge-invariant form

$$P_k = \epsilon_{ki} \int d^2x \, (2\pi \, x_i \, \tau + \frac{1}{\beta} \, E_i B) \tag{4.2.11}$$

The second term is the Poynting vector, the pure electromagnetic contribution to the field momentum.

Thus, independently of derivation, P_k is the correct form of the momentum in our theory, valid in any topological sector and reducing to the naive expression in the trivial sector $N = 0$ and for configurations allowing for free integrations by parts.

Before we discuss the implications of the above formula of the linear momentum on the motion of vortices, we would like to construct in a similar way the correct form of the angular momentum in our model. Again, the Noether expression

$$L_N = - \int d^2x \, \epsilon_{ij} \, [\, x_i \, (\pi \partial_j \Psi + \pi_k \partial_j A_k) + \pi_i A_j \,] \tag{4.2.12}$$

is formally conserved and generates rotations but is divergent in any nontrivial sector. Allow for integrations by parts and ignore surface terms to rewrite it in the form

$$L = \int d^2x \, [\, \frac{1}{2} \mathbf{x}^2 \, \epsilon_{ij} \, (\partial_i \pi \partial_j \Psi + \partial_i \pi_k \partial_j A_k) + \epsilon_{ij} A_i \pi_j \,] \tag{4.2.13}$$

or as a manifestly gauge invariant quantity in terms of the topological density τ defined in section 2

$$L = - \int d^2x \, (\pi \mathbf{x}^2 \tau + \frac{1}{\beta} \, \mathbf{x} \cdot \mathbf{E} B) \tag{4.2.14}$$

Using either one of the last two formulas one can show that for essentially all finite-energy configurations as in the case of the linear momentum, L is well-defined, conserved and generates spatial rotations, i.e. it satisfies

$$\{L, \Psi(\mathbf{x}, t)\} = \epsilon_{ij} x_i \partial_j \Psi$$

$$\{L, A_k(\mathbf{x}, t)\} = \epsilon_{ij} x_i \partial_j A_k + \epsilon_{kl} A_l \tag{4.2.15}$$

L is then the proper definition of the angular momentum when dealing with topologically non-trivial configurations. As already explained it vanishes for the spherically symmetric neutral solutions studied in chapter three.

4.2.3 Vortex motion

In the next chapter we will present details of a numerical simulation of the motion of the flux vortices described above under the influence of various external forces. Here we would like for the sake of completeness to predict analytically and without any approximation the essential features of their dynamical behaviour [27]. It is already apparent that the momentum P_k defined in the previous section is not a measure of the translational motion of a vortex but instead it describes its position. In fact the momentum of a static axially symmetric vortex with charge N centered at $\mathbf{a}$ is $P_k = 2\pi N \epsilon_{ki} a_i$. It is also clear that a localized free vortex of arbitrary shape moving in formation at constant velocity v_i would have $P_k = 2\pi N \epsilon_{ki}(a_i^0 + v_i t)$. For any $v_i \neq 0$ this is forbidden by the linear momentum conservation law. A free vortex is spontaneously pinned as a consequence of momentum conservation.

Let us define the "guiding center" $\mathbf{R}$ of a generic configuration with $N \neq 0$ by

$$R_i \equiv -\frac{1}{2\pi N} \epsilon_{ij} P_j \tag{4.2.16}$$

Since under a rigid displacement of the whole configuration by $\mathbf{c}$, $\mathbf{R}$ changes to $\mathbf{R} + \mathbf{c}$ and for a spherical vortex it coincides with its geometric center, we naturally interpret it as the mean position of the configuration. Note also in support of this interpretation, that $\mathbf{R}$ is related to the first moment

of the topological density τ, so that for nearly spherical configurations $\mathbf{R}$ is close to their "center of topology".

a. In the absence of external forces both N and $\mathbf{P}$ are conserved and

$$\frac{d}{dt}\mathbf{R} = \mathbf{0} \tag{4.2.17}$$

A generic vortex-like configuration produced in the system will of course fluctuate in its details but it will remain pinned at its initial mean position.

b. Consider next the response of such a vortex to an externally prescribed electric current $\tilde{J}_i(\mathbf{x}, t)$. Its effect is studied by adding to the action the term $\delta S = \int d^2x\ dt\ \tilde{J}_i(\mathbf{x}, t)A_i$. For consistency of the model the external current should have zero divergence. The new term in the action modifies the A_i equation of motion 2.2.7 by the substitution $J_i \to J_i + \tilde{J}_i$ on the right-hand side. Because of the external current the momentum and the angular momentum are no longer conserved. Instead, their time derivatives are equal to the external force and torque respectively. Indeed one can easily verify Newton's equation:

$$\frac{d}{dt}P_k = F_k^{Lorentz} = -\int d^2x\ \epsilon_{kl}\tilde{J}_l(\mathbf{x}, t)B(\mathbf{x}, t) \tag{4.2.18}$$

as well as

$$\frac{d}{dt}L = Torque = \int d^2x\ x_i\tilde{J}_iB \tag{4.2.19}$$

Naturally the force on the vortex is opposite to the Lorentz force acting on the external current, while the torque is by definition expressed in terms of the force density $f_k = -\epsilon_{kl}\tilde{J}_lB$ as the integral of $\epsilon_{ij}x_if_j$. We now use 4.2.16 and the fact that for arbitrary $\tilde{J}$ N is still conserved to obtain

$$\frac{dR_k}{dt} = -\frac{1}{2\pi N}\int d^2x\ \tilde{J}_kB \tag{4.2.20}$$

In the idealized situation of a homogeneous throughout the vortex external current the above formula simplifies to

$$\frac{dR_k}{dt} = -\tilde{J}_k(t) \tag{4.2.21}$$

In general, the naive expectation based on the usual Newtonian reasoning and Galilean invariance would be that the vortex should accelerate in the

direction of the force acting on it. Instead, 4.2.16 combined with $dP_k/dt = F_k$ for a generic force F_k, shows that the equation of motion of the mean position of the vortex is

$$\frac{d}{dt}R_k = -\frac{1}{2\pi N}\,\epsilon_{kl}\,F_l \tag{4.2.22}$$

i.e. the vortex moves with speed $|\mathbf{F}|/2\pi|N|$ and at $\pm$ 90^0 relative to the force for positive or negative N respectively. In the special case of the homogeneous external current considered here, the force is also proportional to N and all vortices move with the same velocity equal to minus the external current itself. If in particular the latter is due entirely to the condensate charges taken here by convention positive with unit charge density, its value is exactly equal to minus the velocity of the carriers. Thus the vortex will reorganize itself during a transient period following the onset of the external current and it will move with the same speed but opposite to the current carriers. Furthermore it should be pointed-out that in the context of our field theory model no approximation other than the implicit assumption that the vortex remains localized was necessary. The position interpretation 4.2.16 of the momentum converts Newton's law into an equation giving directly the velocity of the vortex in terms of the applied force, while the ϵ_{ij} of 4.2.16 makes the vortex move at an angle $(N/|N|)$ 90^0 relative to the direction of the external force (Hall-behaviour). The above general conclusion, reached without ever solving an equation of motion, does not depend on the details of the Hamiltonian of the system. Any potential V or any additional higher spatial derivative term in H modifies the detailed profile of the vortex solutions but it does not alter their dynamics.

The guiding center interpretation of the momentum 4.2.16 is not applicable in the case of topologically trivial ($N = 0$) configurations. Newton's law 4.2.18 is of course still true for any external force, but this does not strictly speaking tell us much about the actual motion of the vortex. In contrast to the case of ordinary particle dynamics with Poincaré or even Galilean invariance the relation between momentum and velocity is not a priori known in the present model.

4.3 Electron Motion in a Uniform Magnetic Field

In order to illustrate the analogy with the Hall effect more explicitly, we briefly describe here the canonical structure associated with two-dimensional electron motion in a uniform magnetic field B perpendicular to the plane and an in-plane electric field $\mathbf{E} = -\nabla U$, where $U = U(x_1, x_2)$ is the electrostatic potential. In fact the magnetic field B in the electron problem corresponds to the topological charge N of a vortex, while the electric field $\mathbf{E}$ multiplied by the electric charge of the electron, corresponds to $\mathbf{F}^{Lorentz}$ of eq. 4.2.18. The mass and the charge of the electron as well as the speed of light are set equal to unity.

The electron motion is then governed by the equations

$$\dot{x}_1 = \pi_1 \qquad \dot{x}_2 = \pi_2$$

$$\dot{\pi}_1 = B\pi_2 - \partial_1 U \qquad \dot{\pi}_2 = -B\pi_1 - \partial_2 U \tag{4.3.1}$$

where π_1 and π_2 are the components of the mechanical momentum. These equations may be understood as a hamiltonian system with hamiltonian

$$\mathcal{H} = \frac{1}{2}(\pi_1^2 + \pi_2^2) + U(x_1, x_2) \tag{4.3.2}$$

endowed with the Poisson brackets relations

$$\{\pi_1, x_1\} = 1 = \{\pi_2, x_2\} \qquad \{\pi_1, \pi_2\} = -B \tag{4.3.3}$$

where we display only the nonvanishing Poisson brackets. A more transparent set of variables is obtained by introducing the guiding center coordinates

$$R_1 = x_1 + \frac{\pi_2}{B} \qquad R_2 = x_2 - \frac{\pi_1}{B} \tag{4.3.4}$$

while retaining the π_1 and π_2 as independent variables. The corresponding Poisson brackets read as

$$\{\pi_1, \pi_2\} = -B \qquad \{R_1, R_2\} = \frac{1}{B} \qquad \{\pi_\mu, R_\nu\} = 0 \tag{4.3.5}$$

and the Hamilton equations as

$$\dot{\pi}_1 = B\pi_2 - \frac{\partial U}{\partial R_1} \qquad \dot{\pi}_2 = -B\pi_1 - \frac{\partial U}{\partial R_2}$$

$$\dot{R}_1 = \frac{1}{B}\frac{\partial U}{\partial R_2} \qquad \dot{R}_2 = -\frac{1}{B}\frac{\partial U}{\partial R_1} \tag{4.3.6}$$

where $U = U(x_1, x_2) = U(R_1 - \pi_2/B, R_2 + \pi_1/B)$.

In the absence of an electric field ($U = const.$) the last two equations in 4.3.6 become $\dot{R}_1 = 0 = \dot{R}_2$, implying that the guiding center remains fixed, which is the conservation law associated with invariance under space translations. The conserved quantity associated with invariance under space rotations, which requires that U be axially symmetric, is given by the angular momentum

$$l = x_1\pi_2 - x_2\pi_1 + \frac{B}{2}(x_1^2 + x_2^2) = \frac{B}{2}(R_1^2 + R_2^2) - \frac{1}{2B}(\pi_1^2 + \pi_2^2) \tag{4.3.7}$$

which is also seen to be different from its standard mechanical value $x_1\pi_2 - x_2\pi_1$.

Now in the presence of a general electrostatic potential $U = U(x_1, x_2)$ neither the guiding center remains fixed nor the angular momentum is conserved. Nevertheless some general properties of the electron motion can be derived without a detailed solution of the equations of motion. For instance in the case of a uniform electric field pointing in the x_1-direction, $u = -E\,x_1$, the last two equations in eq. 4.3.6 read $\dot{R}_1 = 0$ and $\dot{R}_2 = -E/B$, and imply that the guiding center drifts in a direction perpendicular to the electric field with constant Hall velocity $V_H = -E/B$. For a more general potential U, the last two equations in 4.3.6 cannot be decoupled from the rest, except in the adiabatic (large b) limit where

$$\dot{R}_1 = \frac{1}{B}\frac{\partial U}{\partial R_2} \qquad \dot{R}_2 = -\frac{1}{B}\frac{\partial U}{\partial R_1} \qquad U \sim U(R_1, R_2) \tag{4.3.8}$$

which may be viewed as a hamiltonian system for the pair of canonically conjugate variables R_1 and R_2 with hamiltonian $U(R_1, R_2)$. As a result

the guiding center again drifts along equipotential lines, i.e. in a direction perpendicular to the electric field, with a Hall velocity whose magnitude is given by $|\nabla U|/B$.

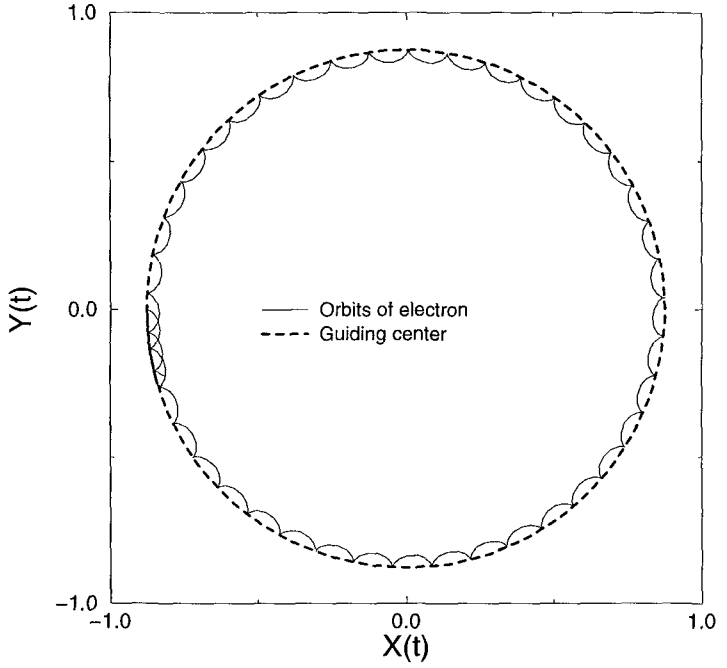

Figure 4.1 : *The trajectory of one of the electrons of the pair (solid line), and the trajectory of its guiding center (dashed line).*

Although the electron pair system is much simpler than the model at hand, it may offer a useful guide for the physical interpretation and the dynamical implications of the results we derived in the previous section. In that context the dynamical behaviour of two interacting vortices as well as that of a vortex-antivortex pair can be parallelized to the motion of an electron-electron and an electron-positron pair respectively. Since we will extensively deal with that aspect of vortex dynamics in the next chapter, we give a short account of the electron analogue.

We consider two electrons initially placed at separation d, with initial velocity $V = 0$, under the influence of a perpendicular magnetic field. As it

can be shown analytically, due to the presence of the magnetic field the two electrons rotate around each other in roughly circular orbits. In Figure 4.1 we plot the trajectories of the electrons for $d = 1.75$ and $B = 4$. Actually we draw only the trajectory of one of the electrons, since the trajectory of the other one is the mirror image of the former, with respect to the center of the coordinate system. Notice that the guiding center of the electron moves along almost circular path while the electron itself performs Larmor precession along that path.

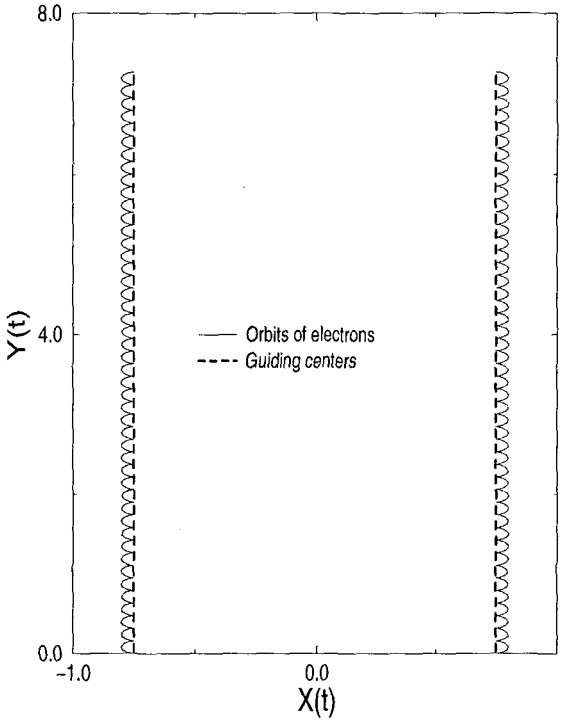

Figure 4.2 : *Trajectories of the electron and the positron (solid line), and of their guiding centers (dashed line).*

In the case of the electron-positron pair at separation d and initial velocity $V = 0$, the two particles instead of rotation, move in formation in a direction perpendicular to the line that connects them. The motion of the electron-positron pair is plotted in Figure 4.2 for $d = 1.5$ and $B = 4$ where

as we see the guiding centers of the particles, move in parallel lines, while the trajectories of the particles oscillate along those lines.

4.4 Discussion

We presented a general treatment of the motion of flux-vortices in the context of our field theoretical model We argued that independently of the details of the Hamiltonian the vortices exhibit Hall-behaviour, like electrons moving on a plane under the simultaneous action of a perpendicular magnetic and an in-plane electric field. An external current was shown from first principles to pull the vortex in the opposite direction. It is tempting to think of our model as a field- theoretic realization of the hydrodynamic model discussed in reference [18] in the vanishing friction limit. The discussion there of vortex motion was based on the phenomenological use of the Magnus force [53] known from fluid mechanics [54] and led to the conclusion that $\mathbf{V} = \tilde{\mathbf{J}}$. Our result (4.21) is exactly the opposite and, to the extent that the model (2.1) captures the essential physics of a superconducting film, it implies the opposite sign Hall effect reported in ordinary as well as high-T_c superconductors [9].

The Hall motion of the vortices derived above is attributed to the radical change in the role of the momentum of the theory as a result of the underlying topology. The Hall behaviour of an isolated vortex is exactly due to the fact that the linear momentum 4.2.11 contains a piece which is equal to the first moment of the topological density. An immediate consequence of this fact combined with the fundamental property 4.2.10 of the momentum is that

$$\{P_1, P_2\} = 2\pi N \tag{4.4.1}$$

We thus conclude that necessary condition for the manifestation of Hall motion is that the translation part of the symmetry algebra of the model admits central extension. It is well-known [55] that this is not possible in the case of the Galilean or the Poincaré algebra in any spatial dimension higher than or equal to two. It is not even true for the Euclidean algebra $E(D)$ for $D \geq 3$. Thus, the Hall behaviour encountered above is expected

a priori only in two-dimensional systems with spatial $E(2)$ algebra, or in D-dimensional systems with translational symmetry alone. In the system at hand one can immediately check that

$$\{L, P_1\} = P_2 \qquad \{L, P_2\} = -P_1 \tag{4.4.2}$$

and verify that it belongs to the first category as expected.

We would also like to stress that although 4.2.8 is true even in theories with canonical momentum π proportional to the time derivative of the complex field, our previous reasoning does not go through since $\mathbf{P}$ is then related to the first moment not of the topological density but of a quantity which actually vanishes for static configurations. Thus, another condition which is necessary is that the equations of motion are first order in the fields which carry the topology in the particular model. In other words, we do not expect Hall- motion of the vortices in the relativistic-like model [8] derived as a dynamical extension of the Ginzburg-Landau theory of a superconductor appropriate for temperatures far below T_c.

On the other hand, the above formalism applies to the motion of vortices in a generalization of the present model which allows for dynamical positiveions forming a lattice, of the (N_h, N_{ss}) with $N_{ss} \neq -2N_h$ vortices of the high-T_c superconductor model proposed in reference [56], as well as to the motion of vortices in easy-plane ferromagnetic films [57], to mention just a few systems of considerable interest.

CHAPTER V
Numerical Results

5.1 Introduction

In the previous chapter we analytically showed how the topological properties of the vortices are related to their dynamics. In particular the vortices were shown to exhibit Hall behaviour and the gross features of their motion were determined using general analytical arguments. Those results acquire particular importance since they may account for the presence of the Magnus force in superconductors, whose origin is still an open question.

In principle the motion of the vortex can be far more rich and complex from what Hall behaviour implies, without any contradiction to the theory. Even in the original Hall phenomenon, in the case where the strength of the magnetic field is very low (or equivalently the strength of the electric field is very high) the Hall motion though still valid for large time scales, fails to describe the motion of the electron at small time scale. In relative systems which exhibit Hall behaviour [58], the results of numerical studies, along with the confirmation of the general picture, revealed systematic patterns in the motion of magnetic bubbles which the theory could not account for. We thus realize that one has to solve in detail the equations of motion to have a thorough picture of the motion of the vortices.

In this chapter we study numerically the dynamics of vortices performing

a large number of simulations. The purpose of this work is twofold :
1) to analytically verify the picture developed in chapter IV, determine the range of applicability of the theory and study the deviations if any from the theoretical idealized picture, and 2) to investigate the finer details of the motion of the vortices.

In section II we review concepts and techniques of lattice gauge theories which played an essential role in the construction of our numerical algorithm. Section III describes in detail the numerical simulations of the motion of a vortex pair. In section IV we refer briefly to the similar problem of the evolution of a vortex-antivortex pair. Finally in section V we study numerically the response of the vortex to the application of an homogeneous external current.

5.2 Lattice Gauge Theories

5.2.1 Discretization schemes

Gauge physics play a fundamental role in our present understanding of physics. Originally invoked to describe electromagnetic interactions ; the notion of a gauge field has been extended and used in successful models of weak and strong interactions. Attempts to unify all these forces are also based on gauge theories and, if the connection in general relativity is recognized as a gauge potential, it appears that all particle interactions may accountable in terms of gauge fields.

Notwithstanding the tremendous success of gauge theories and quantum field theory, there are classes of phenomena in Q.C.D. which due to their non-perturbative nature, resist to any field theoretical approach. To deal with those phenomena, a very interesting alternative has been proposed by K. Wilson [59] : it consists in defining the theory on a lattice (L.G.T.) rather than in continuous space-time.

Every field theory can be defined on a lattice ; all that is required is the replacement of the partial derivatives occurring in the Lagrangian with finite difference operators. However, the lattice formulation of a gauge theory

is particularly elegant and natural. It is strongly related to the geometrical meaning of gauge theories. Though L.G.T. were developed as a regularization scheme and widely applied in Monte-Carlo calculations in quantum chromodynamics, they can also be implemented to any numerical computation which involve gauge fields, in order to achieve better numerical accuracy and credibility.

From computational point of view L.G. formulation is an odd complex and quite artificial discretization scheme. The main technical innovation is that the matter fields are associated with the vertices of the grid, while the gauge fields are associated with the oriented links. Furthermore the formulas which are used for the covariant derivatives are the least unusual. Naturally arises the question, why one should use L.T.G. ? To answer to this query and to bridge the conceptual gap between particle and computational physics, we give a short account of arguments which justify L.G.T. from either numerical and physical point of view. We start by emphasizing the importance of adopting the "right" discretization scheme.

To solve a set of partial differential equations in the computer, one has to use a scheme to transform the differential equations to difference equations. It is well known that the whole performance of the computation is very sensitive to the discretization scheme which is used. A striking example relative to our discussion, is considered below

Suppose we want to study numerically classical electrodynamics in $2+1$ dimensions in the absence of any charge sources. In the $A^0 = 0$ gauge the equations of motion are written

$$\partial_t E^1 = \epsilon_{12}\partial_2 B = \partial_2^2 A^1 - \partial_1\partial_2 A^2$$

$$\partial_t E^2 = \epsilon_{21}\partial_1 B = \partial_1^2 A^2 - \partial_1\partial_2 A^1 \qquad (5.2.1)$$

and the Gauss constraint reads : $\partial_k E^k = 0$. We discretize the system as follows. We define a $2-d$ lattice with lattice spacing $\Delta x = \Delta y = \alpha$ and the field $\mathcal{F}(\mathbf{x})$ is represented by $\mathcal{F}_{i,j}$ where $\mathcal{F} = (A^k, E^k)$. For convenience time is left continuous. The differential operators transform as

$$\partial_k \mathcal{F}(\mathbf{x}) \longrightarrow \frac{1}{2\alpha}(\mathcal{F}_{(i,j)+\hat{k}} - \mathcal{F}_{(i,j)-\hat{k}})$$

$$\partial_k^2 \mathcal{F}(\mathbf{x}) \longrightarrow \frac{1}{\alpha^2}(\mathcal{F}_{(i,j)+\hat{k}} + \mathcal{F}_{(i,j)-\hat{k}} - 2\mathcal{F}_{i,j}) \tag{5.2.2}$$

$$\partial_1 \partial_2 \mathcal{F}(\mathbf{x}) \longrightarrow \frac{1}{4\alpha^2}(\mathcal{F}_{i+1,j+1} + \mathcal{F}_{i-1,j-1} - \mathcal{F}_{i-1,j+1} - \mathcal{F}_{i+1,j-1})$$

A major problem arises when we consider the preservation of Gauss Law in the discrete system. In the continuous system, the Gauss constraint is preserved by the equations of motion i.e. $\partial_t(\partial_k E^k) = \partial_k \dot{E}^k = \partial_k \epsilon_{km} \partial_m B = 0$. To the contrary, implication of the difference equations leads us to the following result

$$\partial_k \dot{E}^k_{i,j} = \frac{3}{2\alpha^2}\partial_k A^k_{i,j} - \partial_2^2 \partial_1 A^1_{i,j} - \partial_1^2 \partial_2 A^2_{i,j} \tag{5.2.3}$$

where for notational simplicity we substituted in 5.2.3 the difference operators with the corresponding differential operators. It is evident that the discrete system fails to reproduce essential features of the continuous system, namely the preservation of gauss constraint, and even more the discrepancy remains in the continuum limit $\alpha \rightarrow 0$. A slight modification of the difference operators is enough to cure this disease. The trick is to write the discretized lagrangian of the system, using a left derivative formula for the differential operators, and then derive the equations of motion. The difference equations which are obtained this way do preserve gauss law. Moreover they have the additional feature of being invariant under discrete gauge transformations. This is not a coincidence. As we state below these two properties of a gauge system are mutually dependent.

The Lagrangian of a gauge system, is by definition invariant with respect to gauge transformations. This means that the time derivative of some components of the gauge fields, do not enter in the Lagrangian, because the gauge transformations contain arbitrary functions of time [60]. Consequently these components are not dynamical variables. Variation of the Lagrangian with respect to these components yields constraint equations, i.e. constraint equations are consequences of the gauge symmetry of the system.

One of the central features and prominent advantage, of the discretization scheme proposed by Wilson is that by construction retains the gauge symmetry of the continuum system. The underlying physical principles of that particular scheme is revealed when recalling the geometrical interpretation of the gauge fields.

5.2.2 The Geometry of Gauge Fields

Weyl was the first who tried to relate a gauge theory with geometry. Einstein's successful formulation of general relativity in 1916 unveiled a profound connection between gravitation and geometry. This discovery inspired Weyl (1919, 1921) to incorporate electromagnetism into geometry through the concept of a space-time dependent (local) scale transformation. His initial attempt to identify the scale factor with the vector potential A_μ was not successful. After the foundation of quantum mechanics it was realized that the correct scale factor should be iA_μ instead of A_μ and that what would be required would be invariance of the theory under space-time dependent phase transformation. However when Weyl finally worked out this approach, he retained his initial terminology [61].

There is a deep geometrical foundation to the gauge field concept. In analogy to the notion of parallel transport in general relativity, gauge potentials specify "transport operators", which can be used to compare orientations in some intrinsic space of matter fields, at different space points. For example consider a field theory in $2+1$ dimensions and a field Ψ which belongs to a definite representation of the gauge group $\mathcal{G}$, which for notational simplicity is identified with the $U(1)$ group. Under an infinitesimal parallel transport, the field $\Psi(\mathbf{x})$ undergoes, because of the local change of axes in internal space, an apparent change

$$\Psi(\mathbf{x}) \longrightarrow \Psi^T(\mathbf{x}\,;\, d\mathbf{x}) = \Psi(\mathbf{x}) + \delta\Psi(\mathbf{x}) \tag{5.2.4}$$

where

$$\delta\Psi(\mathbf{x}) = i\,\mathbf{A}(\mathbf{x})\,\Psi(\mathbf{x})\,d\mathbf{x} \tag{5.2.5}$$

For parallel transport of a finite interval from $\mathbf{x}$ to $\mathbf{x}'$ we can exponentiate

5.2.4 and obtain

$$\Psi^T(\mathbf{x}') = exp[i \int_C \mathbf{A}\, d\mathbf{y}]\ \Psi(\mathbf{x}) \tag{5.2.6}$$

All these suggest that the gauge fields in analogy to the Christoffel symbols of general relativity, are the connection coefficients, because they connect the components of a vector (in an internal space) at a point, to its components at a nearby point. In fact a parallel can be drawn between gauge theory and general relativity in the whole structure of the two theories [62]

To form a properly covariant derivative we have to compare $\Psi(\mathbf{x}+d\mathbf{x})$ not with $\Psi(\mathbf{x})$ but with the value $\Psi(\mathbf{x})$ would have if it were parallel transported from $\mathbf{x}$ to $\mathbf{x}+d\mathbf{x}$. The covariant is then reads (in the limit $\delta x_i \longrightarrow 0$)

$$\mathcal{D}_i\Psi = \tfrac{1}{\delta x^i}\big[\Psi^T(\mathbf{x});\,(-\delta x^i)) - \Psi(\mathbf{x}-\delta x^i)\big]$$

$$\Longrightarrow \mathcal{D}_i\Psi = (\partial_i - iA_i)\Psi \tag{5.2.7}$$

By using equation 5.2.7 for finite δx_i, we can derive the form of the covariant derivative. We discretize space by defining the field $\Psi(\mathbf{x}) \rightarrow \Psi_{i,j}$ on the vertices of a grid with lattice spacing α. The covariant derivative for $\delta x_i = \alpha$, reads

$$\mathcal{D}_k\Psi = \frac{1}{\alpha}\big[\Psi^T_{(i,j)+\hat{k}} - \Psi_{i,j}\big] \tag{5.2.8}$$

where

$$\Psi^T_{(i,j)+\hat{k}} = exp\big[-i\alpha A^k_{i,j}\big]\ \Psi_{(i,j)+\hat{k}}$$

Notice that the form of Ψ^T is immediate consequence of 5.2.5, where due to the discretization of space the value of the gauge field along the link which connects the neighbouring vertices, has been taken constant. The previous example, suggests that on the lattice the gauge dynamical variables should be associated with the oriented links between neighbouring vertices rather than the vertices themselves. Moreover since α plays the role of the infinitesimal displacements of the continuum system, we can take as basic dynamical variables the finite group elements $U^k_{i,j}$ of $\mathcal{G}$

$$U^k_{i,j} = exp[i\alpha A^k_{i,j}]$$

The formulation of the gauge dynamical term also departs from geometrical notions. In the continuum theory, the all important $F_{\mu\nu}$ is associated with a sort of closed path, namely the one defined by the infinitesimal parallelogram of sides dx^μ and dx^ν. The lattice equivalent of the elementary closed loop is the perimeter of a square usually called the plaquette having vertices in 4 neighbouring sites. The corresponding transport operator is denoted by $U^p_{i,j}$

$$U^p_{i,j} = U^1_{i,j} U^2_{i+1,j} U^{*1}_{i+1,j+1} U^{*2}_{i,j+1}$$

In the continuum theory the gauge action is defined in terms of $F_{\mu\nu}$. Similarly, $U^p_{i,j}$ is used for the construction of the lattice gauge action. The requirements that determine the form of the action, is that it must be a gauge invariant function of the plaquette transport operator and that formally shall reduce to the continuum

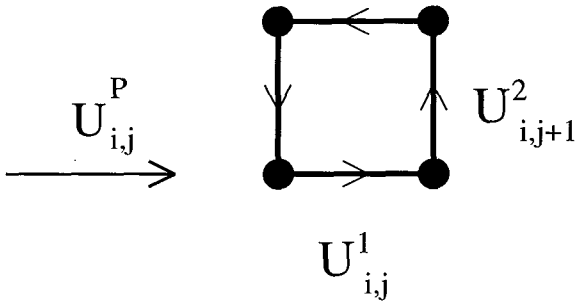

Figure 5.1 : *The Plaquette action* $U^p_{i,j}$

theory as $\alpha \to 0$. Thus we are led to a dynamical term for the gauge variables

$$S_U = \frac{1}{\alpha^2} \sum_{i,j} (1 - \frac{1}{2} Re(U^p_{i,j}) \qquad (5.2.9)$$

Note that there are more than one ways to define a discrete action which meets these constraints, and in literature there are several alternatives [63].

Hitherto we have demonstrated in some detail the basic features of a

gauge theory defined on a lattice as those naturally arise from the geometrical interpretation of the gauge theories. We will proceed further by applying similar considerations in our model Lagrangian 2.2.4 in order to derive the difference equations which then will be integrated numerically.

5.3 The Motion of a Vortex Pair

In this section we consider the physical problem of two vortices initially placed at a distance d from each other. Our objective is to study the time evolution of the vortex pair system induced by their mutual interaction.

The dynamics of the system is determined by equations 2.2.7 which we are unable to treat analytically. Thus we performed a large number of simulations for various values of the parameters κ, β and different separations d.

Difference equations

The computer simulation of any continuous dynamical system presupposes a discretization of its degrees of freedom. In order to maintain as much as possible the symmetries of the continuous system in its discretized form we adopted techniques from lattice gauge field theory [64]. The points

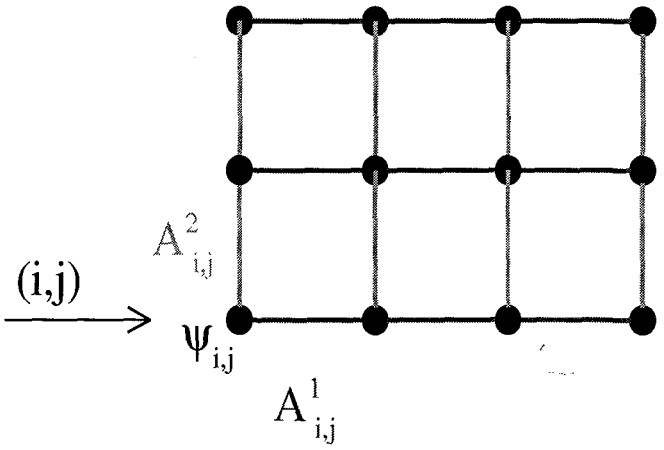

Figure 5.2 : *The 2-dimensional grid which is used to discretize the continuous system*

of space are replaced with a two dimensional lattice (Fig. 5.2) with lattice spacing α. The matter field $\Psi(\mathbf{x})$ is represented by the variables $\Psi_{i,j}$ which live on the vertices of the lattice, while the gauge fields $A_1(\mathbf{x}), A_2(\mathbf{x})$ are represented by $A^1_{i,j}, A^2_{i,j}$, which live on the oriented links of the lattice. (A^1 lives on the links in the x_1 direction and A^2 on the links in the x_2 direction.) The time component of the electromagnetic potential $A_0(\mathbf{x})$ represented by $A^0_{i,j}$ lives also on the vertices of the grid. At that stage time is left continuous. It will be discretized later with time step much smaller than α. The lattice version of the covariant derivative is

$$D_k\Psi_{i,j} = \frac{1}{\alpha}(U^k_{i,j}\Psi_{(i,j)+\hat{k}} - \Psi_{i,j}) \qquad where \qquad U^k_{i,j} = exp(-i\alpha A^k_{i,j}) \tag{5.3.1}$$

Using the above definition for the covariant derivative, the action for the discretized system reads

$$S = \int dt\, \alpha^2 \sum_{i,j} \Big[\frac{1}{2}[\Psi^*_{i,j}(i\partial_t - A^0_{i,j})\Psi_{i,j} + c.c.] + A^0_{i,j} - \frac{1}{2}|D_k\Psi_{i,j}|^2 + \frac{1}{2\beta}\mathbf{E}^2_{i,j}$$

$$- \frac{1}{8}\kappa^2(\Psi^*_{i,j}\Psi_{i,j} - 1)^2 - \frac{1}{\alpha^4}[1 - cos(\alpha(A^1_{i,j} + A^2_{i,j+1} - A^1_{i+1,j} - A^2_{i,j}))]\Big] \tag{5.3.2}$$

where $E^k_{i,j} = -\partial_t A^k_{i,j} - \frac{1}{\alpha}(A^0_{(i,j)+\hat{k}} - A^0_{(i,j)})$. The last term of 5.3.2 corresponds to the dynamical term of the gauge field and as can be easily checked in the $\alpha \to 0$ limit goes to the familiar B^2 term.

The discretized system retains the gauge symmetry which possessed in its continuous form, which in turn ensures that difference equations will preserve Gauss constraint. Specifically, the action 5.3.2 is by construction invariant under the transformation

$$\begin{aligned} \Psi_{i,j} &\to exp[i\Lambda_{i,j}]\Psi_{i,j} \\ A^k_{i,j} &\to A^k_{i,j} + \tfrac{1}{\alpha}(\Lambda_{(i,j)+\hat{k}} - \Lambda_{i,j}) \\ A^0_{i,j} &\to A^0_{i,j} - \partial_t\Lambda_{i,j} \end{aligned} \tag{5.3.3}$$

This is the discrete version of the gauge transformations 2.2.10. As a consequence of the above symmetry the system obeys the constraint

$$\frac{1}{\alpha}\sum_{k=1,2}\{\,(E^k_{(i,j)+\hat{k}}-E^k_{i,j})\,\}\;=\;\beta(\Psi^*_{i,j}\Psi_{i,j}-1) \qquad (5.3.4)$$

which is the discrete version of Gauss law. By varying the action 5.3.2 with respect to $\Psi^*_{i,j}$ and $A^k_{i,j}$ we obtain the following difference equations

$$i\dot{\Psi}\;=\;\frac{1}{2\alpha}\sum_{k=1,2}\{\,U^{k*}_{(i,j)-\hat{k}}(D_k\Psi_{(i,j)-\hat{k}})-(D_k\Psi_{(i,j)})\,\}+\frac{1}{4}\kappa^2(\Psi^*_{i,j}\Psi_{i,j}-1)\Psi_{i,j}$$

$$\frac{1}{\beta}\dot{E^k_{i,j}}\;=\;\frac{i}{2\alpha}[U^k_{i,j}\Psi_{i,j+\hat{k}}\Psi^*_{i,j}-U^{k*}_{i,j}\Psi^*_{i,j+\hat{k}}\Psi_{i,j}]+\frac{1}{\alpha^3}\sum_{l\neq k}\{sin[\alpha(A^k_{i,j}+A^l_{i,j+\hat{k}}$$

$$-A^k_{i,j+\hat{l}}-A^l_{i,j})]-sin[\alpha(A^k_{i,j-\hat{l}}+A^l_{i,j+\hat{k}-\hat{l}}-A^k_{i,j}-A^l_{i,j-\hat{l}})]\} \qquad (5.3.5)$$

In the derivation of the difference equations we have used the gauge symmetry of the system to eliminate the A_0 component. This particular choice of gauge simplifies considerably the equations of motion and make the numerical task more tractable.

Initial data

We begin the simulation with initial data describing two vortices in separation d. The value of d is properly chosed to ensure that the vortices feel each others presence. That particular constraint on d complicates the determination of the initial data in the sense that the system which we want to describe is dynamical. The current problem is more difficult than its equivalent in the study of scattering properties of solitons in relativistic models. There, the solitons are initially supposed to be apart enough, and initial data are constructed quite accurately by proper superposition of isolate soliton solutions. To the contrary in our case one has to introduce a field configuration - the initial state - which essentially corresponds to a snapshot of the dynamical system of two interacting vortices in given distance. Yet that snapshot depends on the details of the process which brought the vortices close to each other.

We overcome this complication as follows. We introduce as initial data an approximate configuration which reproduces the physical properties of the system under consideration. Namely we use the constrained variational calculation presented in chapter *III* to relax the fields to that configuration which minimizes the energy of the system of two vortices at separation d. We expect that this configuration is quite accurate, especially in the limit where the two vortices have approached each other very slowly. We also use the knowledge we obtained from the study of the static sector to restrict to certain values of d ($d = 3 - 7$ for $\kappa \sim 1$ and $\beta \sim 0.1$), which ensure non trivial vortex interaction, but not so strong as to distort considerably the shape of each vortex.

Boundary Conditions

In this kind of simulations the proper treatment of the boundary conditions is important and requires special attention. After some experimentation we boiled down to the adoption of Neumann boundary conditions. This corresponds to setting the covariant derivative in the normal to the boundary direction equal to zero. To do so we fixed the value of the Higgs field at each point of the external layer of the grid equal to their first inner neighbour. Also the values of the gauge fields, which live at the links which connect those neighbours, were set equal to zero. To test the influence of the boundaries in our calculations we ran simulations in bigger grids and confirmed that our results are insensitive to any enlargement of the grid.

Potential Energy

We proceed further by computing the interaction energy between the two vortices, a quantity strongly related to the dynamics of the system. At that point we make a definite choice of the parameters.

We set $\beta = 0.04$ and $\kappa = 1.5$. Implementation of the techniques mentioned in chapter *III* enables us to compute the minimum energy $E(d)$ of the vortex pair for several separations d. By defining the interaction energy as $U(d) = E(d) - 2E_{N=1}$ where $E_{N=1}$ is the energy of a single $N = 1$ vortex, we evaluate $U(d)$ which is then plotted in Fig. 5.3. According to the graph $U(d)$ is repulsive for all distances and falls to zero very quickly. Considering the evolution of two vortices initially kept in separation d one

would naively expect that the two vortices will move further apart in order to minimize their energy. However the analysis of the canonical structure of the model (chapter *III*) implies a different scenario. The vortices are expected to exhibit Hall behaviour, namely they are expected to move in a direction perpendicular to the applied force. Thus it is more likely that the two vortices will rotate around each other in analogy to the motion of two electrons in a plane under the influence of a perpendicular magnetic field.

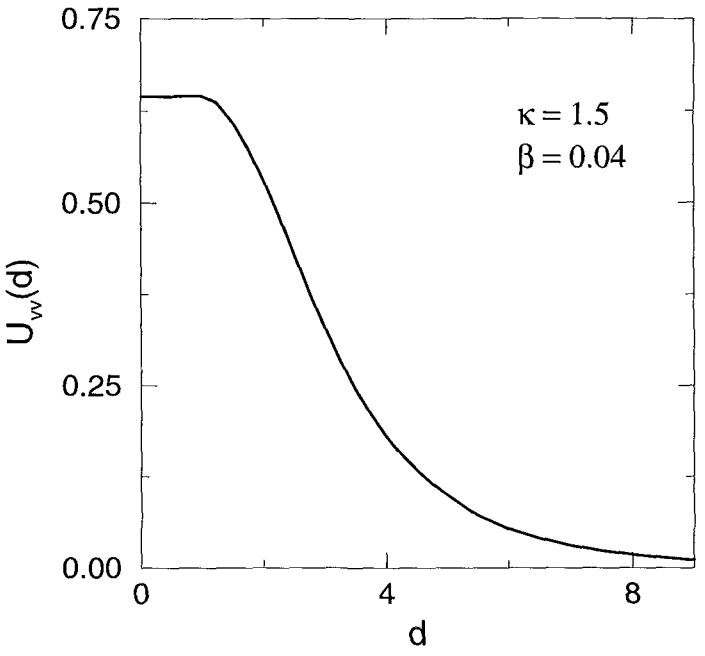

Figure 5.3 : *The interaction energy of two single vortices for* $\kappa = 1.5$ *and* $\beta = 0.04$ *as a function of their separation* d.

The rotation of the vortex pair

We perform the first simulation for initial separation $d = 4$. That particular choice of d ensures that vortices are close enough to yield significant interaction, while at the same time apart enough to describe two well separated objects. Initially the two vortices were located on the x-axis at

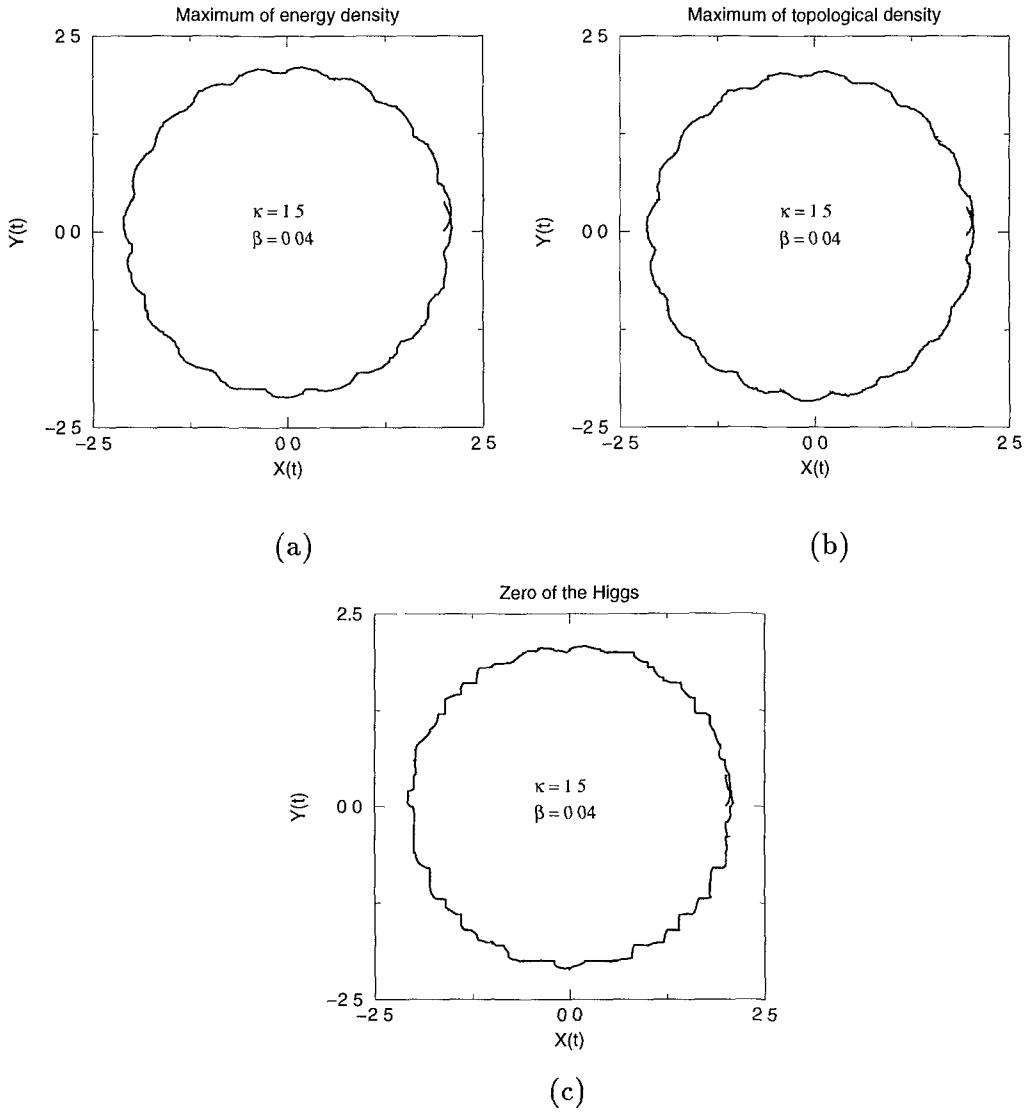

Figure 5.4 : *The trajectory of one vortex of the pair as determined by the location of the maximum of the energy density (fig. 5.4a), of the maximum of the topological density (fig. 5.4b) and of the zero of the scalar field ψ (fig. 5.4c). Time duration t=800.*

positions $(+\frac{d}{2},0)$ and $(-\frac{d}{2},0)$. The motion of the vortices is illustrated in detail in figures 5.4, 5. 5 and 5.6. As it turns out the vortices rotate around each other in roughly circular orbits.

In Fig. 5.4 the trajectory of the "center" of one of the vortices is plotted. To avoid overlapping of the trajectories, we interrupted the simulation when the vortices completed one whole rotation, i.e. at $t = 800$ time units. For the same reason only the trajectory of the vortex which was initially located at the right-half plane is plotted in Fig. 5.4. The other vortexs trajectory is the mirror image with respect to the origin of the coordinate system and thus it is omitted. Because any definition of the center of a non-symmetric extended object is ambiguous we use three different methods to determine the positions of the "centers" of the vortices. Thus in Fig. 5.4a we plot the trajectory of the vortex as this is determined by tracking the maximum of the energy density w. In Fig. 5.4b the maximum of topological density τ (as defined in equation 2.5.9) is tracked, while in Fig. 5.4c we track the location of the zeros of the Higgs field. In principle none of these methods determines accurately the position of a vortex, but it is expected that each of them provides a reasonable description of the overall motion of the vortices Because of this uncertainty these three different measurements of the position do not have to coincide. The fact that they yield quite similar results implies that the vortices perform very organized motion without significant oscillatory activity in their interior.

Apart from the rotation around the origin, a finer periodic motion can be perceived in the trajectory of the vortex. The motion of the vortex is like a cycloid along a cyclic orbit and strongly reminds us of similar patterns which are encountered in the motion of interacting charged particles under the influence of external magnetic fields. We call that finer motion "larmor" motion and we will study it in detail later in this section.

Useful information concerning the shape of the vortices is obtained from Fig. 5.5 where the energy density at specified times is plotted as $3-d$ surface plot. Specifically it is plotted the energy density of the initial state (a) and three snap-shots (b), (c), (d) corresponding to time t = 200, 500, 700 respectively. We see that each of the two energy lumbs is almost spherically symmetric in agreement to previous remark that the vortices are essentially

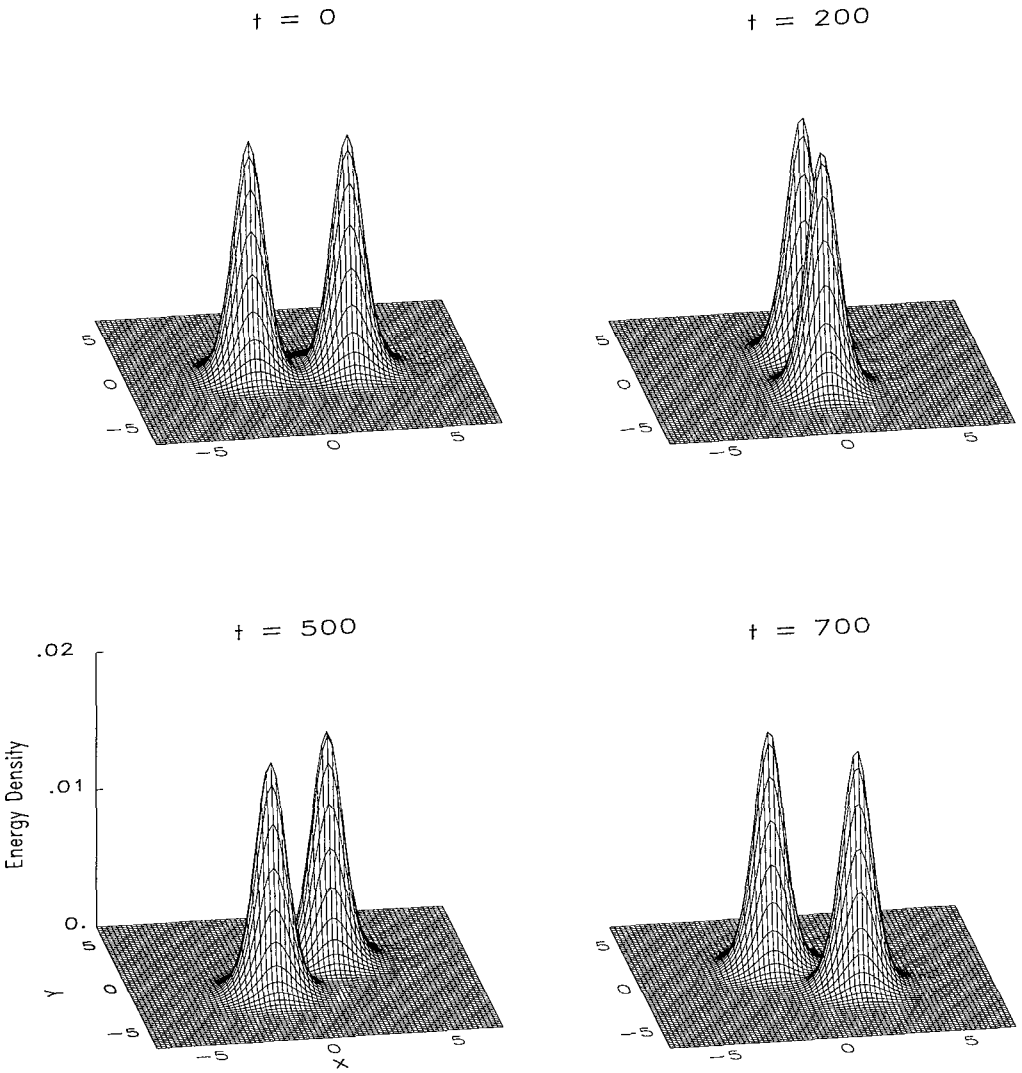

Figure 5.5: *Four snapshots of the profile of the energy density of the vortex pair.*

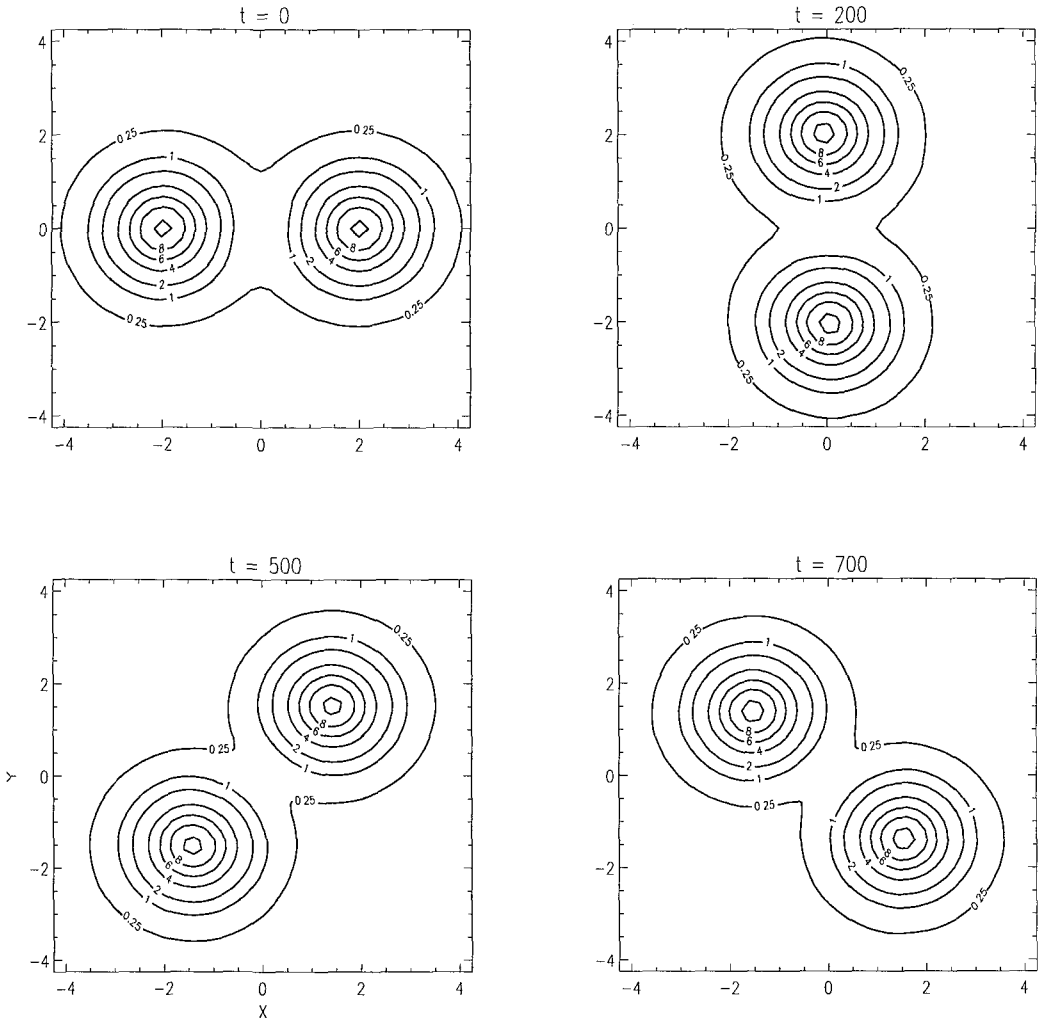

Figure 5.6: *The energy density contours for the same four snapshots as in fig. 5.5.*

undistorted. Even more the shape of the energy profile seems to remain unchanged during the rotation. A more detailed examination including animation of successive snap-shots revealed a small oscillation of the size of the energy lumb. In fact the energy lumb slightly spreads and shrinks with a period equal to that of the larmor motion. Finally in Fig. 5.6 the contours of the energy density are plotted for the same snap-shots, where the rotation of the vortex and the rigidness of its motion are demonstrated beyond any doubt.

Like in any numerical calculation there is a relevant error in our results and their reliability is under question. One way that one can partly check the accuracy of the results is by examining the manner in which the conservation laws are respected during the evolution. We start by considering Gauss law, which is essentially a local conservation law. Its preservation is built in the construction of the difference equations, and according to the results is conserved amazingly well. After a complete period, the total deviation from Gauss law (the sum of deviation over all points of the grid) was less than 10^{-6}. Similarly, the total energy of the system is conserved after the completion of a period up to the third decimal digit i.e. with accuracy better than 0.05%. The total energy W as function of time is plotted in Fig. 5.7 as well as its four components W_e, W_b, W_d and W_v. While the components of the energy are oscillate vividly, their sum is a perfect straight line parallel to the time axis. Angular momentum exhibits a similar behaviour as follows from Fig.5.8, where the angular momentum l and it's two components l_1 and l_2 are plotted. While both components undergo wide oscillations the total angular momentum is conserved reasonably well. Comparison of Fig. 5.4 and Fig. 5.8 reveals a systematic relation between the period of larmor motion and that of angular momentums oscillations. This relation has its origin in the algebraic form of the l_1 component of angular momentum. As it follows from equation 4.2.15 l_1 is proportional to the second moment of the topological density and as such it is a measure of the size of the vortex pair. Due to the larmor motion the size of the pair (the inter-vortex separation) oscillates and that oscillation is reflected in the value of l_1. Note that a periodical pattern with the same period can be also detected in the energy plots after careful examination. It seems that this oscillating behaviour is a general feature of the system.

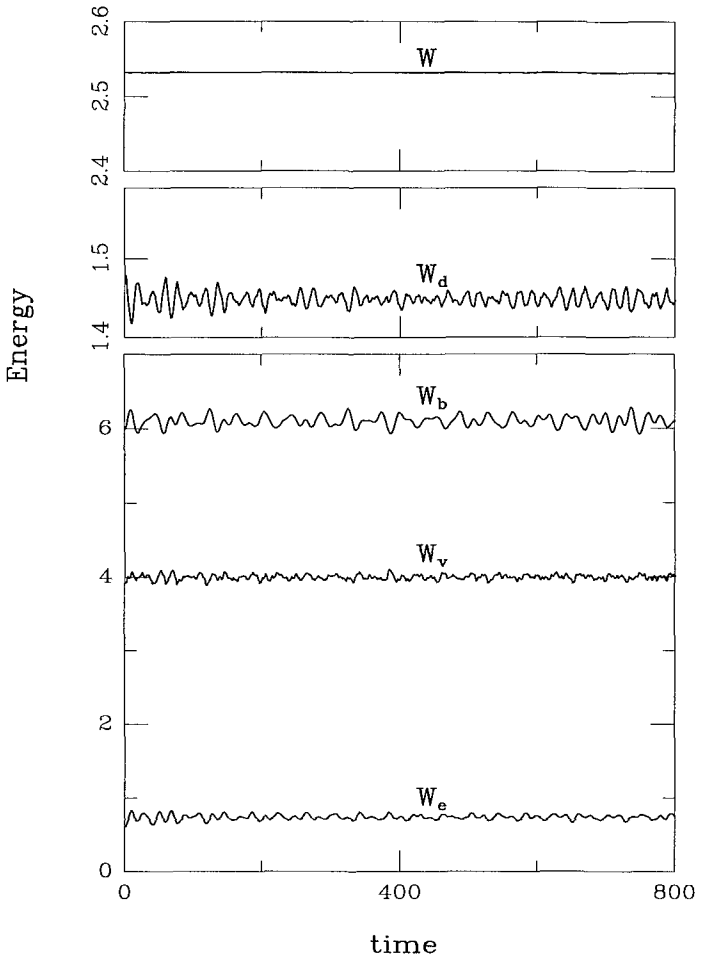

Figure 5.7 : *The time dependence of the various components of the energy of the vortex pair and the total energy W. Note the high accuracy in the conservation of the total energy of the system.*

Another quantity of interest, the total topological charge N is plotted as a function of time in Fig. 5.9. N takes the value 1.993 at $t = 0$ and retains that value, up to small fluctuations during the evolution. The

slight deviation from the $N = 2$ value of the continuum limit is due to the discretization of space.

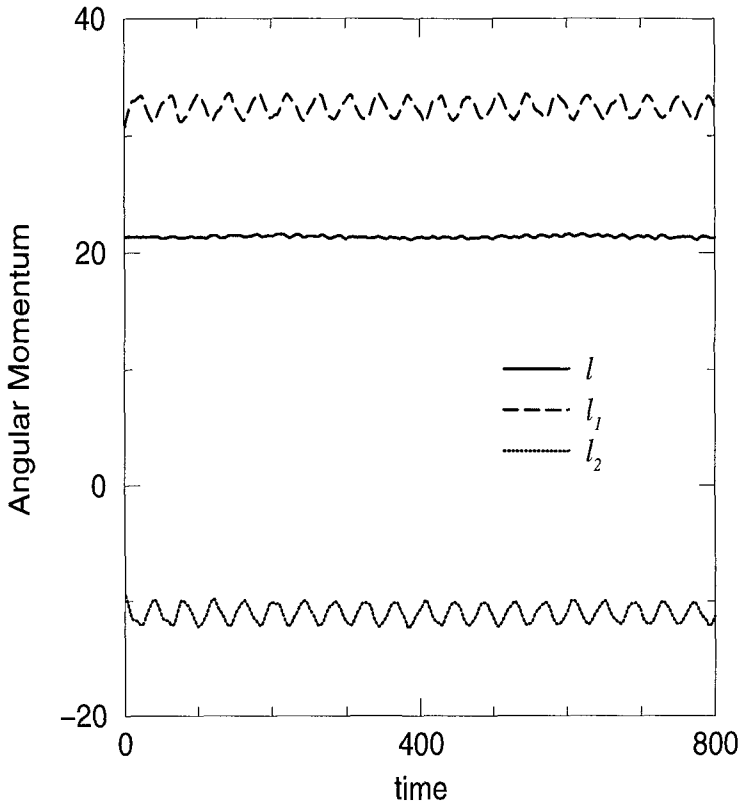

Figure 5.8 : *The two pieces of the angular momentum and their sum. The conservation of the total angular momentum to within 2% is quite satisfactory.*

Last but not least is considered the guiding center of the system (or equivalently the linear momentum) which is a conserved quantity. Due to the symmetry of the initial configuration the guiding center initially coincides with the origin of the coordinate system and remains there through out the simulation.

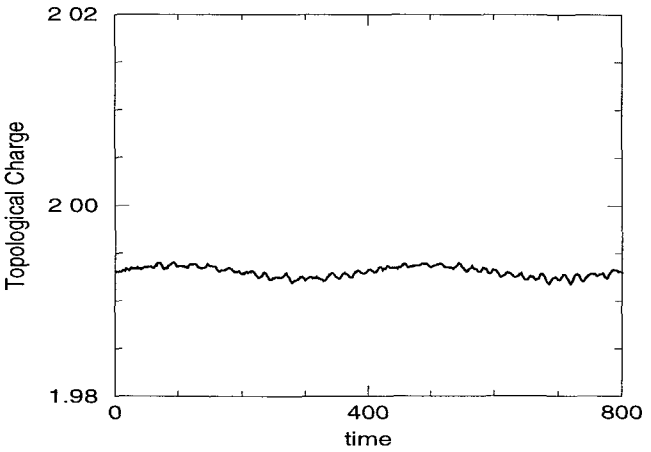

Figure 5.9: *The time evolution of the topological charge of the vortex pair.*

So far, the general picture that arises confirms the Hall behaviour of the system in accordance to the analytical predictions. Furthermore the system is characterized by periodic patterns which - to mention only one of them - in the trajectory plots are manifested as the "larmor motion". The credibility of the results is supported by the high accuracy in the preservation of several characteristic quantities of the system. Within this model we performed a large number of simulations for several values of the parameters. In the subsequent simulations the above properties, i.e. rotation, larmor motion and high accuracy , are to be considered valid unless we explicitly state otherwise.

We now focus in what we called larmor motion. We would like to stress the analogy to the larmor precession encountered earlier in the two electron problem. By comparing Fig 5.4a,b to Fig. 4.1 we see that the orbits of the electrons exhibit exactly the same patterns. Moreover a systematic coresspondence can be established in the details of larmor motion in the two systems. Due to the simplicity of the electron system we can derive analytically some features of the larmor motion. Specifically, when the separation of the two electrons decreases the length and the width of that finer oscillatory motion of the electrons increases. Similar is the effect of

decreasing the strength of the magnetic field or increasing the electron-electron coupling. On the other hand the response of the vortex system in the decrease of d is quite the same. To illustrate that point we performed a number of simulations where κ and β were kept fixed while d varied. The trajectories of the vortices for $d = 2.7, 3.4, 4., 5.$ are plotted in Fig. 5.10.

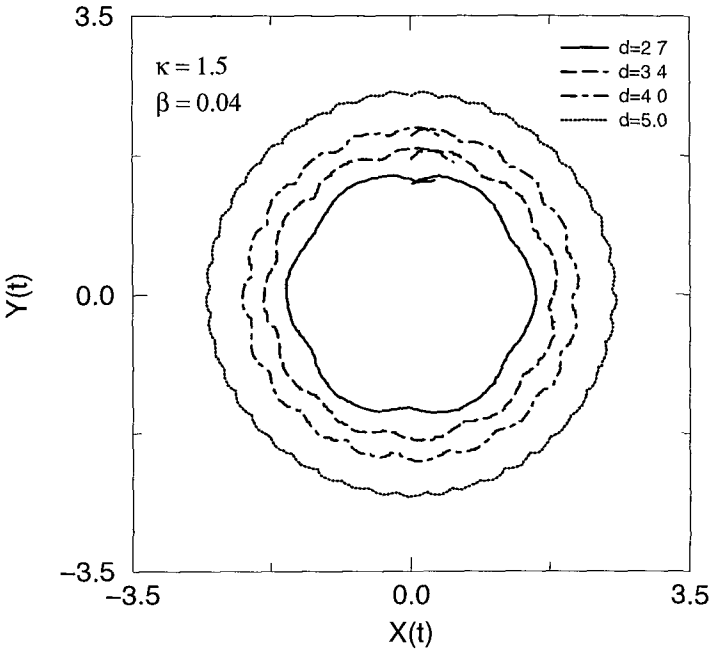

Figure 5.10 : *The dependence of the internal larmor motion of each vortex on their separation d.*

To demonstrate the analogy between the two cases we also plot in Fig. 5.11 the trajectories of the electrons for different separations $d = 1., 1.25, 1.5, 2.$ We also ran another set of simulations to study the dependence of the motion of the vortices on the parameter β. d and κ were kept fixed to the values $d = 3.6$ and $\kappa = 1.5$ while β varied. The resultant trajectories are plotted in Fig. 5.12 for four different values of $\beta = 0.01, 0.02, 0.04, 0.08$. It is worthwhile mentioned that as larmor motion is concerned, variation of β has the same effect to that variation of the magnetic field strength or the electron-electron coupling have in the electron problem. The time duration

for each simulation was the same ($t = 670$). As it is shown in Fig. 5.12 for larger $\beta's$ the arc of the trajectory which is plotted increases, which subsequently implies that the angular velocity also increases. This increase has its origin in the fact that as β grows the form of the potential becomes steeper, which in turn results a stronger interaction between the vortices.

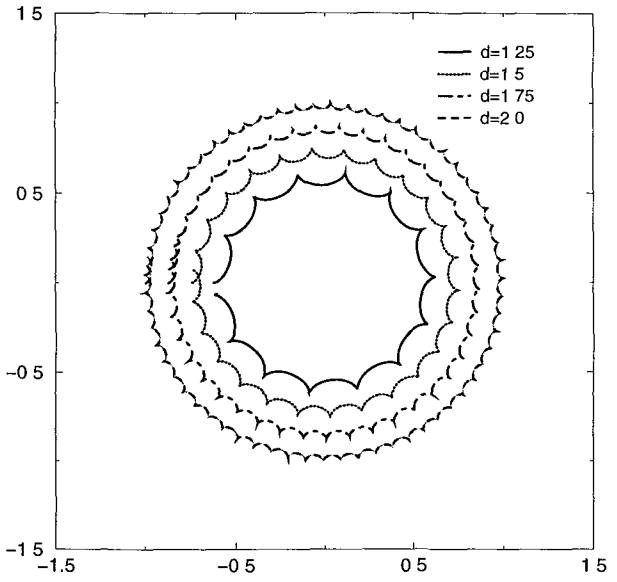

Figure 5.11 : *The dependence of the internal larmor motion of each electron on their separation d.*

Of course one should not take that analogy between B and β literally since the vortex system is far more complicated. Nevertheless we consider this analogy interesting and indicative of the crucial role which the common algebraic structure of the two systems plays.

As we mentioned in the previous chapter there are analytical arguments in support of the "Hall behaviour" of the vortices. Equation 4.2.22 already implies vortexs rotation and even more determines the handedness of the rotation. In fact it follows from 4.2.22 that the way each vortex rotates is determined by the orientation of the external force which acts on it, and thus it depends on the slope of the potential. When the potential between

the vortices is attractive the vortices will rotate clockwise, while they will rotate counter-clockwise if it is repulsive. This is clearly demonstrated in Fig. 5.13 and Fig. 5.14. In Fig.5.13 we plot the vortex-vortex potential for $\kappa = 0.5$ and $\beta = 0.005$.

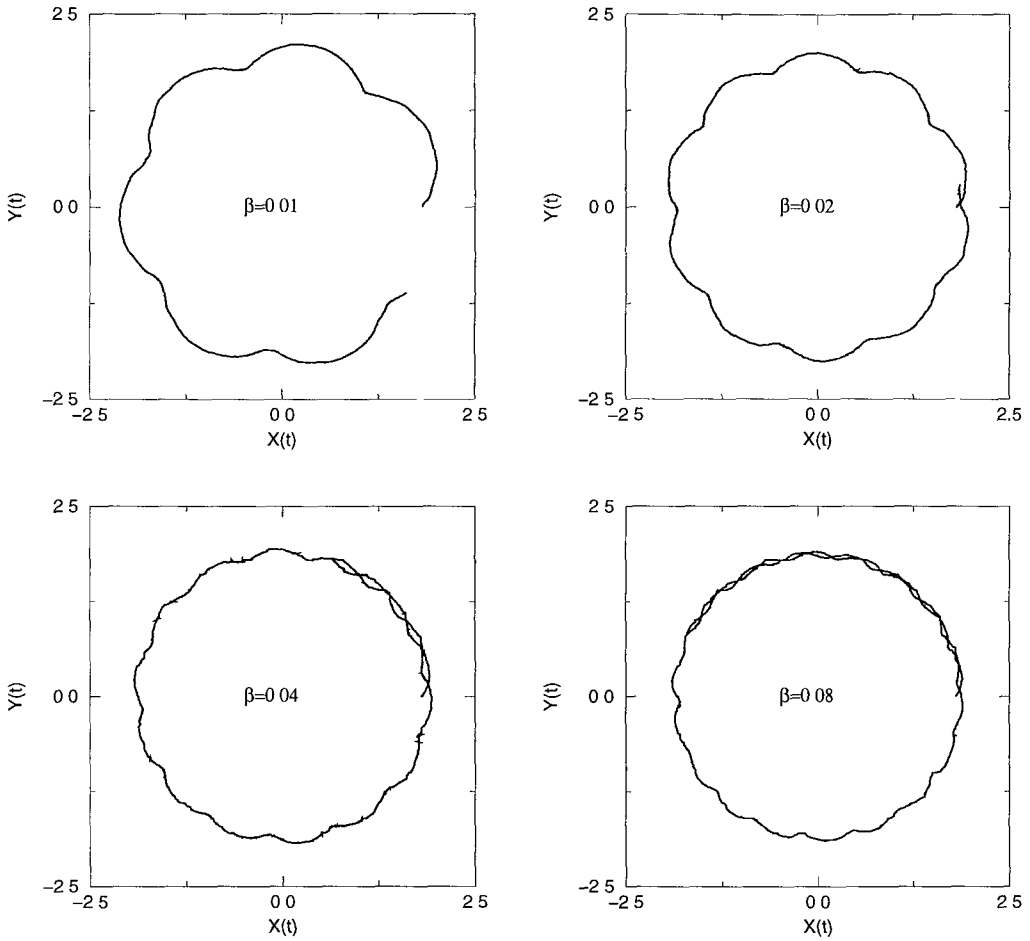

Figure 5.12 : *The vortex motion for various values of the parameter* β

This particular choice of the parameters results a bumb in the form of the potential, i.e. the potential is not monotonous function of d. Then we choose two values of d, $d = 4.5$ and $d = 8$ which correspond to attractive

and repulsive regions of the potential respectively. We run two simulations; one for a vortex pair at separation $d = 4.5$ and another for a vortex pair at separation $d = 8$. The trajectories of the vortices which were initially located at the positive x-axis in each of these two simulations are plotted in Fig. 5.14.

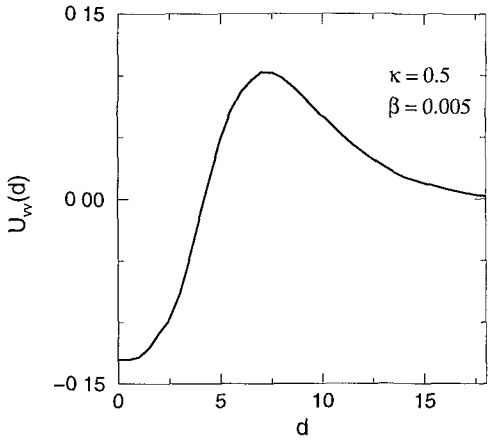

Figure 5.13 : *The interaction energy of two single vortices for* $\kappa = 0.5$ *and* $\beta = 0.005$. *The potential is attractive for small distances and repulsive for* $d \geq 7$.

As it is shown in Fig. 5.14 the direction of the rotation of the vortices is in agreement to our previous prediction. Note that the previous results can be used as a cross check which verifies that in a certain region of the parameters the inter-vortex potential has a bumb [28]. Another feature we encounter in Fig. 5.14 is the quick oscillation of vortexs position, which can be attributed to the fact that internal degrees of freedom of the vortex oscillate vividly. As a consequence the determination of the exact position of the vortex is ambiguous. The maximum of energy density which has been tracked in order to plot Fig. 5.14 does not reflects the exact position of the vortex. Nevertheless the tracking succeeds to describe the overall motion of the vortices which again are in complete agreement to the theoretical prediction. After some experimentation we have come to the conclusion that internal oscillatory activity is a common feature of small $\kappa's$ region. Indicatively for $\kappa = 0.5$, one has to increase β up to values of order $\sim 10^2$ in order to recover rigidness in the motion of the vortex. It seems that

the presence of the potential plays an important role in the coherence of the moving vortex and one has to understand analytically the underlying reason.

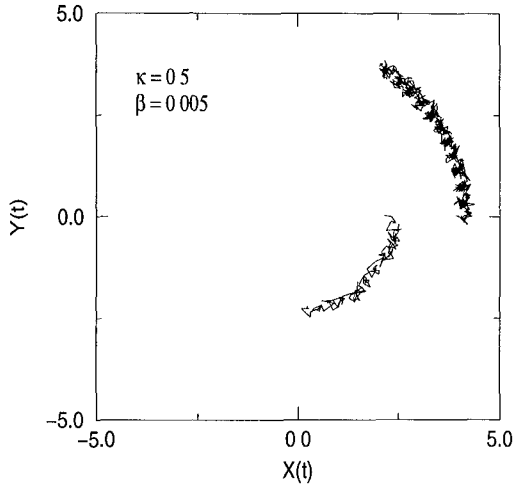

Figure 5.14 : *The interaction energy of two single vortices for* $\kappa = 0.5$ *and* $\beta = 0.005$.

The quantitative comparison of theoretical estimations and numerical results is the next issue we address. A rough estimation of a vortexs revolution period is derived analytically and is then compared to the result obtained through straightforward numerical calculation. The analytical calculation is based on the assumption that each individual vortex behaves like a rigid body which lives in a potential equal to the vortex-vortex potential. When $d \gg L$ we can approximate the two vortices as point particles and then our assumption is valid, but for intermediate $d's$ like those examined here such an approximation is questionable. Although our assumption is not completely justified, the rigidness of the motion of the vortices as that arises from earlier numerical experiments, supports its validity.

The calculation proceeds as follows. The potential $U(d)$ as well as its gradient $F = \frac{\partial U}{\partial d}$ is computed for $\kappa = 1.5$,. and $\beta = 0.04$ (Fig. 5.1). By substituting the value of the gradient for certain d in equation 4.2.22 we obtain the velocity $V(d)$ of each vortexs guiding center and use it to calculate the period of vortexs revolution $T = \frac{2\pi R}{V}$, where $R = \frac{d}{2}$. In Fig. 5.15 the period of the revolution of the vortex pair is plotted as a

function of d. Continuous curve corresponds to the theoretical prediction while triangular points represent the results obtained when simulations were performed for specific separations d. The coincidence of the two curves is remarkable It is quite surprising that the result we obtain with such a crude calculation are in good agreement to those we get from explicit numerical simulations.

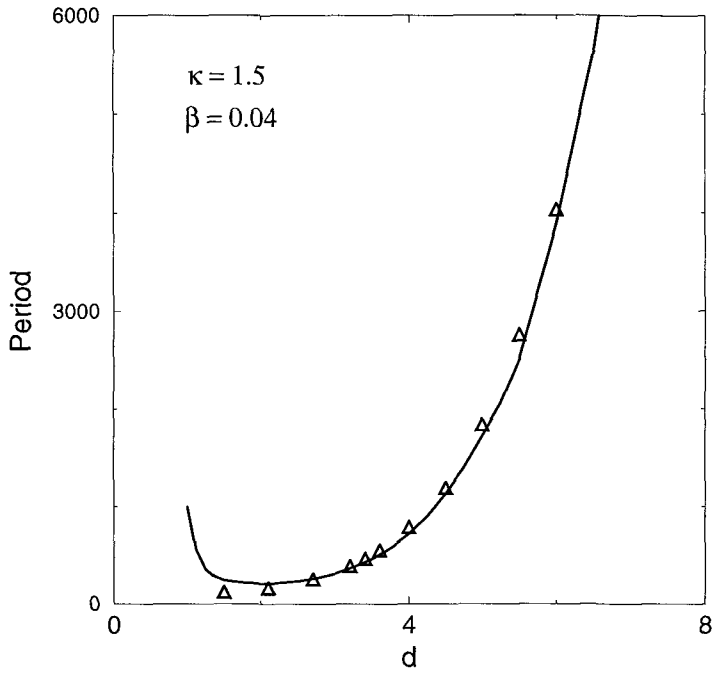

Figure 5.15 : *The period of revolution of the vortices around each other as a function of their separation, computed (solid line) from the theoretical formula and the slope of the curve of Figure 5.1 and from the numerical simulation (triangular points).*

The coincidence of the results is remarkable and indicates that our assumption on the rigidness of the motion of the vortices is valid even for relatively small $d's$ $(2-3$ space units). While commenting on the motion of the vortex earlier we encountered several other indications supporting that picture. The relative difference in the calculation of the period increases

for $d's \leq 2$, a behaviour which is considered natural since for small $d's$ the assumption we did weakens. Relevant to this deviation is the error in the calculation of the gradient of the potential. Successive calculations of the potential and its gradient using bigger grids resulted a 1% error in gradient's evaluation which is quite insignificant.

5.4 Vortex-antivortex pair

Now we modify the previous problem by substituting one of the vortices of the pair with a $N = -1$ antivortex. The system we obtain is equivalent to a vortex -antivortex pair in separation d and this section is devoted to the study of its dynamics. At that point we are in position to appreciate the similarity of our system to that of two charged particles moving in a plane in the presence of a perpendicular magnetic field. Thus to gain some insight to the problem we recall what happens when an electron-positron pair interacts under those circumstances. In that case as we can easily check (see also Fig 4.2) the guiding centers of the particles move along parallel lines while the orbits of the particles perform cycloid motion along those lines. Similarly we expect the vortex and the antivortex to move in formation along parallel trajectories. That picture contradicts intuition which suggests that the vortex and the antivortex will gradually come closer to each other and finally will annihilate to radiation.

A series of simulations were performed for the vortex-antivortex pair system. In the problem at hand, the implementation of any constrained calculation is not possible, and simple superposition methods were invoked to produce the initial data. Namely to construct the initial field configuration, two vortex fields with winding number $N = 1$, and $N = -1$ were superposed according to the rule

$$\begin{aligned} \Psi(\mathbf{x}) &= \Psi^{(1)}(|\mathbf{x} - \tfrac{\mathbf{d}}{2}|)\, \Psi^{(-1)}(|\mathbf{x} + \tfrac{\mathbf{d}}{2}|) \\ \mathbf{A}(\mathbf{x}) &= \mathbf{A}^{(1)}(|\mathbf{x} - \tfrac{\mathbf{d}}{2}|) + \mathbf{A}^{(-1)}(|\mathbf{x} + \tfrac{\mathbf{d}}{2}|) \end{aligned} \qquad (5.4.1)$$

where $\Psi^{(1)}, \mathbf{A}^{(1)}$ are the static fields of the $N = 1$ vortex and $\Psi^{(-1)}, \mathbf{A}^{(-1)}$

are those of the $N = -1$ antivortex. The A_0 field was determined by solving the Poisson equation for the given Ψ configuration. A gauge transformation 5.3.3 was further imposed to the fields to switch to the $A_0 = 0$ gauge.

The trajectories of the vortices in a typical run of a vortex-antivortex pair are illustrated in Fig. 5.16. The exact positions of the centers were determined by tracking the maxima of energy density. The parameters took

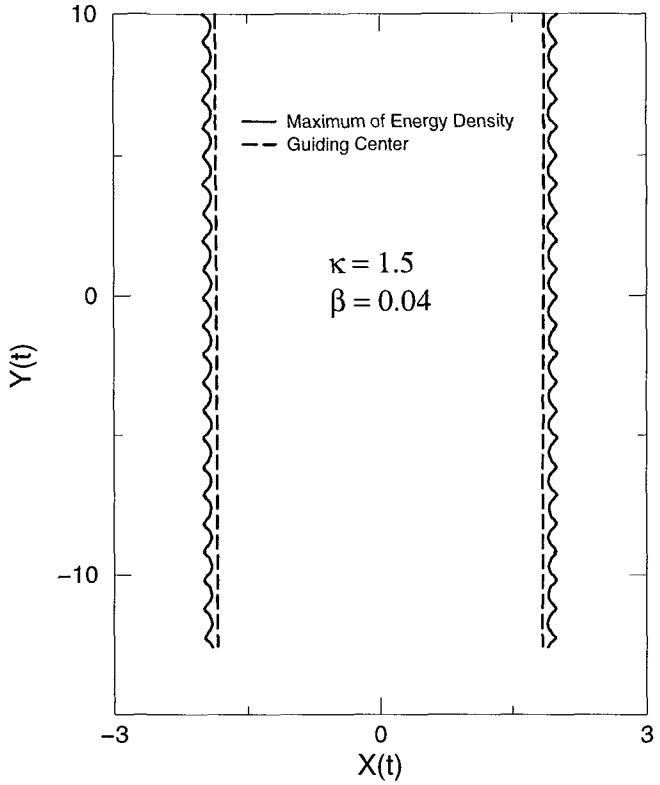

Figure 5.16 : *The typical evolution of an initial vortex-antivortex configuration. The lines shown are the trajectories of the maxima of the energy density of the system.*

the values $\beta = 0.04$, $\kappa = 1.5$, and $d = 4$. Initially the $N = 1$ and the $N = -1$ vortices were placed at the points $(-2, 10)$ and $(2, 10)$ respectively.

The vortices moved in the negative y-direction for 20 space units $\simeq 25$ times their size retaining their initial shape and keeping their initial separation constant. They moved with constant velocity $V_2 = -0.0257$. This value is to be compared to the velocity in the vortex-vortex pair case which for the same values of parameters and separation was found to be $V = 0.016$. The higher velocity in the vortex-antivortex case implies a steeper potential between them than in the case of the vortex pair.

Apart from the parallel transport of vortices, there is finer oscillating motion similar to the "larmor motion" we encountered in the previous section. We ran several simulations to study the details of larmor motion for various values of d and β. It turns out that as in the vortex pair case both length and width of the oscillation are decreasing functions of either d or β. Moreover we verified that (as one would expect) the precession of the electron (or positron) in the electron-positron system exhibits the same response to the decreasing of either the initial distance between the particles or the intensity of the external magnetic field B.

We bring the discussion of the results to an end by making a final comment on boundary effects. As it follows from Fig. 5.16 if we neglect the oscillation originated by the larmor motion, the paths of the two vortices are perfect straight lines parallel to the y-axis. When the two vortices are close enough to the boundaries this picture alters. The vortices move along almost parallel lines but a slight convergence of the trajectories towards each other is observed. When the vortices have moved sufficiently apart from the boundaries ($6 - 7$ space units) the convergence disappears to appear again when the vortices reach close to the negative y-boundaries. By trying different sizes of grids we concluded that this behaviour is a boundary effect sensitive to the absolute separation between the vortex and the boundaries, but insensitive to the size of the grid. In the case of relatively small grids, the convergence of the paths could be misleadingly interpreted as a generic feature of vortex dynamics. To avoid this effect in our simulations the vortices were placed sufficiently apart from the boundaries of the grid.

5.5 Vortex Pull by an External Current

We have previously argued that under the influence of an homogeneous external current the vortex moves with velocity opposite to the applied current. The unusual response of the vortex can be easily realized in the context of Hall behaviour discussed in the previous chapter. Specifically, according to electromagnetic theory when an electric field acts on a vortex of magnetic flux the vortex feels a Lorentz force perpendicular to the plane of the electric and the magnetic field. Combined to the fact that due to the Hall behaviour, the vortex moves in a direction perpendicular to the applied force we find that it actually moves in a direction antiparallel to the electric field.

This is a notable result in the sense that can account for the rather puzzling sign change of the Hall effect which has been observed in the mixed state of the high temperature superconductors [23]-[26]. The sign reversal of the Hall voltage encountered there is attributed to the motion of the vortex with a velocity component opposite to the direction of the transport current.

We perform a number of simulations to investigate the response of the vortex to the external current and to check the theoretical predictions of the previous chapter. The numerical techniques are essentially identical to those described earlier. As initial configurations to our calculations we use isolated static vortex solutions (with charge $N = 1$) placed at the origin of the coordinate system. The external current $\mathbf{J}^e$ is taken parallel to the x-axis with direction to the positive x. In the framework of this model, the introduction of the external current is made possible by the addition of the term $\mathbf{A}\dot{\mathbf{J}}^e$. In turn equations of motion are modified by the substitution $J_i \longrightarrow J_i + J_i^e$ at the right hand side of the second part of 2.2.7.

The task of imposing boundary conditions is slightly problematic. We tried free b.c. as in section III as well as periodic ones and we found the former to be more reliable. Yet some boundary contributions crept in the simulations, caused by the incompatibility of free boundary conditions with the presence of the external current J_x^e at the boundaries. Though we did not manage to eliminate them we were able to isolate their effect and even

more to reduce it by using larger grids.

Numerically it is found more convenient to introduce a current in the form of a strip instead of one occupying the whole space. We assume that in the limit where the width of the strip is much larger than the size of the vortex, the vortex essentially realizes an homogeneous current throughout the whole space and responds accordingly. The exact form of the current is

$$J_y^e = 0 \qquad J_x^e = J_0\, f(y) \tag{5.5.1}$$

where the function f is approximately equal to unity over a strip of width $2L$ and drops to zero outside that strip. A function which meets the above description is

$$f(y) = e^{-(|y|/L)^n} \tag{5.5.2}$$

especially for large n. The reason of introducing the "strip current" is twofold. First it reduces the contribution from the boundaries. Besides, it reduces the rate of the energy flow into the system, which is generated by the external current.

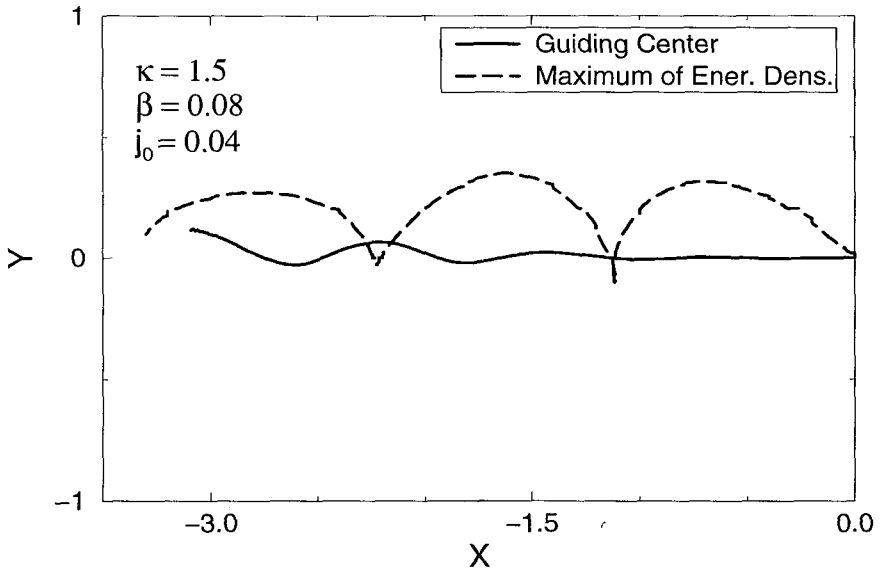

Figure 5.17 : *The trajectory of the vortex as determined by the guiding center (solid line), or the maximum of the energy density (dashed line).*

We perform our first run for $\kappa = 1.5$ and $\beta = 0.08$. The duration of the simulation is 80 time units. The radius of the vortex as that measured by the second moment of the energy density is ≈ 0.85. The value of J_0 is set equal to 0.04 which is one order of magnitude smaller than the average internal current of the vortex. The trajectory of the vortex for approximately 4 times its radius is plotted in Fig. 5.17. The solid line corresponds to the trajectory of the guiding center while the dashed line to that of the maximum of the energy density. There is a marked agreement between the motion of the guiding center and the theoretical predictions. The guiding center initially moves along an almost perfect straight line in the negative x direction which later on is modulated by an oscillatory motion in the y-axis. By experimenting with the size of the grid we realized that this oscillation of the guiding center is a boundary effect, which can be reduced by using larger grid in the cost of increasing the computational time which is needed for the simulations.

Equation 4.2.21 provides a definite prediction for the velocity of the guiding center. Namely the vortex is expected to move in the negative x-direction with a velocity V_x of measure equal to that of the external current. This prediction was also tested numerically and confirmed by the results.

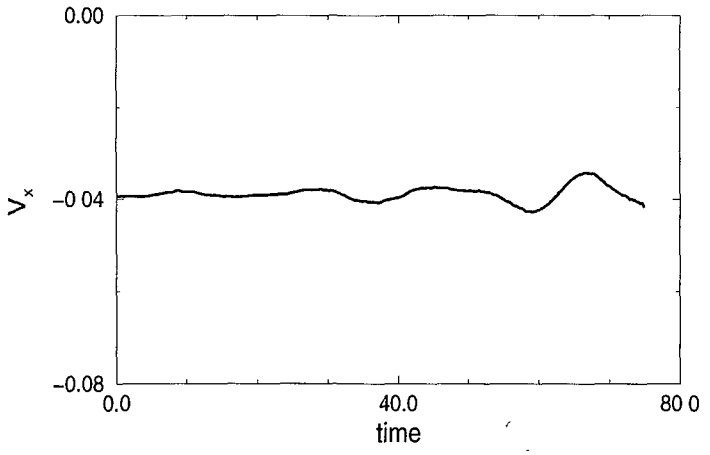

Figure 5.18 : *The x-component of the velocity of the guiding center of the vortex.*

In Fig. 5.18 we plot the x-component of the velocity of the vortex versus time, as this was measured in the previous simulation. As it is shown there, for $0 < t < 35$ the velocity V_x is roughly constant and equal to $-0.98\, J_0$. For larger times an oscillation in the magnitude of V_x turns on, which as earlier, is generated from boundary contributions. The slight deviation of V_x from J_0 is due to the strip form of the current. Actually the velocity of the vortex depends on the width of the strip as this is determined by parameter L. Experimenting with L we found the ratio $-\frac{V_x}{J_0} = 0.89, 0.94$ and 0.98 for $L = 3, 4$ and 5 respectively. For larger L the ratio $-\frac{V_x}{J_0}$ was essentially equal to one indicating that the strip was wide enough for the vortex to realize the external current as homogeneous throughout the whole space. The exact way the current drops to zero does not affect the motion of the vortex. We tried the values $n = 3, 5$ and 8 in eqs. 5.5.2 with $L = 5$, without any significant change in vortexs motion. Of course when L is small it is expected that n becomes important. Smaller value of n effectively means wider strip which in turn results higher velocity for the vortex.

Another feature we encounter in Fig. 5.17 is the Larmor precession of the trajectory of the vortex, as this is tracked through the maximum of the energy density. We are by now familiar to that effect which is reminiscence of the Hall structure of the model. It is thus expected that the Larmor motion will have similar dependence on the parameter β to that traced in the problem of the two vortices, i.e the oscillations will become wider for smaller β.

In Fig. 5.19 the $\beta-$dependence of Larmor motion is illustrated. There the trajectories of the vortex are plotted for $\beta = 0.02, 0.16$ and 0.32. J_0 and κ are fixed to the values 1.5 and 0.02 respectively. The details of Larmor motion are also depend on J_0. When J_0 increases the external force acting on the vortex also increases, which is similar to the effect of decreasing the inter-vortex separation in the vortex pair system. Thus we expect that the width of Larmor oscillations is an increasing function of J_0. We ran a set of simulations and though not quoted here the numerical results confirmed the J_0-dependence of Larmor motion.

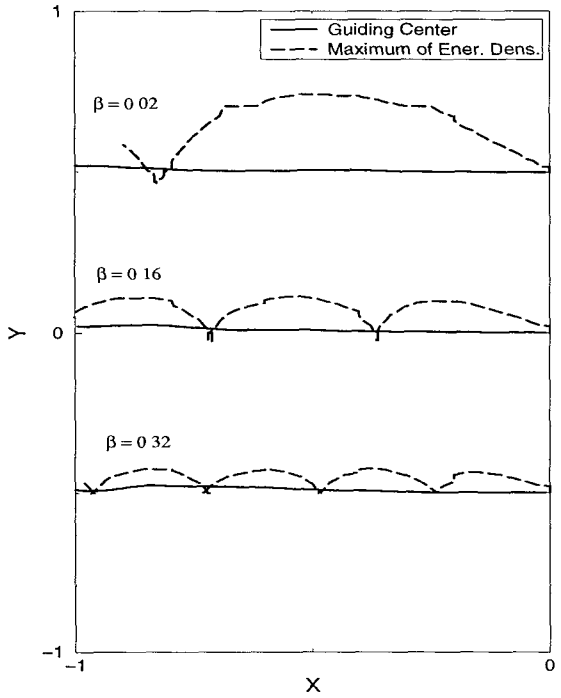

Figure 5.19 : *The dependence of the internal larmor motion of the vortex on parameter β.*

The last question we posed is the evolution of the vortex after the current is turned off. The canonical structure of the system implies that it is impossible for the vortex to move in the absence of external probes. Specifically, according to the discussion in section 4.2, when the current is turned off, the guiding center must froze at the point where is found at that time. On the other hand, because of the current, the vortex absorbs a considerable amount of energy and a part of it is transformed to kinetic energy. Note that the vortex is unable to expel this energy because the energy gap in the spectrum of the model prevents it from emitting radiation. Thus we end up with the puzzling picture of a body which possess kinetic energy and which is pinned at a certain point.

A possible way of reconciling these two contradicting features, is by as-

suming that some internal oscillatory motion is taken place. It turns out that there is an alternative to that explanation. The vortex continues to move, performing an oscillatory motion around the point where the guiding center of the vortex is frozen. This is illustrated in a simulation we performed for $\beta = 0.08$ and $\kappa = 1.5$. The value of J_0 was 0.02 for $0 < t \leq 40$ and then it was turned off. The total duration of the simulation was 125 time units.

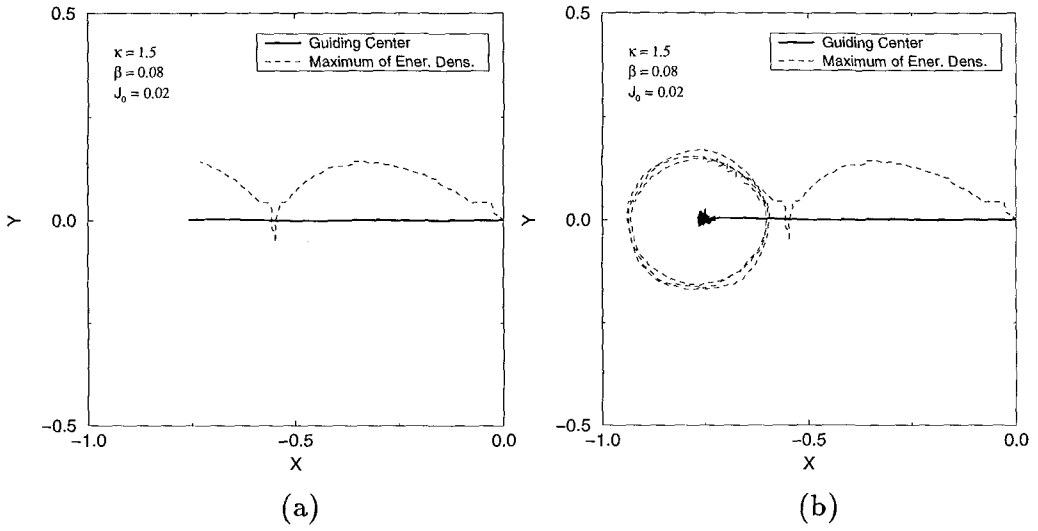

Figure 5.20 : *The motion of the vortex after the current is turned off. (a) the trajectory of the vortex while the current is on, and (b) the subsequent evolution after the current is turned off.*

In Fig. 5.20 we plot the trajectories of both the guiding center and the maximum of the energy density. Plot (a) shows the trajectories till the time where the current vanished, while plot (b) shows the trajectories till $t = 125$. There we see that indeed the guiding center remains at the point where it was found when the current was turned off. To the contrary, the maximum of energy density which due to Larmor motion did not coincide with the guiding center at that time, starts to oscillate around the position of the guiding center. Thus beside any internal oscillation the vortex also

oscillates around the pinned guiding center.

Due to the presence of the current the only quantity which is conserved is the total topological charge. To have an estimate of the accuracy of our routines we followed the evolution of topological charge which was conserved with accuracy 0.1% in all our simulations. All the calculations in this section were performed in a 300×300 grid with grid spacing $\alpha = 0.2$ and time step 0.002. In the above simulations the energy of the system is not constant, but increases with time due to the interaction with the external current. The increasing of energy imposes a constraint to the duration of the simulations since for large times the energy of the system blows up. For example in the first run when the current was turned off ($t = 40$), the energy of the vortex had risen by 20%, while in the first run described in this section, at $t = 80$ the energy of the vortex had been multiplied by a factor of four. Introduction of dissipation - which actually exists in any physical system - to control the energy balance is necessary in order to made feasible the numerical simulation of the motion of the vortex for longer times.

5.6 Discussion

The direct numerical simulation of the motion of a generic vortex-(anti)vortex configuration confirms the Hall behaviour, predicted analytically in a previous publication [27]. The quantitative agreement persists even when the two solitons overlap to the point that they can hardly be considered as two. Physically, this behaviour may not be entirely surprising. It might be described as the well known Hall effect. After all, the vortex of the model is microscopically [28] a non-vanishing electric charge density, which is sustained by the non-linear forces (attractive electrostatic and Ψ self-interactions), and circulates around its center, thus giving rise to the vortex magnetic field. The current is locally perpendicular to the electric field and hence consistent with the absence of energy dissipation. Thus, the overall situation looks similar to the ordinary Hall setting, only the circulating charges are immersed in their own magnetic field and repelled by it, instead of being kept in orbit by an externally prescribed one and quite naturally, a vortex is expected to exhibit the Hall behaviour described here. One may

push the picture even farther by noticing that since the charges as described by the wave-function Ψ, are spread over the entire region of the vortex, they feel the integral of the magnetic field, i.e. the winding number of the configuration, which makes plausible the appearance of N in formulas (4.4.1) and (4.2.22).

Mathematically on the other hand, one is dealing with the most general model describing the dynamics of a condensate wave-function Ψ coupled to the electromagnetic potential, and restricted only by the translational, rotational and gauge invariance of the system. The ion lattice assumed frozen, defines a preferred reference frame and breaks the Poincaré invariance of the underlying fundamental system. Topological or metastable non-topological solitons [65] in models with just these symmetries [37] are expected [28] to exhibit identical Hall behaviour. This is indeed what happens in all the systems examined so far [56], [32], even in ferromagnets which have no physical similarity to a system of charges interacting with the electromagnetic field [51], [66].

Clearly, the next step is to test the predictions of the model at hand against more realistic experimental situations. One should study the static properties of vortices in thin films with finite thickness, and then analyze their response to an external current in the context possibly of an improved model to incorporate dissipation.

5.7 Appendix: The Numerical Algorithm

To solve the initial value problem defined by the system of equations 5.3.5 we used a leapfrog updating scheme [67] where the the time levels of the time derivative term "leapfrogs" the time levels of space derivative terms. Equations 5.3.5 is a mixed system of first order and second order differential equations in time. A leapfrog algorithm for a second order equation is equivalent to the updating of fields and momenta successively, but the coupling of that equation to a first order equation demands special care in the construction of the algorithm. Nevertheless the leapfrog algorithm gives marked improvement in the stability over the simpler approach of updating both fields and their momenta at the same time level.

To perform our simulations we found a 161×161 grid, with lattice spacing $\alpha = 0.15$ of sufficient accuracy. The space resolution of that grid is estimated by calculating numerically the total topological charge N and comparing it to the exact value $N = 2$. It is found to be 1.993 when the formula ?? is used for the topological density and 1.999 when formula ?? was used. The accuracy of the simulations is further estimated by the conservation of energy which is respected in one period's time with accuracy better than 0.1% in all our runs. Another check of the accuracy of our results is provided by performing simulations in bigger grids 251×251 with the same or smaller lattice spacing ($\alpha = 0.1$). The results we obtained were in total agreement to those of the previous runs. We used bigger grid (251×251 with $\alpha = 0.15$) in the vortex-antivortex simulations in order to follow the orbits of the vortices for longer distances. The time step Δt we used in most of our runs was 0.001 or 0.002 but the algorithm was stable and accurate for even bigger time steps. All our simulations were performed on various HP workstations in Crete. A typical run of duration $T \approx 800$ time units with $\Delta t = 0.002$ in a 161×161 grid needed 80 hours CPU time in a HP 735 workstation.

Finally we want to comment on our choice to use lattice gauge formalism. In numerical works on vortex dynamics in relativistic models there are two different discretization schemes in use. The most accurate one is based on techniques from lattice gauge formalism (L.G.T.)[64], [68], [48] especially

designed to preserve the local gauge constraint. In other works [49], [50], conventional discretization schemes (C.D.S.) are invoked to transform the differential equations of the continuum to difference equations. The latter method is less accurate in the sense that the gauge constraint is not very well preserved. Nevertheless the results of the two discretization schemes are in agreement.

In our work we experimented with both alternatives and finally adopted the former. Our choice was motivated by reasons of elegance and functionality. The construction of (L.G.T.) is particularly elegant and natural. On the other hand (C.D.S.) while they may work suffer from serious theoretical trouble. Since they do not preserve gauge symmetry, imposition of any gauge fixing condition is arbitrary and problematic. This disease has no cure and its symptoms are demonstrated in the preservation of the Gauss constraint. In fact this discrepancy is a consequence of the violation of the equation of continuity. Gauge symmetry and continuity equation are closely related[69]. A discretization scheme that does not preserve gauge symmetry results to a set of difference equations which violate equation of continuity and consequently the gauge constraint. Although formally (C.D.S.) suffer serious problems, the relativistic analogue [49], [50] implies that they can be equally effective. And now we come to functionality. Use of (C.D.S.) results violation of Gauss law. The corresponding error is accumulative and increases with time. When that error becomes significant the routine destabilizes. Of course one can always use sufficiently small grid spacing to retain the error at sufficiently small values. But in the non-relativistic system which we study, in contrast to the relativistic analogue, the velocities are very small and one has to wait quite long to see a complete rotation of the vortex. This in turn results a very small grid spacing and consequently a very large grid and the whole numerical task becomes very CPU time consuming.

Bibliography

[1] H. K. Onnes, *Leiden Comm.*, (1911) 1206 ; quoted in D. Shoenberg, *Superconductivity*, Cambridge, New York, (1952) 1

[2] B.S. Chandrasekhar, in *Superconductivity*, Vol. 1, edited by R.D. Parks, M. Dekker, New York (1969) and references therein.

[3] J. Bardeen, L.N. Cooper, and J.R. Schrieffer, *Phys. Rev.* **108**, (1957) 1175.

[4] L. N. Cooper, *Phys. Rev.* **104** (1956) 1189.

[5] V. I. Ginzburg and L. D. Landau, *Zh. Eksp. Teor. Fiz.* **20**, (1950) 1064.

[6] L.P. Gorkov, *Zh. Eksp. Teor. Fiz.* **36** (1959) 1918.

[7] L. Landau and E.M. Lifshitz, *Statistical Physics*, Part 2. Pergamon Press 1980.

[8] N.R. Werthamer, in *Superconductivity*, Vol. 2, edited by R.D. Parks, M. Dekker, New York (1969) and references therein.

[9] A.T. Dorsey, *Phys.Rev.* **B46** (1992) 8376, and references therein.

[10] Ping Ao and D.J. Thouless, *Phys.Rev.Lett.* **70** (1993) 2158.

[11] R.P. Feynman, R.B. Leighton, and M. Sands, *The Feynman Lectures on Physics*, vol. III, Addison-Wesley, 1965. See also R.P. Feynman, *Statistical Mechanics*, Frontiers in Physics, W. A. Benjamin (1972).

[12] H.B. Nielsen and P. Olesen, *Nucl. Phys.* **61B** (1973) 45.

[13] W. Meissner and R. Ochsenfeld, *Naturwiss.* **21**, 787 (1933).

[14] U. Essmann and H. Trauble, *Phys. Lett.* **24A** (1967) 526.

[15] B. S. Deaver and W. M. Fairbank, *Phys. Rev. Lett.* **7** (1961) 43.

[16] R. Doll and M. Nabauer, *Phys. Rev. Lett.* **7** (1961) 51.

[17] J. Bardeen and M.J. Stephen, *Phys. Rev.* **140A** (1965) 1197

[18] P. Nozières and W.F. Vinen, *Philos. Mag.* **14** (1966) 667, and references therein.

[19] Ping Ao *J. of Superconductivity* **8** (1995) 1

[20] M. Hatsuda, M. Sato, S. Yahikozawa and T. Hatsuda *KEK preprint 95-56*, cond-mat 9505158

[21] Ping Ao, D.J. Thouless, and X.M. Zhu *9312099*

[22] I.J.R. Aitchison, Ping Ao, D.J. Thouless, and X.M. Zhu *CERN-TH-7385-94*, 9411047

[23] S.J. Hagen, C.J. Lobb, R.L. Greene, M.G. Forrester and J.H. Kane, *Phys. Rev.* **41B** (1990) 11630

[24] S.J. Hagen, C.J. Lobb, R.L. Greene, M.G. Forrester and J. Talvacchio, *Phys. Rev.* **42B** (1990) 6777

[25] T. W. Jing and N. P. Ong, *Phys. Rev.* **42B** (1990) 10781

[26] S.J. Hagen, C.J. Lobb, R.L. Greene and M. Eddy, *Phys. Rev.* **43B** (1991) 6246

[27] N. Papanicolaou and T.N. Tomaras, *Phys. Lett.* **179A** (1993) 33.

[28] G.N. Stratopoulos and T.N. Tomaras, *Physica* **D89** (1995) 136.

[29] G.N. Stratopoulos and T.N. Tomaras, *Crete preprint 96-10*, hep-th/9601172 to appear in Physical Review **B**

[30] G.N. Stratopoulos and T.N. Tomaras, Work in preparation.

[31] P. Donatis and R. Iengo, *Nucl. Phys.* **B435** (1995) 659-672

[32] P. Donatis and R. Iengo, "Persistent supercurrents in a planar non-relativistic chiral fluid", SISSA preprint (1995).

[33] K.M. Lee, *Phys. Rev.* **49D** (1994) 4265

[34] R. Rajaraman, *Solitons and Instantons* (North-Holland, Amsterdam, 1982.)

[35] S. Coleman, *Aspects of Symmetry*, Cambridge University Press 1988.

[36] S. Coleman, *Nucl. Phys.* **262B**, 263 (1985).

[37] R. Friedberg, T.D. Lee and A. Sirlin, *Phys. Rev.* **13D**, 2739 (1976).

[38] L. Jacobs and C. Rebbi, *Phys. Rev.* **B19** (1979) 4486.

[39] L. Perivolaropoulos, *Phys. Rev.* **D48** (1993) 5961, and references therein.

[40] G.H. Derrick, *J. Math. Phys.* **5** (1964) 1252.

[41] A.A. Abrikosov, *Sov. Phys. JETP* **5** (1957) 1174.

[42] D. R. Tilley and J Tilley, *Superfluidity and Superconductivity*, Adam Hilger (1990)

[43] M.F. Atiyah and N. Hitchin, (The geometry and dynamics of magnetic monopoles) (Princeton Uviv. Press, Princeton 1988).

[44] N.S. Manton, *Phys. Lett.* **192B**, 177 (1981).

[45] R.S. Ward, *Phys. Lett.* **158B**, 424 (1985).

[46] R.A. Leese, M. Peyrard and W.J. Zakrzewski, *Nonlinearity* **3**, 773 (1990).

[47] M. Peyrard, B. Piette and W.J. Zakrzewski, *Nonlinearity* **5**, 563 (1992).

[48] E Myers, C. Rebbi and R. Strilka, *Phys. Rev.* **45D** (1992) 1355.

[49] E.P.S. Shellard, P.J. Ruback, *Phys. Lett.* **209B** (1988) 262.

[50] P. Laguna and R.A. Matzner, *Phys. Rev.* **41D** (1990) 1751.

[51] N. Papanicolaou and T.N. Tomaras, *Nucl. Phys.* **360B** (1991) 425.

[52] See for instance T.D. Lee, *Particle Physics and Introduction to Field Theory*, Harwood Academic Publishers 1981.

[53] J. Friedel, P.G. de Gennes and J. Matricon, *Appl. Phys. Lett.* **2** (1963) 119.

[54] G.K. Batchelor, *An Introduction to Fluid Dynamics* , Cambridge University Press 1967.

[55] J-M. Lévy-Leblond in *Group Theory and its Applications*, Ed. E.M. Loebl, Academic Press 1971.

[56] X.G. Wen and A. Zee, *Phys. Rev. Lett.* **62** (1989) 2873.

[57] F.G. Mertens, A.R. Bishop, G.M. Wysin and C. Kawabata, *Phys. Rev.* **B39** (1989) 591.

[58] N. Papanicolaou and W.J. Zakrzewski, *Physica D* **80** (1995) 225.

[59] K. G. Wilson, *Phys. Rev.* **D14** (1974) 2455.

[60] Les Houches 1975 *Methods in field theory* North-Holland Publishing Company, (1976).

[61] T. P. Cheng and L. F. Li, *Gauge theory of elementary particle physics*, Oxford University Press (1984).

[62] L. H. Ryder, *Quantum Field Theory* , Cambridge University Press (1985) 124.

[63] C. Rebbi, *Lattice Gauge Theories and Monte Carlo Simulations*, World Scientific Publishing Co (1983) 9, and references therein.

[64] M. Creutz, L. Jacobs and C. Rebbi, *Phys. Rep* **95** (1983) 201.

[65] C. Bachas and T. N. Tomaras, *Phys. Rev.* **D51**, R5356 (1995).

[66] N. Papanicolaou and W.J. Zakrzewski, "Dynamics of Magnetic Bubbles in a Skyrme Model", Crete preprint (1995)

[67] W.H. Press, S.A. Teukolsky, W.T. Vetterling and B.P. Flannery, *Numerical Recipes in Fortran*, Cambridge University Press (1992).

[68] K.J.M. Moriarty, E Myers and C. Rebbi, *Comput. Phys. Commun.* **54** (1989) 273.

[69] L. D. Landau and E. M. Lifshitz, *The Classical Theory of Fields*, Pergamon Press (1980)

[70] R.P. Huebener, *Magnetic Flux Structures in Superconductors*, Springer 1979.

[71] Qiang Li, J.R. Clem and D.K. Finnemore, *Phys.Rev.* **B43** (1991) 12843.

[72] N. Papanicolaou, *Physica D* **74** (1994) 107.